TÉCNICO LISBOA

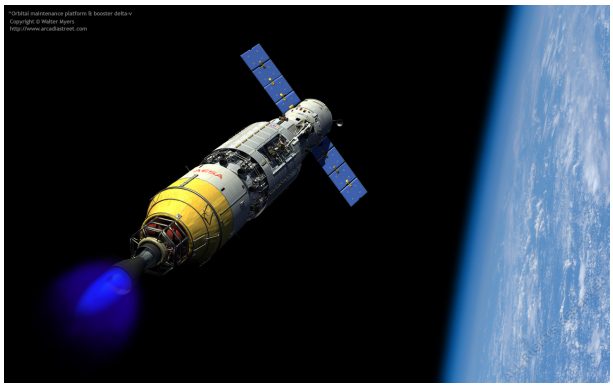

Low-Thrust Orbit Transfers Between Two-Body Keplerian Orbits

Mariana Gonçalves de Araújo Sá

Thesis to obtain the Master of Science Degree in

Engineering Physics

Supervisor: Prof. Dr. Rui Manuel Agostinho Dilão

Examination Committee

Chairperson: Prof. Dr. Ilídio Pereira Lopes
Supervisor: Prof. Dr. Rui Manuel Agostinho Dilão
Member of the Committee: Prof.ª Dra. Ana Maria Ribeiro Ferreira Nunes

December 2020

Acknowledgments

Ao Professor Rui Dilão pela sua orientação, simpatia, dedicação e motivação durante todo o desenvolvimento da minha tese. Mesmo em tempos pandémicos e a 300 quilómetros esteve sempre disponível para esclarecer as minhas dúvidas e problemas com as simulações. Muito obrigada.

Às minhas três pessoas favoritas do mundo inteiro: aos meus pais, por serem o meu maior pilar em todas as etapas da vida e por nunca me deixarem desistir do que sabem que é importante para mim; à Leonor, por ser a melhor irmã, amiga e confidente que podia ter. Ao meu pai agradeço mais uma vez todas as correções que fez a esta tese e que, com certeza, contribuiram para que ficasse mais completa.

Aos meus quatro avós e titi por todo o carinho, mimo e dedicação que sempre me deram. Sou uma sortuda!

À minha família da capital: Beatriz, Nuno, Rita, Bárbara, Francisco, Inês e Diogo e ainda à Cláudia e Rafaela. Recordarei sempre com muito carinho estes três anos que passámos juntos! Um agradecimento especial à Rita e à Beatriz, por toda a ajuda que me deram com o *Mathematica*; ao Diogo, por todas as caminhadas e sessões televisivas (de elevada cultura!) durante os meses em que partilhámos casa e ao Nuno, por ter sido o melhor companheiro que podia ter arranjado para passar o Estado de Emergência, pela leitura e correção de partes desta tese, e por, apesar de já não estar comigo diariamente, continuar sempre presente nos momentos cruciais.

À Beatriz Pereira, pela mensagem quase semanal "então, que tal vai isso?" e por todo o apoio durante esta "batalha".

Por último, mas não menos importantes, aos meus amigos de sempre, Ana Sofia, Mafalda, Miguel, Sofia, Sobral, Cristina e Rita Lino, e aos "Barroqueiros", Bianca e Xico, por, mesmo agora estando eles no Porto e eu em Lisboa, continuarem assiduamente na minha vida.

Resumo

Em órbita, os satélites descrevem órbitas Keplerianas em torno de um corpo primário. Contudo, por vezes, pode ser necessário alterar as suas trajetórias e, portanto, transferi-los para outras órbitas. Uma mudança de trajetória implica uma mudança na velocidade do veículo espacial, controlada acionando os pequenos propulsores que este possui.

Nesta tese de mestrado, para controlar a direção dos gases de escape dos propulsores, considerámos manobras não-impulsivas e, em particular, transferências *low-thrust*. Estas transferências implicam uma taxa constante e bastante longa de combustão dos gases de escape e podem ser iniciadas em qualquer instante de tempo independentemente da posição do satélite. Estes dois aspetos representam melhorias significativas relativamente às transferências de Hohmann, que são realizadas essencialmente no *apoapsis* e *periapsis* da órbita inicial.

Foi desenvolvido um novo algoritmo para transferências entre duas órbitas Keplerianas no mesmo plano. Para isso, controlámos as constantes de movimento do problema de Kepler: os vetores momento angular e Laplace-Runge-Lenz e a energia efetiva do satélite, usando um controlo do tipo *bang-bang*. As órbitas inicial e final são Keplerianas e completamente definidas pelos valores destas constantes.

As transferências foram simuladas para órbitas elípticas, circulares e hiperbólicas com momento angular constante e energia efetiva variável, com energia efetiva constante e momento angular variável e com ambas estas grandezas variáveis. Para além disso, estudámos o caso particular de transferências entre duas órbitas circulares e usámos o vetor de Laplace-Runge-Lenz para rodar a orientação das linhas dos apsides.

Palavras-chave: Transferência de órbitas, órbitas Keplerianas, Teoria de Controlo, Controlo *bang-bang*, Sistemas Dinâmicos

Abstract

When on orbit, satellites describe Keplerian orbits around a primary body. However, it may be necessary to change their trajectory and, therefore, transfer them to other orbits. A change in the trajectory implies a change in spacecraft speed, which is done through the burning of its rocket engines.

In this master thesis, for the maneuvering of the thrusters exhaust direction, we considered non-impulsive maneuvers and, in particular, low-thrust transfers. These transfers imply a constant and long burn fires and can be applied at any instant of time regardless of the satellite position. These two aspects represent significant improvements over Hohmann transfers, which are essentially performed at the apoapsis and at the periapsis of the initial orbit.

We developed a new algorithm for plane transfers, i.e., a general satellite transfer between two Keplerian orbits in the same plane. To do this, we controlled the constants of motion of the Kepler problem: angular momentum and Laplace-Runge-Lenz vectors and effective energy, using a *bang-bang* type control. The initial and final orbits are Keplerian and are completely defined by the values of these constants.

We simulated transfers between elliptical, hyperbolic and circular orbits with constant angular momentum, with constant effective energy and with both variable angular momentum and effective energy. Furthermore, we studied a particular case of transfers: between two circular orbits, and used Laplace-Runge-Lenz vector to rotate the orientation of the lines of apsides.

Keywords: Orbit transfers, Keplerian orbits, Control Theory, *Bang-bang* Control, Dynamical Systems

Contents

List of Tables

List of Figures

Glossary

Notation

Greek symbols

α Laplace-Runge-Lenz azimuthal angle in the plane of the orbit. $\Delta\alpha$ is this angle variation. (SI unit: rad)

Δ Variation of a variable when it is followed by a variable. Otherwise, it is a polynomial discriminant.

ϵ Control parameter. (dimensionless)

ϕ Control longitude escape angle measured in the reference frame S. (SI unity: rad)

γ Rate of mass lost by the satellite per unit of mass. (SI unity: s^{-1})

σ Control parameter used to simplify the choice of ϕ according with the sign taken in the equations of motion $(= \pm 1, 0)$. (dimensionless)

θ Position azimuthal angle in the reference frame S. (SI unity: rad)

τ Normalized time variable. (dimensionless)

μ Standard gravitational parameter $(= GM)$. For the Earth, $\mu \simeq 4 \times 10^{14} m^3 s^{-2}$. (SI unity: $m^3 s^{-2}$)

Latin symbols

$\vec{A}$ Laplace-Runge-Lenz vector and A is its magnitude. (dimensionless)

G Universal gravitation constant ($\simeq 6.67 \times 10^{-11} m^3 kg^{-1} s^{-2}$). (SI unity: $m^3 kg^{-1} s^{-2}$)

H When $= 0$, it is the effective energy of the Keplerian orbit but when $\neq 0$ is the total effective energy of the satellite. (dimensionless)

$\vec{L}$ Angular momentum vector and L is its magnitude. (dimensionless)

$\mathcal{L}$ Lagrangian.

M Mass of the primary body. (SI unity: kg)

m Mass of the secondary body or satellite. (SI unity: kg)

$\vec{r}$ Position vector in the reference frame S and r denotes the distance between the satellite and the primary mass. (SI unity: m)

S Reference frame centred at the primary body system.

t Time variable. (SI unity: s)

$\vec{u}_{rel}$ Velocity vector of the exhaust gases (mass lost by the satellite) measured in the satellite reference frame and u is its magnitude. (SI unity: ms^{-1})

x, y Cartesian coordinates in the reference frame S. (SI unity: m)

Subscripts

0 Initial value.

x, y Cartesian components in the reference frame S.

Superscripts

$*$ Fixed point.

Acronyms

LRL Laplace-Runge-Lenz

Chapter 1

Introduction

In the latter half of the twentieth century, rockets were developed and overcame the gravity force. Thus, the space exploration era had begun: in 1957, the first human-made object to orbit the Earth, the satellite Sputnik 1, was launched and the first human space flight occurred in 1961. After that, many other missions took place and others are still currently in progress, such as the famous Hubble Space Telescope, launched in 1990. However, it did not always go as expected and some accidents happened: in 1986 and 2003 the space shuttles Challenger and Columbia, respectively, exploded during their launch and killed all the members of the crews.

There is still much work to do regarding space exploration and a fundamental part of that is the application of orbital maneuvers, i.e., the transfer of a spacecraft or satellite between orbits. An example is a set of GPS satellites in which one of them crashed and it is necessary to replace it, sending another satellite to its position. This is a problem of high complexity and many new strategies of transfers have been developed, involving optimization criteria to minimize both the costs and the transfer time. These optimization criteria lead us to Control Theory and, in particular, to Pontryagin's Maximum Principle.

To transfer a spacecraft between two orbits, it is necessary to change its velocity, which is done through the burning of the rocket engines on the spacecraft. To do that we have two types of maneuvers: impulsive and non-impulsive. The difference between them is that the former consists of instantaneous burn fires with high-thrust chemical propulsion systems at some chosen points of the orbit, while in the latter the burn fires are applied during a longer time period. The main example of impulsive maneuvers is the Hohmann transfers. Low-thrust transfers are examples of non-impulsive control with low energy consumption. This will be described in detail in Section 1.2.

The main goal of this master thesis is to develop a new algorithm for plane transfers based on the control and optimization of the constants of motion of the Kepler problem. These constants are angular momentum and Laplace-Runge-Lenz vectors and energy. This project is an extension of [1], where 2-dimensional transfers with constant angular momentum and with constant effective energy have been considered. In this thesis, we have extended these techniques to all possible Keplerian orbits, eliminating convergence problems and situations where non reachable targets exist. The main results of this thesis are exposed in [3].

1.1 Motion of a Rocket

Since the main goal of this dissertation is to study the transfer of a spacecraft between two orbits, we must know that the spacecraft has rocket engines, which are fired when we want to change the spacecraft velocity (speed and/or direction). These are known as thrusters. At the bottom of the rocket, there are big thrusters (left picture of Figure 1.1) that expel exhaust gases so that the gravity is overcome and the rocket takes off. On the sides of the spacecraft, there are small boxes with a set of small thrusters disposed in different directions (right picture of Figure 1.1). On orbit, we can control the rocket orientation by boosting the small thrusters.

Figure 1.1: On the left, thrusters at the bottom of the rocket Saturn V. On the right, a rocket stage and in the zoom are the rocket engines which are boosted to control a spacecraft. Both pictures were taken from reference [1].

To derive the rocket equation of motion we assume that m is the instantaneous mass of the rocket, which is moving with velocity $\vec{v}$ relative to an inertial frame. To control the rocket motion we fire a booster with velocity $\vec{u}$ relative to the rocket. The exhaust gases are expelled at the rate $\frac{dm}{dt}$ with velocity $\vec{v}+\vec{u}$. Then, the rocket equation of motion [4] is

$$\vec{F} = \frac{d(m\vec{v})}{dt} - (\vec{v}+\vec{u})\frac{dm}{dt}, \tag{1.1}$$

where, in this case, $\vec{F}$ is simply the gravitational force, $\vec{F_g}$. This expression can easily be simplified into

$$\vec{F_g} = m\frac{d\vec{v}}{dt} - \vec{u}\frac{dm}{dt}. \tag{1.2}$$

From here, if we consider that the motion of the rocket is upward and, consequently, the gas exhaust's motion is downward, the equation (1.1) is written as

$$-mg = m\frac{dv}{dt} - u\frac{dm}{dt}, \tag{1.3}$$

where $\frac{dm}{dt} = -k$ and $\vec{u} = u\hat{z}$. k and u are positive constants. Since $m(t) = m_0 - kt > 0$, equation (1.3)

can be integrated and we obtain the equation for the rocket speed as a function of time:

$$v(t) = v(0) + u \ln \frac{m_0}{m_0 - kt} - gt, \tag{1.4}$$

where m_0 is the initial mass of the rocket.

At this point, we have the necessary conditions to understand some of the most used orbital maneuvers.

1.2 Orbital Maneuvers

Since we are interested in changing the orbit of a satellite, we must recall that the orbital maneuvers can be impulsive or non-impulsive. Impulsive maneuvers consist of quasi-instantaneous burn fires usually with high-thrust chemical propulsion systems, while the non-impulsive ones consist of long burn fires usually with low-thrust electrical propulsion systems.

Initially, only impulsive maneuvers were carried out, but the situation changed with the appearance of ionic motors and others. These new technologies are very efficient, with a specific impulse several times higher than chemical propulsion, but with a smaller force, which implies that to be useful they have to work for long periods of time, i.e., continuously.

In the following sections, we will present an example of each of these orbital maneuvers (Hohmann and low-thrust orbit transfers) to understand the impulsive and non-impulsive maneuvers, respectively.

1.2.1 Hohmann Transfer

The Hohmann transfer is a method of performing the transfer of two co-planar circular orbits through an elliptical orbit, where the energy expenditure is minimized [5]. To do this, it takes two maneuvers in which boosts are fired, causing changes in the rocket velocity. Each of these maneuvers is impulsive, i.e., it occurs instantaneously, so that the rocket remains at the same position at the final of the boost. This idea came from Walter Hohmann in 1925 [6].

The geometry of a Hohmann transfer can be seen in Figure 1.2. Let us suppose that we want to transfer a satellite in a circular orbit with radius r_1 to one with radius $r_2 > r_1$, minimizing the expenditure of energy. We chose a point in the initial orbit and we apply an impulsive and tangential thrust, leading to a velocity increase $\Delta\vec{v_1}$. The rocket is now following an elliptical transfer orbit. Then, we chose another point of this new orbit and we again apply an impulsive thrust. The chosen points must be the periapsis (r_1) and the apoapsis[1] (r_2) of the transfer orbit, respectively. The rocket velocity is now $\Delta\vec{v_2}$, changing the elliptical orbit to a circular one with a larger radius. This process is reversed if we want to change from an orbit with a radius r_2 to another with a radius $r_1 < r_2$.

To compute the velocity changes in this transfer, we use the energy conservation equation [4] as

$$\frac{v^2}{2} - \frac{\mu}{r} = -\frac{\mu}{2\alpha}, \tag{1.5}$$

[1] Periapsis and apoapsis are the closest and the farthest points of the orbit to the primary body, respectively.

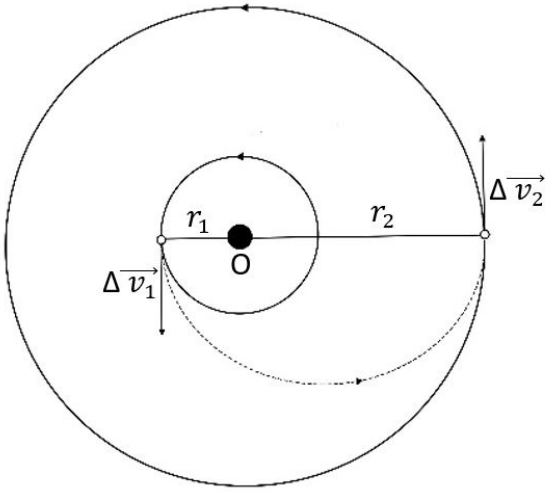

Figure 1.2: Geometry of a Hohmann transfer orbit.

where $v = |\vec{v}|$ is the absolute value (the speed) of the rocket velocity, α is the semi-major axis of the conic section and $\mu = GM$, with M being the mass of the primary body and G the gravitational constant. The left term is related to the specific orbital energy for a Keplerian orbit and the right one with properties of the conic sections [7].

Using equation (1.5) and subtracting the speeds before and after each thrust in each chosen point, we obtain the maneuvers' velocity [4]. As for the first thrust, before the rocket is in a circular orbit with $r = \alpha = r_1$ and we can write:

$$\frac{v_1^2}{2} - \frac{\mu}{r_1} = -\frac{\mu}{2r_1} \implies v_1 = \sqrt{\frac{\mu}{r_1}}; \tag{1.6}$$

after, it is in an elliptical orbit with $r = r_1$ and $\alpha = \frac{r_1+r_2}{2}$, which leads to a new velocity v_1':

$$v_1' = \left[\frac{2\mu}{r_1}\left(\frac{r_2}{r_1+r_2}\right)\right]^{\frac{1}{2}}. \tag{1.7}$$

Therefore, the amount of speed that must be added to the rocket in the first maneuver is given by the subtraction of equations (1.7) and (1.6):

$$\Delta v_1 = v_1' - v_1 = \left[\frac{2\mu}{r_1}\left(\frac{r_2}{r_1+r_2}\right)\right]^{\frac{1}{2}} - \left(\frac{\mu}{r_1}\right)^{\frac{1}{2}}. \tag{1.8}$$

For the second thrust, the method is analogous. Before the boost, when the rocket arrives at the apogee of the elliptical transfer orbit, $r = r_2$ and $\alpha = \frac{r_1+r_2}{2}$; after this, $r = r_2$ and $\alpha = r_2$. Then, the velocity change for the second thrust is:

$$\Delta v_2 = \left(\frac{\mu}{r_2}\right)^{\frac{1}{2}} - \left[\frac{2\mu}{r_2}\left(\frac{r_1}{r_1+r_2}\right)\right]^{\frac{1}{2}}. \tag{1.9}$$

The total speed change is given by $\Delta v_1 + \Delta v_2$ and the total energy change is proportional to $(|\Delta v_1| + |\Delta v_2|)^2$. Since we apply the maneuvers to increase the speed of the spacecraft, the order of the subtractions (1.8) and (1.9) was chosen such that velocity changes in an outward transfer were

positive. Also, notice that it takes one-half of the period of the elliptic orbit transfer to complete the Hohmann transfer, i.e., the time between maneuvers is given by the third Kepler's law [7]:

$$\Delta t = \pi \sqrt{\frac{r_1^3}{\mu}}. \tag{1.10}$$

Although there are other types of transfers with a set of two impulsive thrusts, the main example of orbit transfer is the bi-elliptic one, with a set of three impulsive thrusts of maneuvers [4], but we will not study it here.

1.2.2 Low-Thrust Orbit Transfer

Unlike the Hohmann transfers, some maneuvers require small amounts of fuel but they take a considerable amount of time to reach the required high velocity. These transfers are known as low-thrust and usually have an electrical propulsion system, often using plasma thrusters, such as, for example, Hall thrusters. Furthermore, while Hohmann transfers have to start at the periapsis or apoapsis of the initial orbit, this new type of transfer allows us to start at any point in the orbit. Figure 1.3 shows an example of a low-thrust maneuver, where the trajectory is a spiral until reaching the final orbit.

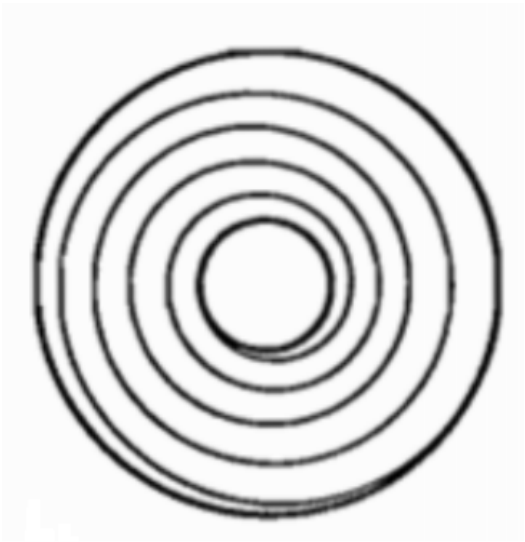

Figure 1.3: Example of a low-thrust transfer. Picture taken from reference [2].

Let us consider the problem of transfer from a lower to a higher circular orbit, i.e., we want to increase the semi-major axis a of the orbit and, consequently, the total two-body gravitational energy (per mass unit) $\epsilon = -\frac{\mu}{2a}$, [7]. Taking the derivative of this equation with respect to time, we obtain

$$\frac{d\epsilon}{dt} = \frac{\mu}{2a^2}\frac{da}{dt}. \tag{1.11}$$

The rate at which the propulsion system performs work (power per mass unit) on the spacecraft is

$$\frac{d\epsilon}{dt} = \vec{A} \cdot \vec{v}, \tag{1.12}$$

where $\vec{A}$ and $\vec{v}$ are the acceleration and the velocity of the vehicle, respectively. Since we are interested in optimizing this rate, the inner product $\vec{A} \cdot \vec{v}$ must be maximized, implying the alignment of these two vectors. If we consider low accelerations, the spacecraft orbit remains nearly circular at each point, resulting in a slow outward spiral trajectory. The vehicle instantaneous velocity is approximated by the velocity of the circular orbit, $v_c = \sqrt{\frac{\mu}{a}}$.

If we match equations (1.11) and (1.12), we obtain an equation of motion for the semi-major axis of the orbit:

$$\frac{da}{dt} = \frac{2}{\sqrt{\mu}} a^{\frac{3}{2}} A, \tag{1.13}$$

which is easily separated in a and t. If, then, we integrate both sides, we have the duration of a transfer:

$$\Delta t = \frac{\sqrt{\mu}}{A} \left(a_0^{-\frac{1}{2}} - a^{-\frac{1}{2}} \right). \tag{1.14}$$

The total speed change is given by the product of the time interval during which thrusters are turned on with the rocket constant acceleration:

$$\Delta v = A(t - t_0) = \sqrt{\mu} \left(a_0^{-\frac{1}{2}} - a^{-\frac{1}{2}} \right), \tag{1.15}$$

which is equal to the difference between the speeds at the initial and final orbits.

Low-thrust transfers have been analyzed during the past decades. In the 1960s spacecrafts that used solar-electric panels to power an electric engine were studied. These vehicles are called solar-electric transfer vehicles and have low-thrust levels on the order of hundredths to thousandths of g (gravitational acceleration). Transfer times are very long and their trajectories have a spiral shape. In 1967, Dickerson and Smith [8] derived the required conditions for optimal solar-electric powered flights. They used variational calculus techniques from classical optimization theory and presented several numerical examples to illustrate the general solar-electric formulation. In 1968, a planetary orbiter spacecraft propelled by solar-electric panels was proposed by Sauer [9] and it could deliver to Mars a larger payload than conventional rockets.

In the 1970s, NASA started its Solar Electric Propulsion (SEP) stage program, which is still in effect. In 1975, Oglevie *et al.* [10] found that to maintain the optimal path is necessary to point the solar arrays towards the sun. The goal of the SEP program is to obtain highly efficient orbit transfers as well as develop "technologies necessary for robotic and human exploration-class solar-electric transportation systems"[2]. In 2015, a 12.5-kilowatt (kW) Hall thruster with magnetic shielding was successfully tested and it was able to operate continuously for years. Currently, NASA is working on SEP technologies needed to affordably enable human missions to the Moon and Mars in a more economically. Such technologies are expected to maintain the spacecraft position around the Moon and transfer it to other orbits. The first crew will be sent to Mars around 2030 [11].

Furthermore, in the late 1980s, *ELectric Insertion Transfer Experiment* (ELITE) program was developed by the U.S. Air Force with the aim of building and testing a pioneer of an operational electric orbit

[2]https://www.nasa.gov/mission_pages/tdm/sep/index.html

transfer vehicle [12, 13].

The first Moon mission by the European Space Agency (ESA) had an electric propulsion system which sent SMART-1[3] to the Moon with just 82 kilograms of Xenon fuel. The mission started in 2003 and ended three years later with extreme success, testing new communication and navigational techniques. Besides, it had solar panels which used an advanced type of gallium-arsenide solar cells instead of the silicon cells used so far.

Other examples of satellites that used electric thrusters are the U.S. Air Force's Advanced Extremely High Frequency satellite [14], that used Hall effect thrusters, and the European Space Agency's ARTEMIS satellite [15], which used an onboard ion propulsion engine. Besides, in 2015, two all-electric telecommunication satellites were launched on SpaceX's Falcon 9 rocket [16].

As we can conclude, electrical propulsion is currently considered a revolutionary technology for the new generations of satellites and many stakeholders all over the world have been investing in increasing its competitiveness.

1.2.3 Orbit Plane Change Transfers

So far, we only considered orbit transfers in the same plane. However, this is not very realistic. Real maneuvers include changes in the orientation of a satellite orbital plane and are therefore one of the most expensive transfers. This plane change also implies a change in the direction of the velocity vector, which is found by subtracting the velocity vectors of the orbits. To simplify, assuming that both orbits have the same speed v and considering the triangle in Figure 1.4, it is possible to demonstrate, by a geometrical calculation, that the required velocity change, Δv, is

$$\Delta v = 2v \sin\left(\frac{\theta}{2}\right). \tag{1.16}$$

We must emphasize this result because it shows that plane changes are, in fact, very expensive maneuvers in terms of propellants. For example, if we consider $\theta = 60°$, the required change in speed is equal to the current speed, which allows us to conclude that this change can be very large. In this case, it requires a rocket large enough to launch the payload in the first place, which, in turn, requires a huge booster [7].

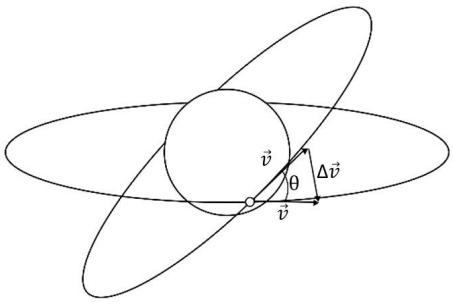

Figure 1.4: Plane change of an initial orbit to another. The orbits are both circular, differing only by their relative angle.

[3] https://www.esa.int/Enabling_Support/Operations/SMART-1

1.3 Optimal Control Theory

It seems logical that, if we want to control a spacecraft, we must know how to control it and also how to do it optimally to minimize costs and transfer time. For this reason, we need to understand some topics related to optimal control theory. This theory aims "to determine the control signals that will cause a process to satisfy the physical constraints and at the same time minimize (or maximize) some performance criterion" [17] and it can be applied in many different fields, such as biology, hydrology, and economics.

In 1696, Bernoulli proposed a challenge that became known as the *Brachystochrone problem* [18]: considering two points A and B in a vertical plane, what is the curve between these two points for which a free-falling body takes the shortest time when acted by the gravitational force? One year later he published his solution, which involves a minimization over a set of curves with some dynamical constraints, marking the emergence of optimal control. Although many well-known names in Mathematics and Physics - in which Euler, Lagrange, Hamilton, among other, are included - have devoted themselves to improve the formalism of optimal control theory, it was Pontryagin around 1956 who gave the biggest contribution to this theory through the formulation of the *Pontryagin's Maximum Principle*.

1.3.1 *Pontryagin's Maximum Principle*

Consider a dynamical system defined by the differential equations

$$\frac{dx_i}{dt} = f_i(\vec{x}(t), \vec{u}(t)), \qquad i = 1, ..., n, \tag{1.17}$$

where $\vec{x}(t) \in \mathbb{R}^n$ and $\vec{u}(t) \in U$ is a set of control parameters in a closed and limited domain $U \in \mathbb{R}^m$. To simplify, it will be used the *bang-bang* control [19], where $\vec{u}(t)$ is a continuous function defined by parts.

We want to find an optimal control $\vec{u}(t)$ and the corresponding path $\vec{x}(t)$ such that the dynamical system defined by (1.17) evolves to $\vec{x_1}$ at a time t_1, according to a given set of initial conditions $\vec{x_0}$, that minimizes or maximizes the functional

$$J = \int_{t_0}^{t_1} f_0(\vec{x}(t), \vec{u}(t))dt, \tag{1.18}$$

where f_0 is a control function. A particular case is the minimum time control, where $f_0 = 1$ and $J = t_1 - t_0$ [20].

Introducing a new variable $x_0 = J$, equations (1.17) and (1.18) can be rewritten as

$$\begin{cases} \frac{dx_0}{dt} = f_0(\vec{x}, \vec{u}) \\ ... \\ \frac{dx_n}{dt} = f_n(\vec{x}, \vec{u}) \end{cases} . \tag{1.19}$$

The initial condition for this new variable is $x_0(t_0) = 0$. From here, the phase space of the system (1.19) has dimension $n + 1$ and we assume that $x = (x_0, ..., x_n)$.

To construct a Hamiltonian system, we define new variables $\lambda_0, \lambda_1, ..., \lambda_n$, which are the conjugated momenta, and new differential equations:

$$\frac{d\lambda_i}{dt} = -\sum_{j=0}^{n} \lambda_j \frac{\partial f_i(\vec{x}, \vec{u})}{\partial x_i}, \qquad i = 0, ..., n. \tag{1.20}$$

Since there are solutions of (1.19) globally in time and since equation (1.20) is linear in λ_i, when a solution $\vec{x}(t)$ and an admissible command $\vec{u}(t)$ are introduced, we can conclude, by the Floquet's theorem [20], that the system of equations (1.20) has a unique solution. Therefore, the Pontryagin's Hamiltonian is

$$\mathbb{H}(\vec{\lambda}, \vec{x}, \vec{u}) = \sum_{j=0}^{n} \lambda_j f_j(\vec{x}, \vec{u}), \tag{1.21}$$

and the Hamilton's canonical equations are

$$\begin{cases} \frac{dx_i}{dt} = \frac{\partial \mathbb{H}}{\partial \lambda_i} = f_i \\ \frac{d\lambda_i}{dt} = -\frac{\partial \mathbb{H}}{\partial x_i} = -\sum_{j=0}^{n} \lambda_j \frac{\partial f_i}{\partial x_i} \end{cases}, \tag{1.22}$$

where $i = 0, ..., n$. The set of equations (1.22) is the combination of (1.20) and (1.21). The Hamiltonian (1.21) has dimension $2n + 1$.

If system of equations (1.19) has a solution for $u(t) \in U$ commands, we can solve equations (1.20) and obtain the Hamiltonian (1.21). Thus, the Hamiltonian $\mathbb{H}$ is parameterized by $u(t)$ and we define a new function

$$M(\vec{\lambda}, \vec{x}) = \sup_{u \in U} \mathbb{H}(\vec{\lambda}, \vec{x}, \vec{u}). \tag{1.23}$$

Pontryagin's Maximum Principle states that, in order to a control $u(t)$ to be optimal, there must be functions $\lambda_0(t), ..., \lambda_n(t)$ such that: a) the function $\mathbb{H}(\vec{\lambda}, \vec{x}, \vec{u})$ has a maximum at the point $u(t)$, i.e., $\mathbb{H}(\vec{\lambda}, \vec{x}, \vec{u}) = M(\vec{\lambda}, \vec{x})$ and b) at the final time $t = t_1$, $\lambda_0(t_1) \leq 0$ and $M\left(\lambda(t_1), x(t_1)\right) = 0$.

When the equations (1.22) are easy to solve, the control is determined by eliminating the time variable from these equations. When that is not possible, we have to resort to other techniques, such as control of the conservation laws [20]. In Chapter 5, we will apply this control type to the Kepler problem, simultaneously controlling the energy and the angular momentum vector of a satellite.

1.4 The trajectory optimization problem associated with the low-thrust propulsion systems

The trajectory optimization problem associated with low-thrust propulsion system has been studied for many decades in the context of a variety of missions. As a rule, the criteria for optimizing trajectories are based on decreasing the time or on the expense of the propellant of a transfer and requires the solution of an ideal control problem that consists of applying variational calculation methods. The first studies in the field appeared around 1960 ([21, 22] as examples). Edelbaum became known for deriving

an analytic expression for the maximum inclination between two circular orbits with a constant acceleration and fixed transfer time [23]. In the same paper, he also derived an analytic expression for the total speed variation necessary to perform transfers between certain inclined circular orbits. After almost more than ten years, Flandro continued Edelbaum's work for transfers between elliptic orbits [24].

Already in the 70s, Brusch and Vincent found multiple transfers between specific initial and final orbits, for both optimal and non-optimal transfer trajectories [25].

In his master thesis in 1982, Alfano used two timescales, one faster and one slower, to determine small changes in orbital elements for a single (high-thrust) and many (low-thrust) revolutions, respectively [26]. Three years later, Wiesel and Alfano separated these timescales into two problems and recapitulated Edelbaum's solution over one orbit for the "fast" time scale. They also managed for the first time the application of optimal control principles to the "slow" timescale problem over the entire transfer [27].

In 1983, Redding and Breakwell analyzed impulsive and near-impulsive transfers between circular orbits for prediction of the initial conditions for low-thrust transfers [28]. To do this, they resorted to Lawden's "primer vector" theory [29], which provides us with information about the direction of the spacecraft impulse and exact and optimal solutions for the transfers (Chapter 2 of [30]).

Four years later, Hargraves and Paris [31] used direct methods for trajectory optimization converting the optimal control problem into a nonlinear control problem. In their PhD thesis, Spencer [32], in 1994, and Herman [33], one year later, gave more information on this work and, in the 2000s, they met and wrote a paper on trajectory optimization techniques based upon higher-order collocation for Earth-orbit transfer problems [34]. The range of thrust accelerations used was from approximately 1 to 10^{-3} g.

In 1991, Stewart and Melton presented a multi-variable perturbation solution using a fixed steering law and found a relatively low error when compared with the numerical solution [35]. Also around that time, Bauer found a near-optimal, low-thrust spiral transfer, where the eccentricity remains near zero during all the transfer [36]. Two years later, Alfano and Thorne considered optimal control formulation with polar coordinates for analyzing coplanar circular transfers [37]. However, in the 90s, Kechichian was probably the one who published more articles in this field: he developed a set of studies for low-thrust transfers from circular or near circular orbits and even reformulated Edelbaum's theory for low-thrust transfers but now using Optimal Control Theory [38, 39, 40, 41, 42].

At the turn of the XXI century, studies about low-thrust trajectories optimization continued to be developed: Marasch and Hall divided the optimization problem into a set of optimal control subproblems solved with an indirect optimization technique and with polar coordinates, which simplifies the analysis of planar and circular trajectories [43]; Ferrier and Epenoy used a dynamical model based on equinoctial elements in which they applied Pontryagin's minimum principle [44] and Caillau and Noailles studied the minimum time of a coplanar transfer of a satellite around the Earth starting from a low and very eccentric initial orbit until reaching a geostationary terminal one [45]. The maximum thrust available was about 0.3N. A study about the same problem appeared some years later but now intending to maximize the final mass, or of minimizing the consumption [46, 47].

Colasurdo and Casalino, in 2004, took Edelbaum's formalism again and extended it to the quasi-

circular approximation for the spacecraft trajectory [48] and a more accurate extension of the same subject was pursued by Kluever in 2011 [49].

At the 2005 IEEE Aerospace Conference emerged a paper about designed algorithms for low-thrust orbit transfers between two orbits using the Q-law [50].

To prove the complexity and the diversity of orbital maneuvers, it was created in 2006 the Global Trajectory Optimization Competition (GTOC)[4], which is already in its 10^{th} edition. This event gathers "the best aerospace engineers and mathematicians worldwide challenge themselves to solve a “nearly-impossible” problem of interplanetary trajectory design". World-renowned institutions participated in this competition, such as ESA Concepts Team, Moscow State University and NASA's Jet Propulsion Laboratory (JPL). The last one already won three first places since the first edition. In March 2016 a paper was released based on the techniques reported in past GTOC editions, where low-thrust missions neglecting effects of a third body gravitational attraction were the main focus [51].

In 2015 at the Université Nice Sophia Antipol, Helen Clare Henninger, a master student, studied satellite transfers under the influence of two massive bodies (Earth-Moon system) in the case of low-thrust propulsion [52]. Also in this year, a group of Italian researchers presented a selection of possible electric propulsion systems for small satellites based on several requirements [53].

Another relevant contribution to this field is an article published in 2017 in which some numerical methods based on aerospace problems are discussed and compared [54]. These results may help us to choose the best method for each simulation in this thesis.

The most important reference for our work is a master dissertation of an Engineering Physics student from Instituto Superior Técnico in 2017 [1]. In line with what we are going to study, Mariana Fernandes considered transfers between Keplerian orbits in the same plane through the variation of the constants of motion of the Kepler problem during the entire transfer. To perform the simulations, she used the software *Mathematica*.

In a 2018 paper, we can read about a new dynamic model of a thrusting spacecraft used for computing low-thrust orbit-raising trajectories to the geosynchronous equatorial orbit [55]. To demonstrate that, some numerical examples corresponding to planar and non-planar orbit-raising scenarios were presented.

In a private communication to Professor Rui Dilão in 2019, we had access to a paper draft written by Matthew Swenson and João Fonseca, where they studied a novel method of 2D orbital transfers defining an eccentricity manifold and using direct collocation over angular momentum and energy space [56]. This method is valid for closed and open orbits.

Regarding published books related to Optimal Control, the first was published in 1963 by Derek Lawden [29]. Sixteen years later it was Jean-Pierre Marec's turn with *Optimal Space Trajectories* [57]. More recently, in 2010, *Spacecraft Trajectory Optimization* by Bruce A. Conway came up with a "collection variety of both analytical and numerical approaches to trajectory optimization" [30]. Besides, two more recent contributions of orbits determination and treatment also deserve to be mentioned: the books by W. E. Wiesel *Modern Orbit Determination* (2003, second edition 2010) [58] and *Modern Astrodynamics*

[4] `https://sophia.estec.esa.int/gtoc_portal/`

(2003, second edition 2010) [59].

Nowadays and after almost 70 years, the trajectory optimization problem is a subject still studied by the scientific community and many techniques using different methods have been implemented and demonstrate efficient trajectories for most types of problems. Some examples of these techniques use homotopy [47], shooting methods [50] and collocation methods coupled with linear programming [34].

In this master thesis, we use another numerical integration method, which is 4^{th} order Runge-Kutta, an iterative method to numerically solve ordinary differential equations that conserve energy and angular momentum [60].

1.5 Objectives

The goal of our project is to design new strategies for orbit transfers of satellites between two-dimensional two-body Keplerian orbits, starting at any instant or point in the orbit, based on different optimization criteria. This will be done by controlling the constants of motion of the Kepler problem, which are the angular momentum vector $\vec{L}$, the energy E and the Laplace-Runge-Lenz (LRL) vector $\vec{A}$. The latter gives us the orientation and shape of the orbits. Notice that, during the transfer the orbit is non-Keplerian and the constants of motion stop being invariant. Using this, we will control the low-thrust propulsion system of the spacecraft in which the intensity and direction of the gases expelled by the thrusters are chosen and the final Keplerian orbit is reached.

We present three different types of transfers: i) with constant angular momentum, ii) with constant effective energy and iii) with both variable angular momentum and effective energy. We also study a particular case: transfers between circular orbits. The third constant of motion (Laplace-Runge-Lenz vector) is used to rotate the final orbit so that it is in the same orientation as that of the initial orbit.

1.6 Thesis outline

We start Chapter 2 with the 2-dimensional equations of motion of the variable mass Kepler problem, where we present all the mathematical formalism behind this problem.

In Chapters 3 and 4, we study transfers with constant angular momentum and with constant effective energy, respectively.

After that, in Chapter 5 we proceed with two methods to obtain transfers with both variable angular momentum and effective energy: the simplest method is described in Section 5.1, the most efficient in Section 5.2 and we compare these two methods in Section 5.3.

In Chapter 6, we combine the previous types of transfers to implement a transfer between two circular orbits, and, finally, in Chapter 7 we present a method to rotate the orientation of the final orbit to match the initial using the Laplace-Runge-Lenz vector.

In Chapter 8, we discuss the obtained results and present some ideas for future work.

In Appendix A, we present the mathematical formalism used in Chapter 3 when approaching circular orbits.

Chapter 2

Control of the Kepler problem with varying mass

We start this work by presenting the mathematical formalism for the two-dimensional variable mass Kepler problem. We derive the equations of motion for a Keplerian orbit as well as the constants of motion of this problem, that cease to be invariant when the transfer begins. At the end of the chapter, we also derive the expression for the energy cost of a transfer.

2.1 Mathematical Formalism

The spacecraft or satellite motion is approximated by that of a variable mass point, subject to the gravitational attraction of one primary massive body (the center of gravitational force) with mass M. We consider that the motion is described in a two-dimensional configuration space with coordinates $(x, y) \in \mathbb{R}^2$. As we saw in Section 1.1, the satellite has mass m and it has its own propulsion system which, when turned on, causes spacecraft to lose mass and gain speed. Therefore, the equation of motion is given by

$$m\frac{d^2\vec{r}}{dt^2} - \frac{dm}{dt}\vec{u}_{rel} = -\frac{GmM}{r^3}\vec{r}, \tag{2.1}$$

where $\vec{r} = (x, y) \in \mathbb{R}^2$, G is the universal gravitational constant ($G = 6.67408 \times 10^{-11} m^3 kg^{-1} s^{-2}$) and $\vec{u}_{rel} = (u_x, u_y)$ is the velocity of the mass lost by the satellite measured in its referential frame. If we assume a satellite with a large mass compared to the mass lost by the propulsion system we make the approximation

$$\frac{1}{m}\frac{dm}{dt} = \gamma, \tag{2.2}$$

where $\gamma < 0$ is a constant. Replacing this equation into (2.1) and rewriting it in its two components:

$$\begin{cases} \ddot{x} = -\mu\frac{x}{r^3} + \gamma u_x(t) \\ \ddot{y} = -\mu\frac{y}{r^3} + \gamma u_y(t) \end{cases}, \tag{2.3}$$

where $\mu = GM$[1] and $\gamma\vec{u}_{rel} = (\gamma u_x(t), \gamma u_y(t))$. So, we eliminate the satellite mass present in equation (2.1). Initially, the propulsion system is off, $\vec{u}_{rel} = 0$, but when it is turned on we have that

$$(u_x, u_y) = (u\cos\phi, u\sin\phi)\,, \tag{2.4}$$

where ϕ is the escape angle of the satellite.

The system of equations (2.3) is derived from the time-dependent Lagrangian

$$\mathcal{L} = \frac{1}{2}\left(\dot{x}^2 + \dot{y}^2\right) + \frac{\mu}{r} + \gamma x u_x + \gamma y u_y. \tag{2.5}$$

Using polar coordinates, $(x, y) = (r\cos\theta, r\sin\theta)$, we can rewrite equations (2.3) as:

$$\begin{cases} \ddot{r} = -\frac{\mu}{r^2} + r\dot{\theta}^2 + \gamma u_x\cos\theta + \gamma u_y\sin\theta \\ \frac{d}{dt}L_z = -r\gamma u_x\sin\theta + r\gamma u_y\cos\theta \end{cases}, \tag{2.6}$$

where $L_z = r^2\dot{\theta}$ is the angular momentum of the satellite. Here we admit that the movement of the satellite occurs in the (x, y) plane.

To simplify the parametric dependence of equations (2.6), we introduce new radial and temporal variables $s = \frac{r}{r_0}$ and $\tau = \zeta t$, where r_0 and ζ are constants to be determined below. Then, by equation (2.5), the new Lagrangian becomes

$$\bar{\mathcal{L}} = \zeta^2 r_0^2\left[\frac{1}{2}\left(\dot{s}^2 + s^2\dot{\theta}^2\right) + \frac{\mu}{r_0^3\zeta^2}\frac{1}{s} + \frac{\bar{\gamma}}{r_0}s\left(\bar{u}_x\cos\theta + \bar{u}_y\sin\theta\right)\right], \tag{2.7}$$

where now the dot ($\dot{}$) denotes the derivative with respect to τ, $\gamma = \zeta\bar{\gamma}$ and $u_{x,y} = \zeta\bar{u}_{x,y}$. Choosing $\zeta^2 r_0^2 = 1$ and $\mu/(r_0^3\zeta^2) = 1$, we obtain $\zeta = 1/\mu$ and $r_0 = \mu$. Introducing the definitions of u_x and u_y in equation (2.4), the rescaled radial variable and the control parameter $\epsilon = \bar{\gamma}\bar{u}/r_0 = \mu^3\gamma u$ into equation (2.7), we finally obtain the control equations

$$\begin{cases} \ddot{s} = \frac{L_z^2}{s^3} - \frac{1}{s^2} + \epsilon\cos\left(\theta - \phi\right) \\ \frac{d}{d\tau}L_z = -\epsilon s\sin\left(\theta - \phi\right) \end{cases}. \tag{2.8}$$

The satellite is under control only if $\varepsilon \neq 0\ (< 0)$. Otherwise, equations (2.8) describe the Keplerian trajectory of the satellite in the two-dimensional rescaled configuration space.

Using the Lagrangian and Hamilton's equations we obtain the conserved total energy of the satellite without propulsion control. The Hamiltonian becomes

$$H = \frac{1}{2}\left(\dot{x}^2 + \dot{y}^2\right) - \frac{\mu}{r} = \frac{1}{2}\left(\dot{s}^2 + \frac{L_z^2}{s^2}\right) - \frac{1}{s}. \tag{2.9}$$

[1] Equations (2.3) are valid in the limit $m/M \to 0$. Otherwise, (x, y) are the coordinates of the secondary body relative to the centre of mass of the two-body system with varying mass, and $\mu = \mu(t) = G(M + m(t))$.

When the control is turned on $(\epsilon \neq 0)$, the new Hamiltonian is

$$H = \frac{1}{2}\left(\dot{s}^2 + \frac{L_z^2}{s^2}\right) - \frac{1}{s} - \epsilon s \cos\left(\theta - \phi\right) \tag{2.10}$$

and we can use (2.9) and (2.8) to find:

$$\frac{dH}{d\tau} = \epsilon\left[\dot{s}\cos\left(\theta - \phi\right) - s\dot{\theta}\sin\left(\theta - \phi\right)\right]. \tag{2.11}$$

From here, we conclude that the energy is not conserved.

The third constant of motion is the Laplace-Runge-Lenz (LRL) vector [61]. This vector describes the shape and the orientation of an orbit and is defined mathematically by the formula[2]

$$\vec{A} = \vec{\dot{s}} \times \vec{L} - \frac{\vec{s}}{s}, \tag{2.12}$$

which corresponds to

$$\begin{aligned} \vec{A} &= \left(\dot{\bar{y}}L_z - \frac{\bar{x}}{s}\right)\hat{x} - \left(\dot{\bar{x}}L_z - \frac{\bar{y}}{s}\right)\hat{y} = \\ &= \left[\left(\dot{s}\sin\theta + s\dot{\theta}\cos\theta\right)L_z - \cos\theta\right]\hat{x} - \left[\left(\dot{s}\cos\theta - s\dot{\theta}\sin\theta\right)L_z + \sin\theta\right]\hat{y}, \end{aligned} \tag{2.13}$$

for an orbit on the xy plane, where $\vec{s} = (\bar{x}, \bar{y}) = (x, y)/r_0$ and $\hat{x}$ and $\hat{y}$ are the usual Cartesian versors.

In most transfers, the final orbit has a different orientation than the initial one. Thus, the rotation between the two orbits is another parameter that we intend to analyze and this is done using the LRL vector. In Chapter 7 we find a detailed analysis of the process to obtain orbits with the same orientation.

In this thesis, we only consider transfers between orbits with positive angular momentum ($L_z > 0$). Thus, the trajectories are counterclockwise in the configuration space and clockwise in the phase space. The case $L_z < 0$ can be solved by a different choice (orientation) of the Cartesian reference frame and $L_z = 0$ correspond to collision trajectories.

The energy has a local minimum for the circular orbit, which corresponds to the fixed point $(s^*, \dot{s} = Lz^2, 0)$. This implies that the regions with energies below this minimum value are inaccessible. Therefore, $H \in [H(s^*), +\infty]$. While points with $H < 0$ and $H = 0$ correspond to elliptical and parabolic orbits, respectively, points with $H > 0$ correspond to hyperbolic escape trajectories. In this work, we consider transfers between elliptical, circular (a particular case of elliptical orbits), and hyperbolic orbits.

According to reference [1], there is a critical value for ϵ, $\epsilon_{lim} = -\frac{4}{27}$. If $\epsilon \leq \epsilon_{lim}$, the orbits in phase space are always open, so we consider $\epsilon > \epsilon_{lim}$ and, for the simulations, we choose $\epsilon = -0.1$, just like the one chosen in that reference. As ϵ increases, transfers take longer to be completed.

As a starting point of our project, we test the idea of controlling the trajectory of the transfer by actuating directly on the energy and the angular momentum. We consider transfers between two Keplerian orbits with i) constant angular momentum and variable effective energy, ii) constant effective energy and variable angular momentum, and iii) effective energy and angular momentum both variable.

[2]Note that here we defined this vector per mass unit and now it is dimensionless.

When the desired final orbit is reached, i.e., when both energy and angular momentum are again constant, it is possible to perform a rotation on the LRL vector until it reaches the orientation of the initial orbit. This is discussed in Chapter 7.

Throughout this project, we use the 4^{th} order Runge-Kutta numerical integration method built-in NDSolve of *Mathematica- version 12.2*. In addition, we resort to the **WhenEvent**[*event, action*] [3] command to impose control conditions. This command simplifies the writing and reading of the program since it specifies an action when the event is detected in NDSolve.

2.2 Energy cost (or expenditure) of a transfer

This section is dedicated to the study of the energy cost of a transfer between two Keplerian orbits.

In Orbital Mechanics, the energy cost of a transfer is equal to the work done by the control force. Under these conditions, by equation (2.2), we obtain its expression

$$E_{cost} = \int_0^{\Delta\tau} \frac{dm}{dt}\vec{u}_{rel} \cdot d\vec{r} = \int_0^{\Delta\tau} \gamma m(t)\vec{u}_{rel} \cdot \vec{v}dt. \tag{2.14}$$

Then, by equations (2.3) and (2.4), the energy cost is written as

$$E_{cost} = m(0)\gamma u \int_0^{\Delta\tau} e^{\gamma t}\left(\dot{x}\cos\phi + \dot{y}\sin\phi\right)dt, \tag{2.15}$$

where $\Delta\tau$ is the transfer time and $m(0)$ is the satellite mass at the initial time of the transfer.

Using polar coordinates this expression is rewritten as

$$E_{cost} = m(0)\epsilon \int_0^{\Delta\tau} e^{\gamma t}\left[\dot{s}\cos\left(\theta-\phi\right) - s\dot{\theta}\sin\left(\theta-\phi\right)\right]dt, \tag{2.16}$$

We will not make calculations of this energy expenditure for any transfer simulation since it depends on the initial satellite mass and the gamma parameter. Since the gamma parameter is given by the satellite manufacturer and in our project we are considering a general satellite, we find it unreasonable to calculate the energy cost. However, we think it would be an asset for those who read our work if we deduced this expression for the energy expenditure, equation (2.16).

[3] https://reference.wolfram.com/language/ref/WhenEvent.html

Chapter 3

Transfers with constant angular momentum

In this section, we are going to study transfers between Keplerian orbits with a constant angular moment, but different effective energies. In other words, the satellite is initially in an orbit with a certain angular momentum L_{z0} and a certain effective energy H_0 and we need to transfer it to another orbit with the same angular momentum $L_{zf} = L_{z0}$ but with a different effective energy H_f. Transfers start at time $\tau = 0$, with effective energy H_0, and stop when the final effective energy H_f is reached. These transfers are carried out under very specific control conditions, which are presented below.

3.1 Control choices

Since the angular momentum must be constant throughout the transfers $(dL_z/d\tau = 0)$, by the second equation of (2.8), we must impose that $\sin(\theta - \phi) = 0$ and we obtain two control conditions: $\phi = \theta$ or $\phi = \theta \pm \pi$, i.e., when the propulsion system is turned on $(\epsilon \neq 0)$ its orientation follows one of these conditions. The system of equations (2.8) and equation (2.11) are rewritten as:

$$\begin{cases} \ddot{s} = \frac{L_z^2}{s^3} - \frac{1}{s^2} + \epsilon\sigma \\ \dot{\phi} = \dot{\theta} = \frac{L_z}{s^2} \\ \dot{H} = \epsilon\sigma\dot{s} \end{cases}, \tag{3.1}$$

where $\epsilon = -0.1$ is a fixed value and $\cos(\theta - \phi)$ is replaced by σ, which can take the values -1, 1 or also 0 when the control parameter is off for sake of simplification, according to each imposed condition.

There are two types of transfers: i) $H_f > H_0$ and ii) $H_f < H_0$. To the first case, $dH/d\tau > 0$, from the last equation of (3.1) we have that if $\dot{s} > 0$ implies that $\sigma = -1$ and if $\dot{s} \leq 0$, $\sigma = 1$. However, according to the orbital phase space, these conditions are sufficient only for the first case ($H_f > H_0$). When the effective energy decreases along with the transfer, we must be careful with the orbit geometry. First, we have to calculate the fixed points corresponding to each control parameter $\sigma = 0$ and ± 1. To do that, we

make a variable change in the first equation of (3.1) such that $\dot{s} = y$ and, therefore, the fixed points are given by solving

$$\dot{y} = 0 \Rightarrow \frac{L_z^2}{s^3} - \frac{1}{s^2} + \sigma\epsilon = 0, \tag{3.2}$$

in order to s. Based on Figure 4.3 from reference [20], we classify the fixed points depending on σ value and the results are summarized in Table 3.1.

σ	fixed point	fixed point classification
0	$s_0^* = L_z^2$	stable center type
1	s_1^*	stable and center type center type
-1	s_{-1}^* and s_{-2}^* $(L_z \leq 1.1)$	s_{-1}^*: stable s_{-2}^*: unstable and saddle-type

Table 3.1: Fixed points stability to constant angular momentum transfers depending on the control parameter value.

When $\sigma = 0$ there is one fixed point which coincides with circular orbit with radius $s_0^* = L_z^2$ and, consequently, with the minimum effective energy, $H_0 = H(s_0^*, 0) = -1/(2L_z^2)$. This fixed point is Lyapunov stable and center type. When $\sigma = 1$ equation (3.2) has three solutions but only one is real, s_1^*, and corresponds to a fixed point which is also Lyapunov stable and center type. The case where $\sigma = -1$ is more complicated because it depends on the chosen ϵ and L_z values. In this work, as $\epsilon = -0.1$, there are always three solutions depending on the L_z value:

- if $L_z > L_{zlim} = 1.1033$, only one of the solutions is real but negative, which implies that there are no fixed points;

- if $L_z \leq L_{zlim} = 1.1033$, the three solutions are real but only two are positive and correspond to the fixed points, s_{-1}^* and s_{-2}^*, where $s_{-2}^* > s_{-1}^*$. s_{-1}^* is Lyapunov stable and center type and s_{-2}^* is unstable and saddle type.

In Figure 3.1 we present the phase space trajectories to each σ value, where we choose $L_z = 1$. For the case where $\sigma = -1$ we also choose $L_z = 1.3$ to understand the geometry of the orbits when $L_z < L_{zlim}$ and $L_z > L_{zlim}$.

After studying the phase spaces for each value of the control parameter and verifying that there are no fixed points when $\sigma = -1$ and $L_z > L_{zlim}$, we conclude that using this control value transfers would be limited by a certain angular momentum value: $L_z \leq L_{zlim}$. As we intend to obtain transfers regardless of the final angular momentum value, we have to ignore this control parameter and, through the last equation of system (3.1), make the control choices: $\sigma = 1$ if $\dot{s} > 0$ and $\sigma = 0$ if $\dot{s} \leq 0$. Thus, the control conditions are chosen for the two possible cases of transfers with constant angular momentum and are summarized in Table 3.2.

Despite that, if we look closely at the orbital phase spaces overlapping with $\sigma = 0$ and $\sigma = 1$, we find that in the region between the fixed points there must be a specific choice of the control condition when $H_0 > H_f$. This region is represented in Figure 3.2 and it is problematic when we want the satellite final

orbit to be circular. If we choose a point with $\dot{s} < 0$ and, therefore, $\sigma = 0$, and follow the direction of the arrows, eventually we will arrive at $\dot{s} = 0$. In the next instant, due to the conditions described in Table 3.2, $\dot{s}$ would be positive and, therefore, $\sigma = 1$. However, if we follow the direction of the arrows, this does not happen and we continue with $\dot{s} < 0$. In this region, the solution to this problem is to leave the control off when $\dot{s} = 0$. The satellite will remain in the same orbit (with $\sigma = 0$) and the control will only be switched on again when that orbit intersects another orbit with $\sigma = 1$ and that leads us to the desired effective energy. The intersection between the orbits with $\sigma = 0$ with $\sigma = 1$ occurs when

$$s = s_i = \frac{L_z^2}{2\epsilon s_a^2} - \frac{1}{\epsilon s_a} + \frac{1}{2\epsilon L_z^2} + L_z^2, \tag{3.3}$$

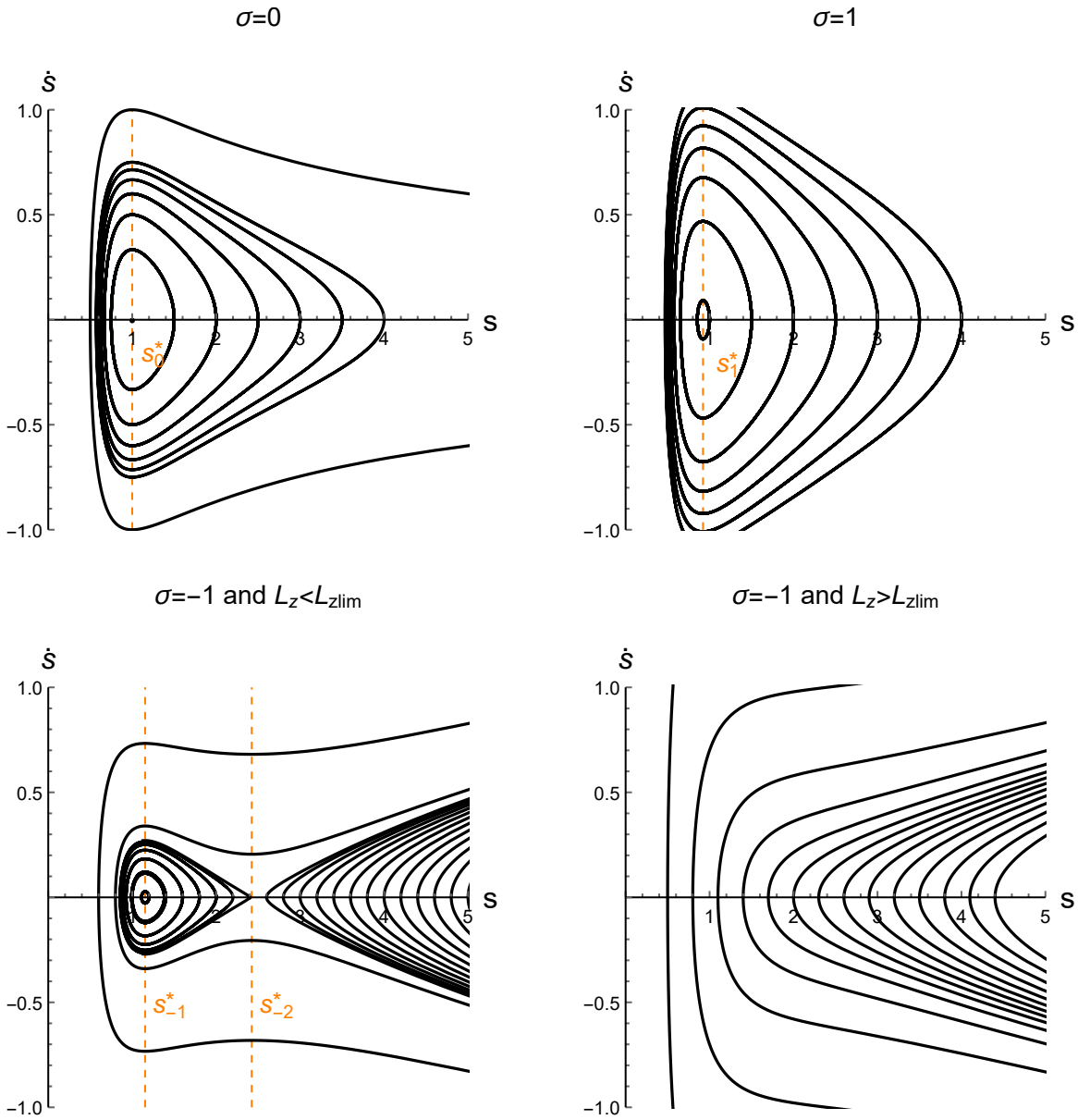

Figure 3.1: Orbital phase space for each σ value with a constant angular momentum $L_z = 1$. In the second figure from the bottom line, we show the phase space for a constant angular moment $L_z = 1.3$, since we observe a difference between the phase spaces for $L_z \leq L_{zlim}$ and $L_z > L_{zlim}$. The dashed vertical orange lines highlight the fixed points positions.

	$\dot{s} \leq 0$	$\dot{s} > 0$
$\dot{H} > 0$	$\sigma = 1$	$\sigma = -1$
$\dot{H} < 0$	$\sigma = 0$	$\sigma = 1$

Table 3.2: Final control conditions for transfers with constant angular momentum.

where s_a is the s value when $\dot{s} = 0$ and σ remains off. All calculations performed until we obtain this expression are described in Appendix A.

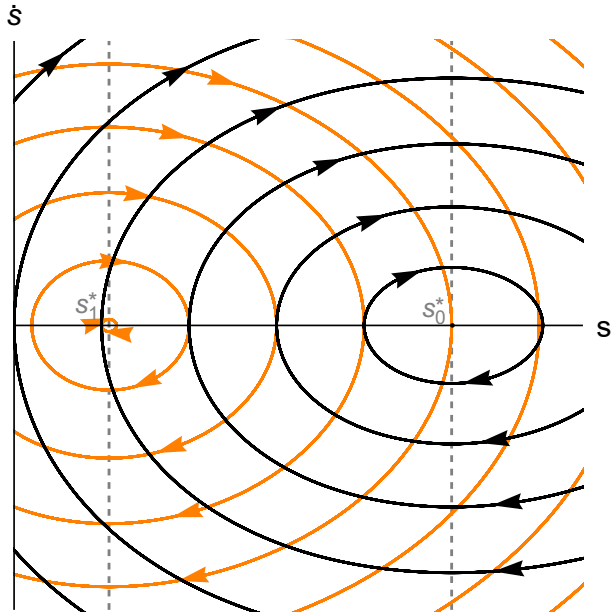

Figure 3.2: Orbital phase space for control parameters $\sigma = 1$ (orange) and $\sigma = 0$ (black) with a constant angular momentum $L_z = 1$. The vertical dashed lines highlight the fixed points positions.

3.2 Simulations

Transfers with constant angular momentum can be circular, elliptical, or hyperbolic. Some examples of transfers involving these conic orbits are summarized in Table 3.3, where $\Delta\tau$ is the dimensionless transfer time.

Let us consider the first example in Table 3.3: a transfer between two elliptical orbits with initial and final effective energies of $H_0 = -0.1972$ and $H_f = -0.25$, respectively. The angular momentum is purposely chosen as $L_z = 1.3 > L_{zlim}$ to prove that with the two controls parameters described in Table 3.2 it is possible to obtain transfers with decreasing effective energy for angular momentum values greater than the limit value that we would have if we used the control parameter $\sigma = -1$. This is the main reason why we start the examples in case ii). This transfer starts at the point $(s_0, \dot{s}_0 = 4, 0)$ with $\theta_0 = 0$ and takes a normalized time transfer $\Delta\tau = 14.8$ (dimensionless) to reach the final effective energy. In the first two plots of Figure 3.3 are represented the phase space and the configuration space of the satellite trajectory. We observe an orientation change between the initial and final orbits but this problem will be solved in Chapter 7 using the Laplace-Runge-Lenz vector. In the graphics of the second line of

case	L_z	orbit geometry	initial conditions	H_f	$\Delta\tau$
ii)	1.3	elliptic to elliptic	$s_0 = 4$ $\dot{s}_0 = 0$ $\theta_0 = 0$ $H_0 = -0.1972$	-0.25	14.8
ii)	0.6	elliptic to elliptic	$s_0 = 1.3$ $\dot{s}_0 = -0.2$ $\theta_0 = \frac{\pi}{2}$ $H_0 = -0.6427$	-0.8	9.8
i)	1.4	circular to hyperbolic	$s_0 = 1.96$ $\dot{s}_0 = 0$ $\theta_0 = \frac{3\pi}{2}$ $H_0 = -0.2551$	0.2	11.7
i)	0.8	hyperbolic to hyperbolic	$s_0 = 0.3022$ $\dot{s}_0 = -0.1$ $\theta_0 = \frac{\pi}{2}$ $H_0 = 0.2$	0.5	2.4
ii)	1	hyperbolic to circular	$s_0 = 0.4589$ $\dot{s}_0 = -0.1$ $\theta_0 = \pi$ $H_0 = 0.2$	-0.5	45.8

Table 3.3: Examples of transfers with constant angular momentum. Note that all quantities are dimensionless, except the polar angle θ_0 which is measured in radians.

this figure, we see the polar angle variation as well as the control choice variation that is made using the data from Table 3.3. In the last line of this figure, we prove that angular momentum remains constant during all the transfer and we conclude that in fact we can obtain transfers without the control parameter $\sigma = -1$ and ensuring that transfers occur regardless of the chosen L_z value. However, until H_f the control parameter remains zero during almost the entire transfer and, consequently, this increases the transfer time. The bright spot is that, by equation (2.16), this problem will not affect the energy cost since when $\sigma = 0$, ϵ is also zero and this will not contribute to the integral of this equation.

The second example in Table 3.3 is a transfer between two elliptical orbits with decreasing effective energy. We choose a constant angular momentum $L_z = 0.6$ and initial and final effective energies $H_0 = 0.6427$ and $H_f = -0.8$, respectively. The transfer starts at $(s_0, \dot{s}_0 = 1.3, -0.2)$ with $\theta_0 = \pi/2$ and is depicted in Figure 3.4. In the first two plots of this figure are represented the phase space trajectory and the configuration space, where we also observe a final orbit orientation change. In the four graphs below that figure, we see the polar angle variation as well as the control choice variation following the data in Table 3.3. As expected, the angular momentum of the orbit remains constant throughout the transfer which takes a normalized time $\Delta\tau = 5.8$ to be completed. Note that, in the last plot, effective energy decreases by step levels. This is due to the fact that we only use $\sigma = 0$ and $\sigma = 1$. In fact, with these control choices, transfers end up being slower but only then do we guarantee that they happen for whatever the angular momentum value.

The last three examples of Table 3.3 are intended to reinforce that this model is also valid when considering open orbits (hyperbolic trajectories), i.e., with $H > 0$.

In Figure 3.5 is depicted a transfer with $L_z = 1.4$ between a circular orbit with $H_0 = -0.2551$ and a

hyperbolic orbit with $H_f = 0.2$. The transfer initial point is $(s_0, \dot{s}_0 = 1.96, 0)$ with $\theta_0 = 3\pi/2$. The control choice parameter follows (central plot on the left of Figure 3.5) the conditions summarized in Table 3.2 in only two steps, so the orbit effective energy increases monotonically until H_f is reached, as can be observed on the last plot of Figure 3.5. The normalized transfer time is $\Delta\tau = 11.7$.

It is also possible to simulate transfers between two hyperbolic orbits. An example of this is shown in Figure 3.6, where the constant angular momentum is $L_z = 0.8$ and the initial and final effective energies are $H_0 = 0.2$ and $H_f = 0.5$, respectively. The transfer start at the point $(s_0, \dot{s}_0 = 0.3022, -0.1)$ with $\theta_0 = \pi/2$. In the first plot of the second line of this figure, the control choice parameter follows the conditions summarized in Table 3.2 in only one step and the orbit effective energy increases monotonically until H_f is reached. The transfer takes a normalized time $\Delta\tau = 2.4$ to be completed.

The last example is the most complex: a transfer simulation between an hyperbolic ($H_0 = 0.2$) and a circular ($H_f = -0.5$) orbits with $L_z = 1$ and this is presented in Figure 3.7. The starting point of the transfer is $(s_0, \dot{s}_0 = 0.4589, -0.1)$ with $\theta_0 = \pi$. In the first two plots, we see the satellite orbital phase space as well as its configuration space. Below these, in the plots of control parameter variation and of effective energy variation, there are levels that correspond to the control being off. Again, it is a consequence of choosing the control parameter indicated in Table 3.2 for the case where the effective energy decreases. Furthermore, for the satellite to reach a final circular orbit, we have to impose a particular condition: when $s_1^* < s < s_0^*$ and $\dot{s} = 0$, we keep the value of s (which we call $s_a = 0.9887$); in the next instant, when $\dot{s} > 0$, we do not turn on the control as it would be supposed and the satellite remains in a Keplerian orbit. The control is only switched on again when s reaches the value indicated by equation (3.3), which corresponds to the intersection with the orbit with $\sigma = 1$, which leads the satellite directly into the circular orbit. The normalized time of this transfer is 45.8.

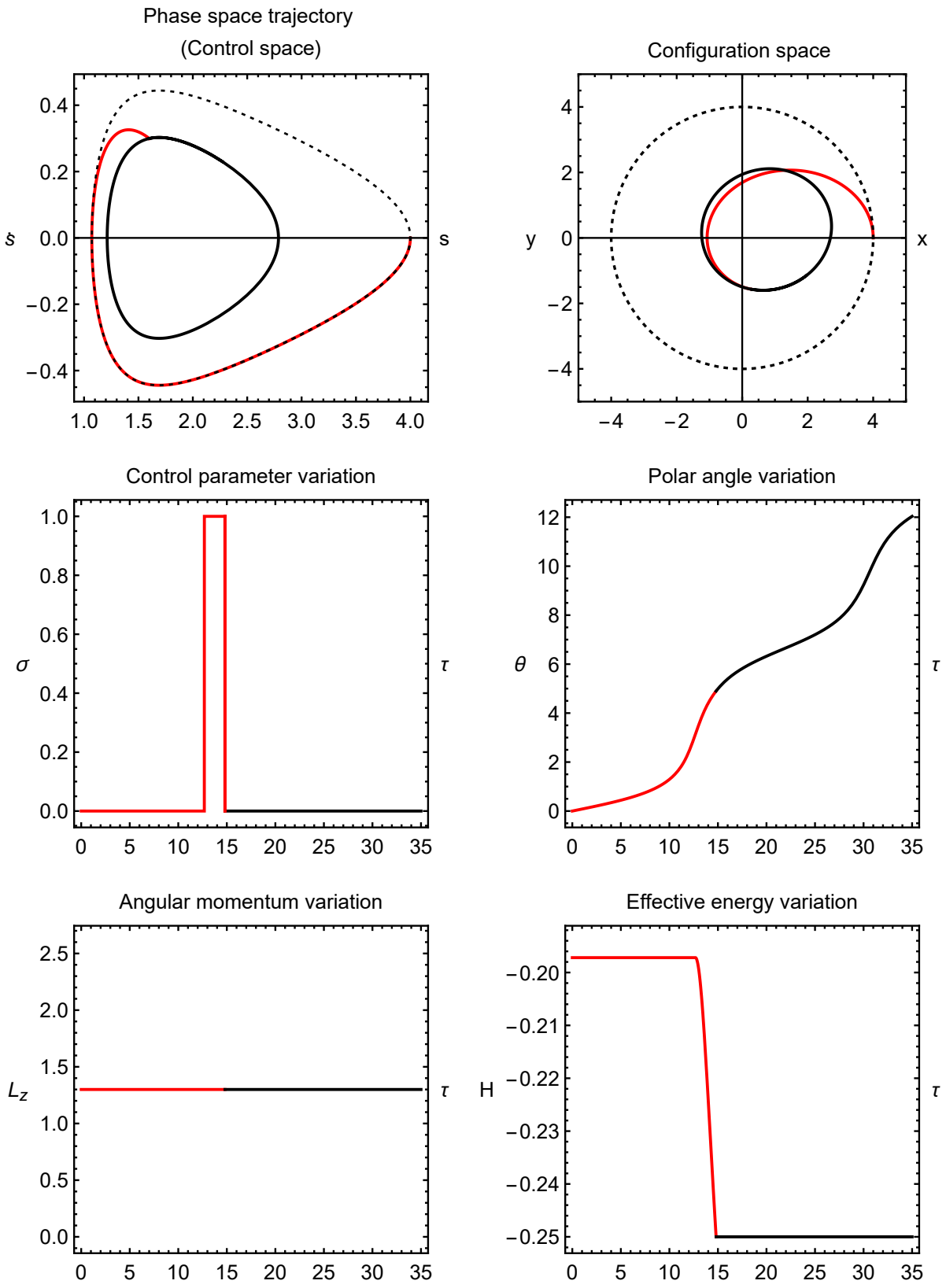

Figure 3.3: Simulation of a transfer with constant angular momentum ($L_z = 1.3$) between two elliptical orbits: the initial with an effective energy ($H_0 = -0.1972$) and the final with ($H_f = -0.25$). The initial orbit is represented by the dashed line, the transfer by the red line and the final orbit by the black one. The transfer starts at the point $(s_0, \dot{s}_0, \theta_0) = (4, 0, 0)$ and takes $\Delta\tau = 14.8$ to be completed.

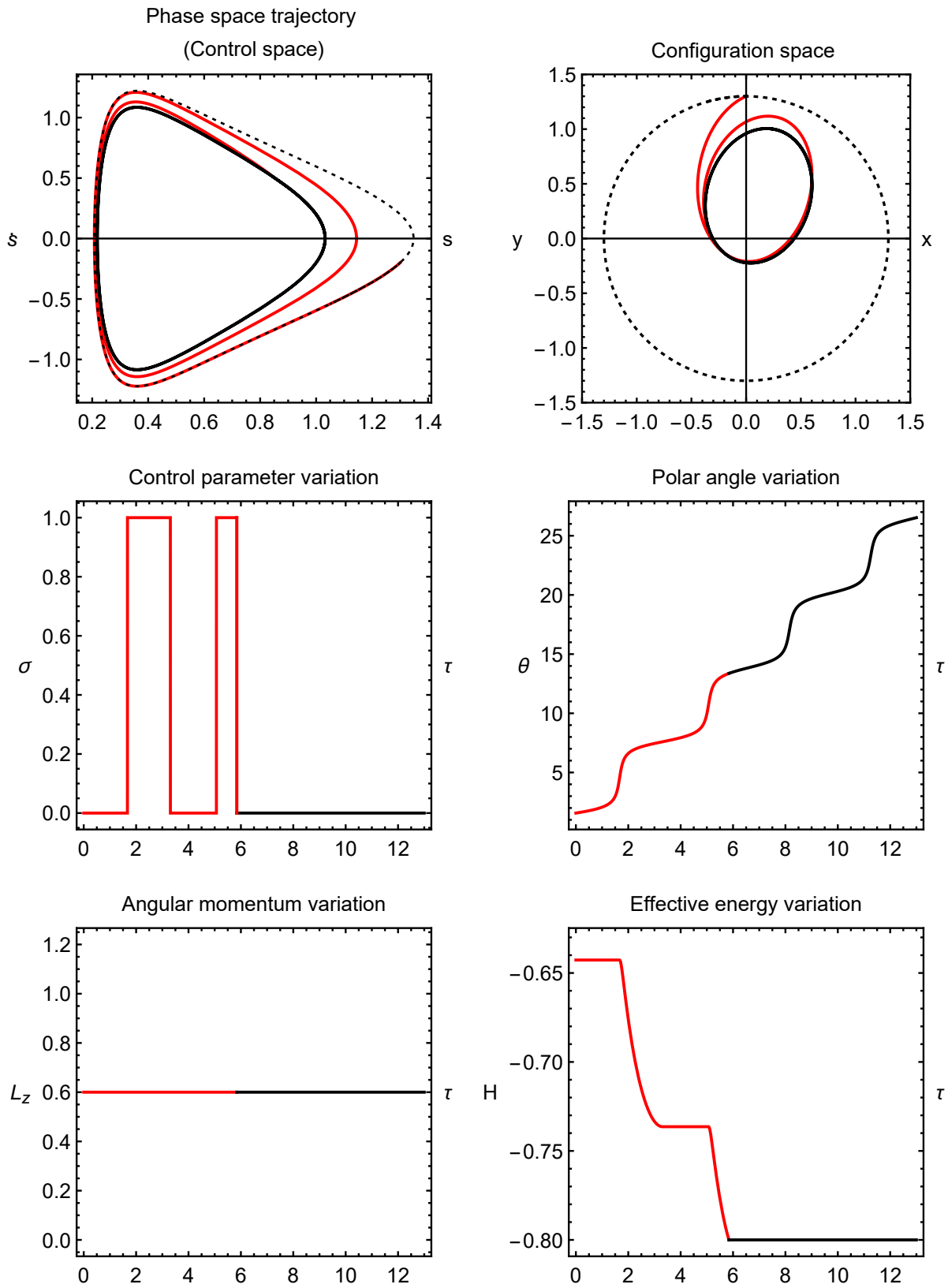

Figure 3.4: Simulation of a transfer with constant angular momentum ($L_z = 0.6$) between two elliptical orbits: the initial with an effective energy ($H_0 = -0.6427$) and the final with ($H_f = -0.8$). The initial orbit is represented by the dashed line, the transfer by the red line and the final orbit by the black one. The transfer starts at the point $(s_0, \dot{s}_0, \theta_0) = (1.3, -0.2, \pi/2)$ and takes a normalized time $\Delta\tau = 9.8$ to be completed.

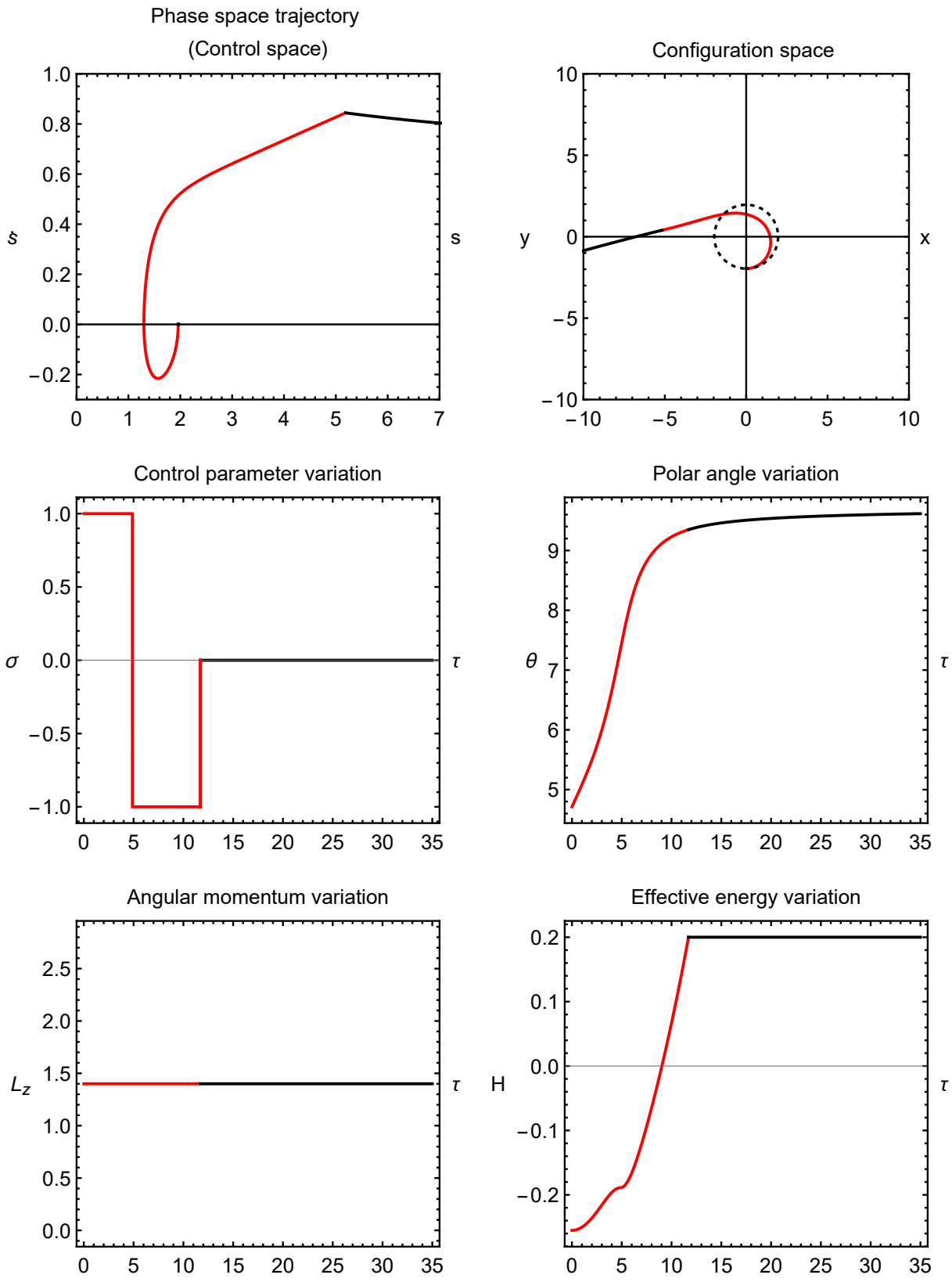

Figure 3.5: Simulation of a transfer with constant angular momentum ($L_z = 1.4$) between circular and hyperbolic orbits: the initial with an effective energy ($H_0 = -0.2551$) and the final with ($H_f = 0.2$). The initial orbit is represented by the dashed line, the transfer by the red line and the final orbit by the black one. The transfer starts at the point $(s_0, \dot{s}_0, \theta_0) = (1.96, 0, 3\pi/2)$ and takes a normalized time $\Delta\tau = 11.7$ to be completed.

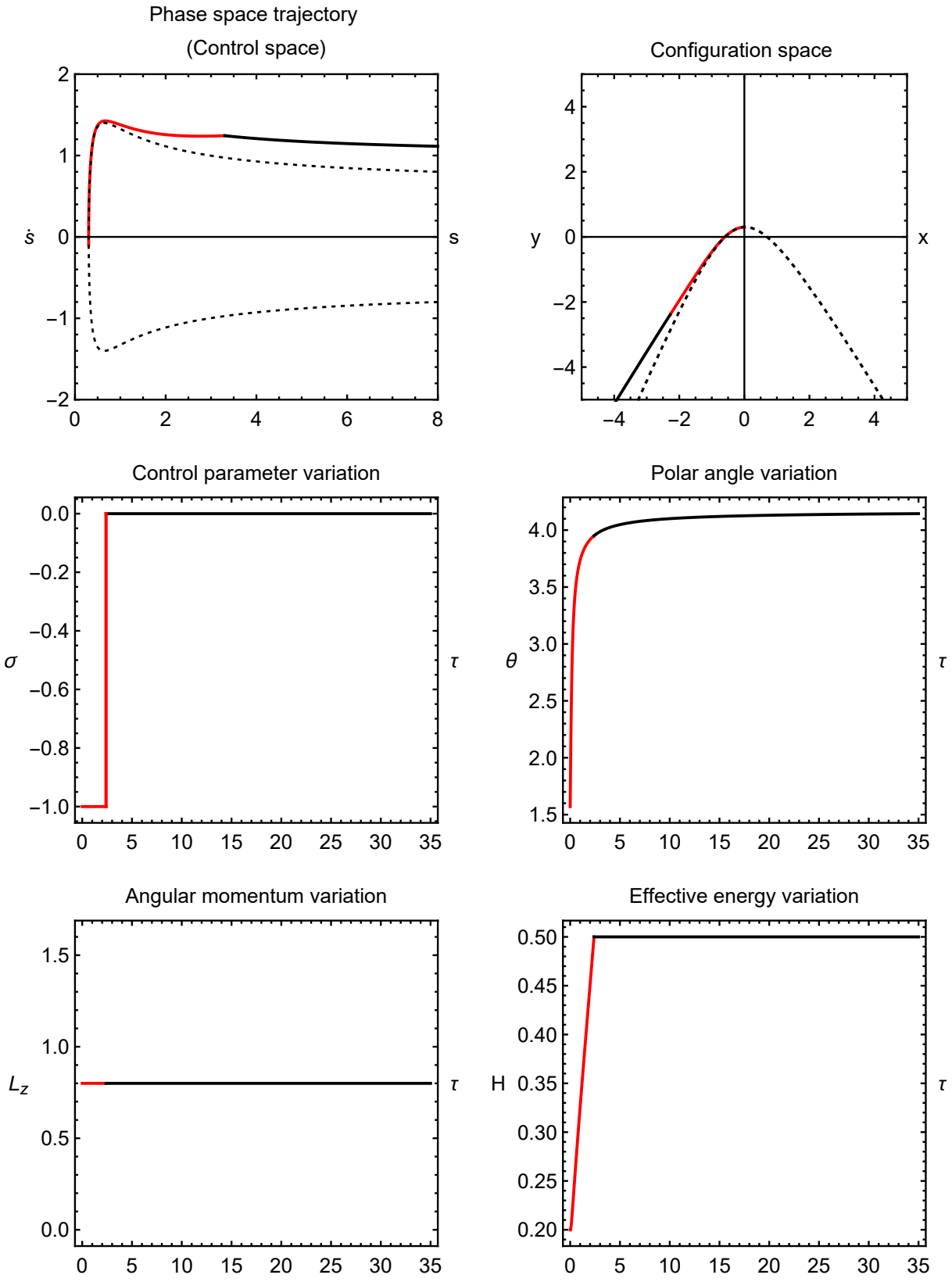

Figure 3.6: Simulation of a transfer with constant angular momentum ($L_z = 0.8$) between two hyperbolic orbits: the initial with an effective energy ($H_0 = 0.2$) and the final with ($H_f = 0.5$). The initial orbit is represented by the dashed line, the transfer by the red line and the final orbit by the black one. The transfer starts at the point $(s_0, \dot{s}_0, \theta_0) = (0.3022, -0.1, \pi/2)$ and takes a normalized time $\Delta\tau = 2.4$ to be completed.

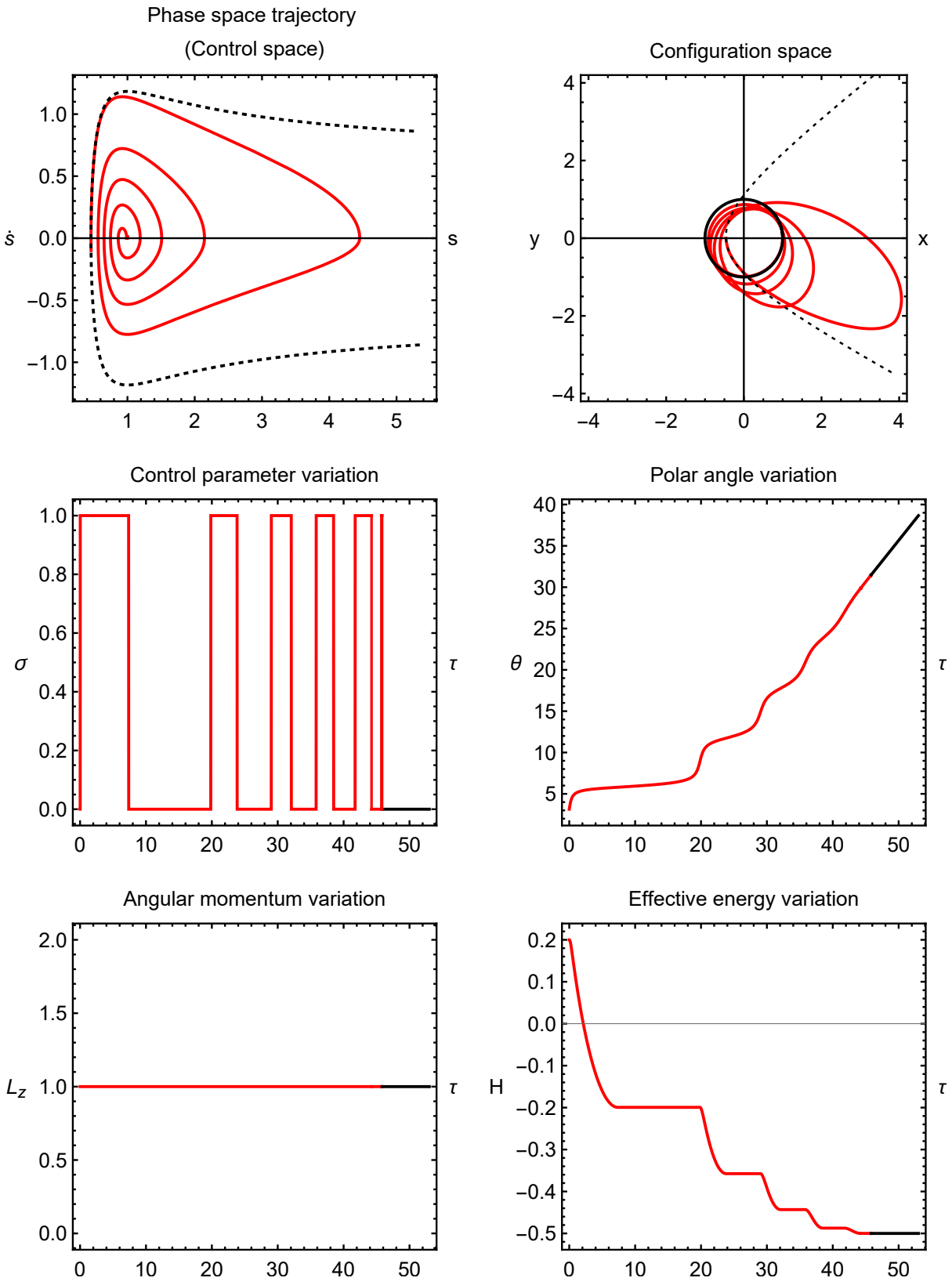

Figure 3.7: Simulation of a transfer with constant angular momentum ($L_z = 1$) between hyperbolic and circular orbits: the initial with an effective energy ($H_0 = 0.2$) and the final with ($H_f = -0.5$). The transfer starts at the point $(s_0, \dot{s}_0) = (0.4589, -0.1)$ with $\theta_0 = \pi$ and its time is 45.8 (dimensionless). The initial orbit is represented by the dashed line, the transfer by the red line and the final orbit by the black one.

Chapter 4

Transfers with constant effective energy

We now consider transfers with constant effective energy, which start at time $\tau = 0$ with angular momentum L_{z0} and stop when the final angular momentum value L_{zf} is reached. We also consider that the initial and final values of angular momentum have the same sign (in this case, the plus sign) so that during a transfer the value of the angular momentum is never zero.

4.1 Control choices

If we equal the equation (2.11) to zero we have the control condition corresponding to energy conservation ($\dot{H} = 0$) which is given by

$$\phi = \theta - \arctan \frac{\dot{s}}{s\dot{\theta}}, \tag{4.1}$$

where $\dot{\theta} = \frac{L_z}{s^2}$. From here, we can obtain the expressions for $\sin(\theta - \phi)$ and $\cos(\theta - \phi)$ which are given by

$$\begin{cases} \sin(\theta - \phi) = \frac{s\dot{s}}{\sqrt{s^2\dot{s}^2 + L_z^2}} \\ \cos(\theta - \phi) = \frac{|L_z|}{\sqrt{s^2\dot{s}^2 + L_z^2}} \end{cases}, \tag{4.2}$$

and rewrite the equations of motion (2.8):

$$\begin{cases} \ddot{s} = \frac{L_z^2}{s^3} - \frac{1}{s^2} + \epsilon\sigma\sigma_c \frac{|L_z|}{\sqrt{L_z^2 + s^2\dot{s}^2}} \\ \frac{d|L_z|}{dt} = -\epsilon\sigma\sigma_c \frac{s^2\dot{s}}{\sqrt{L_z^2 + s^2\dot{s}^2}} \end{cases}, \tag{4.3}$$

where $\sigma_c = 1$ and σ can take the values ± 1 or also 0 when the control parameter is off for sake of simplification, according to each imposed condition.

If $L_{z0} > L_{zf}$, we must have $H \geq -1/(2L_{z0}^2)$, and if $L_{z0} < L_{zf}$, then $H \geq -1/(2L_{zf}^2)$. This will be better understood in Chapter 6. Therefore, we can consider two types of transfers: i) $L_{z0} > L_{zf}$ and

ii) $L_{z0} < L_{zf}$. Similar to transfers of the previous chapter, the case i) has no problems and the control conditions are

$$L_{z0} > L_{zf} : \begin{cases} \text{if } \dot{s} < 0 \wedge L_{z0} > L_{zf} \Rightarrow \sigma = 1 \\ \text{if } \dot{s} \geq 0 \wedge L_{z0} > L_{zf} \Rightarrow \sigma = -1 \\ \text{otherwise } \Rightarrow \sigma = 0 \end{cases} . \tag{4.4}$$

For the ii) case, it is necessary to analyze the geometry of the orbits.

To calculate the fixed points, we have to write the expression of $\ddot{s}$ as a function of H, because we are considering transfers with constant effective energy. To do this, we solve the expression (2.9) in order to L_z^2 and substitute it in the first of equation (4.3):

$$\ddot{s} = -\frac{1}{s^2} + \frac{2Hs^2 + 2s - \dot{s}^2 s^2}{s^3} + \sigma\epsilon \frac{L_z}{\sqrt{L_z^2 + s^2\dot{s}^2}}. \tag{4.5}$$

Then, we do a variable transformation, $\dot{s} = y$, and the fixed points are given by solving

$$\dot{y} = 0 \Rightarrow -\frac{1}{s^2} + \frac{2Hs^2 + 2s}{s^3} + \sigma\epsilon = 0, \tag{4.6}$$

in order to s, where $\dot{s} = 0$, according to each σ value.

When the control parameter is turned off, the fixed point is $(s_0^*, \dot{s}) = (-\frac{1}{2H}, 0)$. When $\sigma = \pm 1$, there are two solutions to each case but only one corresponds to a fixed point, depending on the chosen H value. These fixed points are called s_1^* and s_{-1}^* according to the σ value. All the fixed points are Lyapunov stable of center type [20].

However, to s_{-1}^*, there is a limitation in the effective energy values. If $H^2 < |\epsilon|$, the s^* values are complex and there are no fixed points. Again, similar to what was done in the previous chapter, to overcome this obstacle and since we intend to obtain transfers regardless of the final effective energy value, we ignore the control parameter $\sigma = -1$. Thus, by the last equation of system (4.3), we choose the control conditions: $\sigma = 1$ if $\dot{s} > 0$ and $\sigma = 0$ if $\dot{s} \leq 0$.

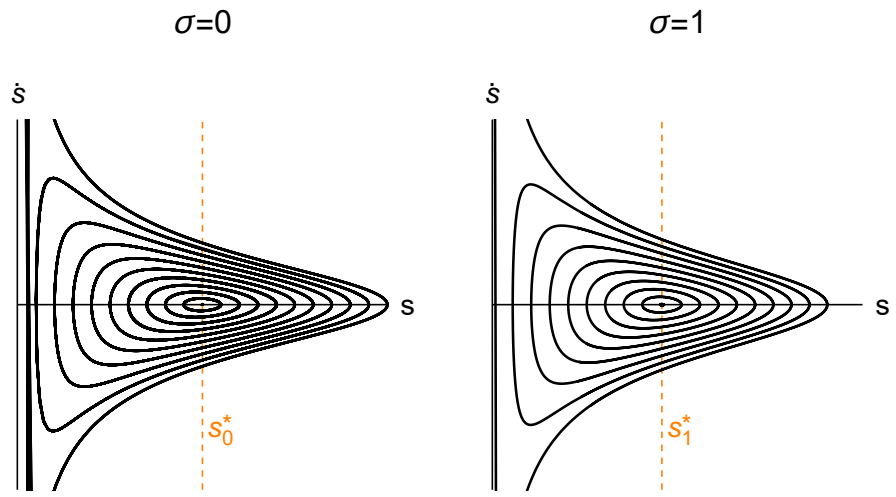

Figure 4.1: Orbital phase space for each σ value with a constant effective energy $H = -0.5$. The dashed vertical orange lines highlight the fixed points positions.

We continue our analysis through the orbital phase space associated with each chosen value of the control parameter. These are represented in Figure 4.1 for a certain effective energy: $H = -0.5$. Once the chosen value is negative the orbits are always closed.

If we overlap the orbital phase spaces with $\sigma = 0$ and $\sigma = 1$, we find a problematic region between the fixed points ($s_1^* \leq s \leq s_0^*$), which prevents us from transferring the satellite to a circular orbit. This region is depicted in Figure 4.2. If we choose a point with $\dot{s} < 0$ and, therefore, $\sigma = 0$, and follow the direction of the arrows, eventually we will arrive at $\dot{s} = 0$. In the next instant, due to the conditions described above, $\dot{s}$ would be positive and, therefore, $\sigma = 1$. However, if we follow the direction of the arrows, this does not happen and we continue with $\dot{s} < 0$.

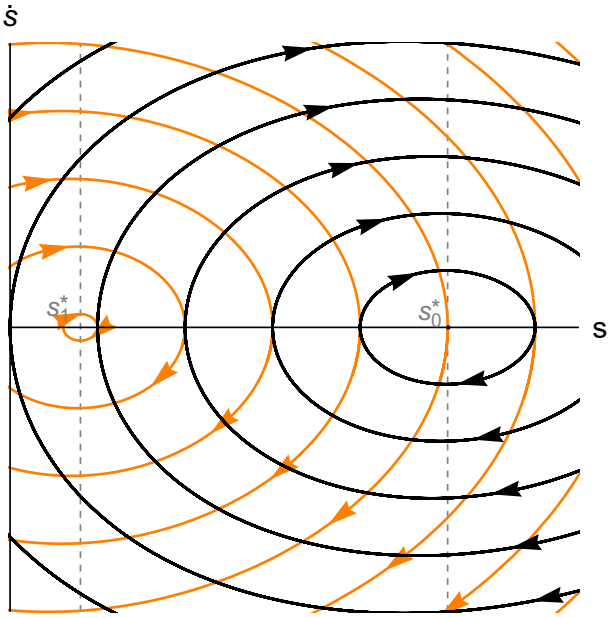

Figure 4.2: Orbital phase space for control parameters $\sigma = 1$ (orange) and $\sigma = 0$ (gray) with a constant effective energy $H = -0.5$. The dashed vertical gray lines highlight the fixed points positions.

Therefore, we have to implement a new strategy for transfers with $H < 0$ and $L_{z0} < L_{zf}$: firstly, we transfer the satellite to an almost circular orbit with constant energy (until $s_1^* \leq s \leq s_0^*$ and $\dot{s} = 0$) and then we make a sequence of three transfers: 1) with increasing energy and constant angular momentum, 2) with constant energy and decreasing angular momentum and 3) with decreasing energy and constant angular momentum. Under these conditions, all the transfers have stable bounded orbits.

So, the control conditions to transfers with $L_{z0} < L_{zf}$ are

$$
\begin{aligned}
H > 0, L_{z0} < L_{zf} : & \begin{cases} \text{if } \dot{s} > 0 \wedge L_{z0} < L_{zf} \Rightarrow \sigma = 1 \\ \text{otherwise } \Rightarrow \sigma = 0 \end{cases} \\
H < 0, L_{z0} < L_{zf} : & \begin{cases} \text{if } \dot{s} > 0 \wedge L_{z0} < L_{zf} \Rightarrow \sigma = 1 \\ \text{if } \dot{s} = 0 \wedge s \in [s_1^*, s_0^*] \wedge L_{z0} < L_{zf} \Rightarrow \sigma_c = 0 \\ \text{otherwise } \Rightarrow \sigma = 0 \end{cases}
\end{aligned}
\tag{4.7}
$$

4.2 Simulations

Such as transfers with constant angular momentum, transfers with constant effective energy can also be circular, elliptical, or hyperbolic and we can find some examples of these transfers in Table 4.1. However, since the effective energy remains constant during all the transfer, the satellite can only be transferred between closed orbits ($H < 0$) or transfers between open orbits ($H > 0$).

In Figure 4.3 we show the result of a transfer simulation between two hyperbolic orbits with a decrease of the angular momentum ($L_{z0} = 0.7969$ and $L_{zf} = 0.2$) and constant effective energy ($H = 0.2$). The main characteristics of this transfer are shown in the first example of Table 4.1. The phase space trajectory and the configuration space are represented in the first two plots in Figure 4.3. At the bottom of this figure, we can see the obtained control parameter variation, the plot of the decreasing angular momentum until it reaches the value of L_{zf} and the plot of the effective energy that remains constant during all the transfer time. The transfer takes a normalized time $\Delta\tau = 3.0$ to be completed.

Now we analyze a transfer between a circular and an elliptical orbits with a decrease of the angular momentum and constant effective energy ($H = -0.5$). The angular momentum of the initial and final orbits are $L_{z0} = 1$ and $L_{zf} = 0.4$, respectively. In Table 4.1 we summarize the initial and final conditions of this transfer as well as the respective transfer time. The simulation transfer is depicted in Figure 4.4. In the first two plots are represented the phase space trajectory and the configuration space, where we can observe a change in orientation between the initial and final orbits. At the bottom of this figure, we can see the control parameter variation obtained, which varies several times until reaching the desired value L_{zf}. Of course that the effective energy remains constant during the $\Delta\tau = 15.0$ of the transfer.

In Figure 4.5, we show a transfer with constant effective energy $H_0 = -0.2$ and $\varepsilon = -0.1$, between Keplerian orbits with angular momenta $L_{z0} = 0.6$ and $L_{zf} = 1$. Since $H \geq -1/(2L_{zf}^2) = -0.5$, the final orbit is accessible. The trajectories in phase and configuration spaces are represented in the first two

case	H	orbit geometry	initial conditions	L_{zf}	$\Delta\tau$
i)	0.2	hyperbolic to hyperbolic	$s_0 = 0.3$ $\dot{s}_0 = 0$ $\theta_0 = 0$ $L_{z0} = 0.7969$	0.2	3.0
i)	-0.5	circular to elliptic	$s_0 = 1$ $\dot{s}_0 = 0$ $\theta_0 = 0$ $L_{z0} = 1$	0.4	15.0
ii)	0.2	elliptic to elliptic	$s_0 = 0.1878$ $\dot{s}_0 = -0.2$ $\theta_0 = \pi$ $L_{z0} = 0.6$	1	2.9
ii)	-0.5	elliptic to circular	$s_0 = 0.4013$ $\dot{s}_0 = -0.1$ $\theta_0 = 0$ $L_{z0} = 0.8$	1	48.8

Table 4.1: Examples of transfers with constant effective energy. All the quantities are dimensionless, except the θ_0 which is measured in radians.

plots. The transfer starts at $(s_0, \dot{s}_0) = (0.1878, -0.2)$ of the initial orbit and with an angle $\theta_0 = \pi$. In the plots below these, we present the control parameter, the polar angle, the angular momentum, and effective energy variations. The control parameter follows the conditions described in equation (4.7) in only one step level with $\sigma = 1$, allowing the angular momentum to increase monotonically until L_{zf} is reached.

In Figure 4.6, we simulate the transfer of a satellite starting in an initial elliptic orbit with angular momentum $L_{z0} = 0.8$ to the circular orbit with radius $s = 1$ and effective energy $H = -0.5$ (angular momentum $L_{zf} = 1$). The initial conditions of the transfer are $(s_0, \dot{s}_0) = (0.4013, -0.1)$, and $\theta_0 = 0$. In this figure are presented trajectories of phase and configuration spaces as well as the control parameter, angular momentum, and effective energy variations. This example is more complex than the others presented because the circular orbit is not directly reachable. We had to implement the strategy defined at the end of Section 4.1. First of all, we transfer the satellite to an almost circular orbit with constant effective energy, and when $s_1^* < s < s_0^*$ and $\dot{s} = 0$ are reached, we start a transfer with increasing effective energy and constant angular momentum (similar to those studied in the previous chapter) until a value relatively close to H is reached, which in this case was $H = -0.4$. When this happens, a transfer with constant effective energy and decreasing angular momentum is started and it ends when L_{zf} is reached. After this, the satellite is transferred with decreasing effective energy and constant angular momentum until the circular orbit by the method described in the last example of Section 3.2. The normalized total time of this transfer is $\Delta\tau = 48.8$.

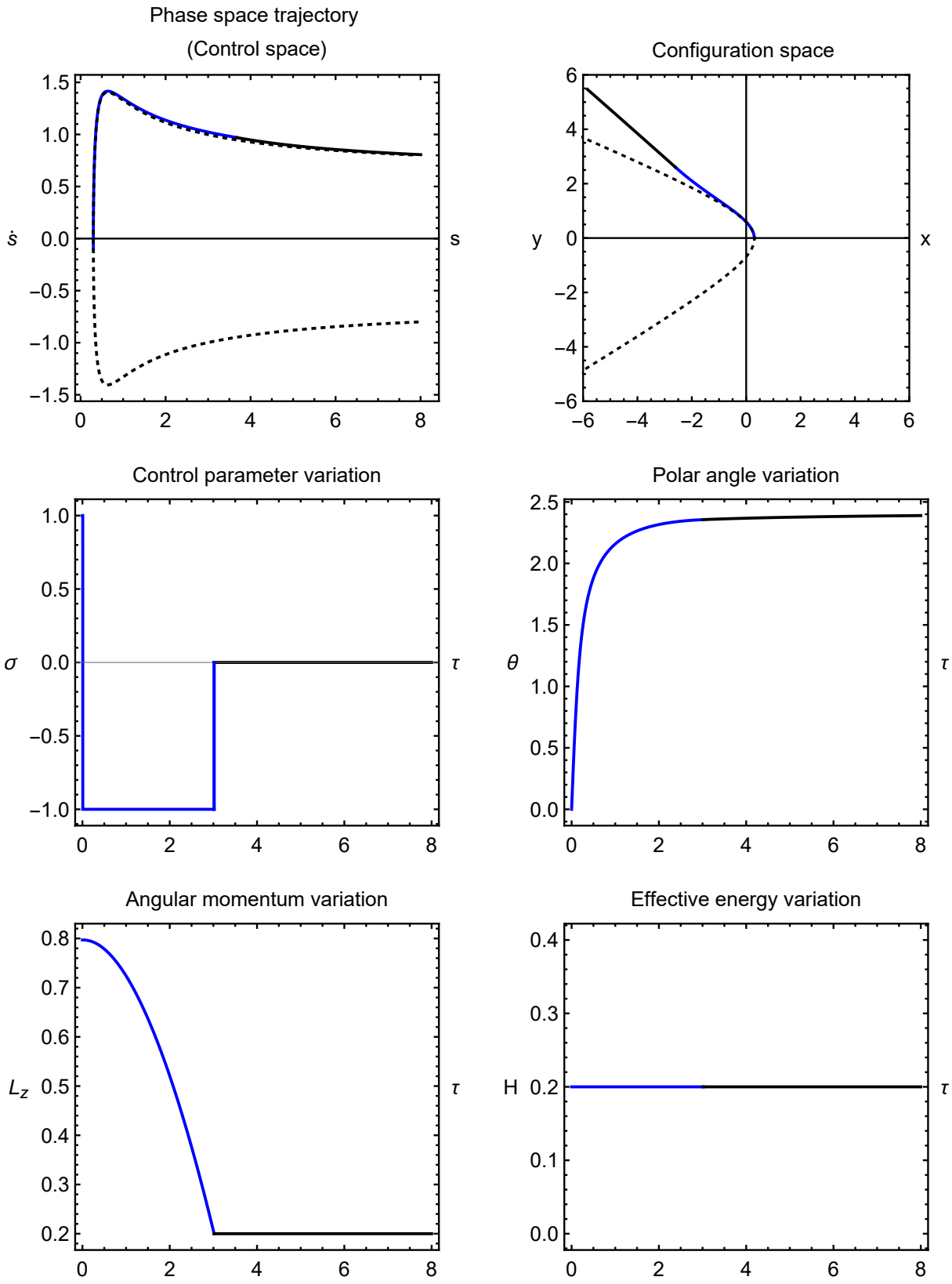

Figure 4.3: Simulation of a transfer with constant effective energy ($H = 0.2$) between two hyperbolic orbits: the initial with an angular momentum ($L_{z0} = 0.7969$) and the final with ($L_{zf} = 0.2$). The initial orbit is represented by the dashed line, the transfer by the blue line and the final orbit by the black one. The transfer starts at the point $(s_0, \dot{s}_0) = (0.3, -0.1)$ with $\theta_0 = 0$. The normalized transfer time is $\Delta\tau = 3.0$.

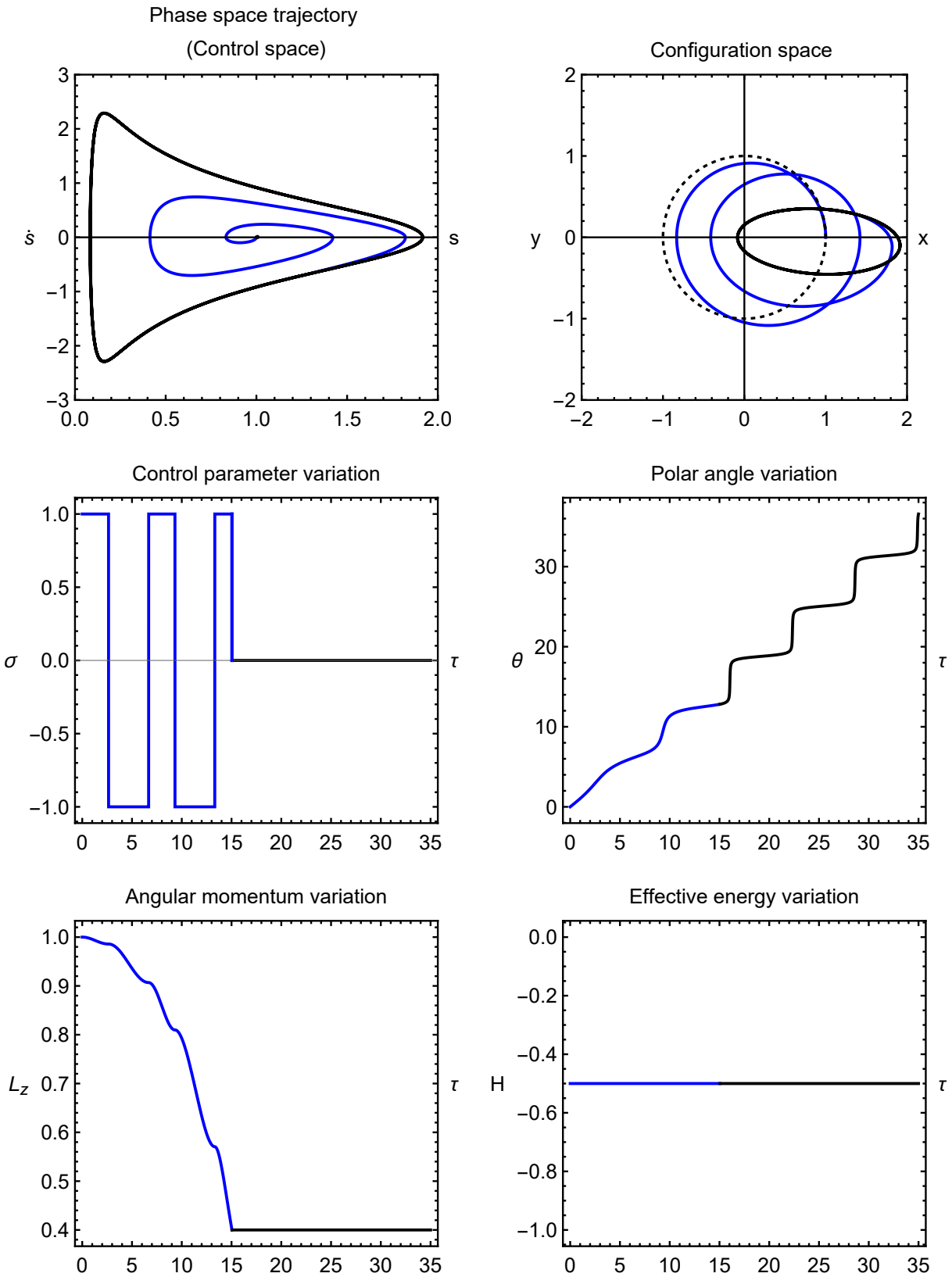

Figure 4.4: Simulation of a transfer with constant effective energy ($H = -0.5$) and between circular and elliptical orbits: the initial with an angular momentum ($L_{z0} = 1$) and the final with ($L_{zf} = 0.4$). The initial orbit is represented by the dashed line, the transfer by the blue line and the final orbit by the black one. The transfer starts at the point $(s_0, \dot{s}_0) = (1, 0)$ with $\theta_0 = 0$. The normalized transfer time is 15.0.

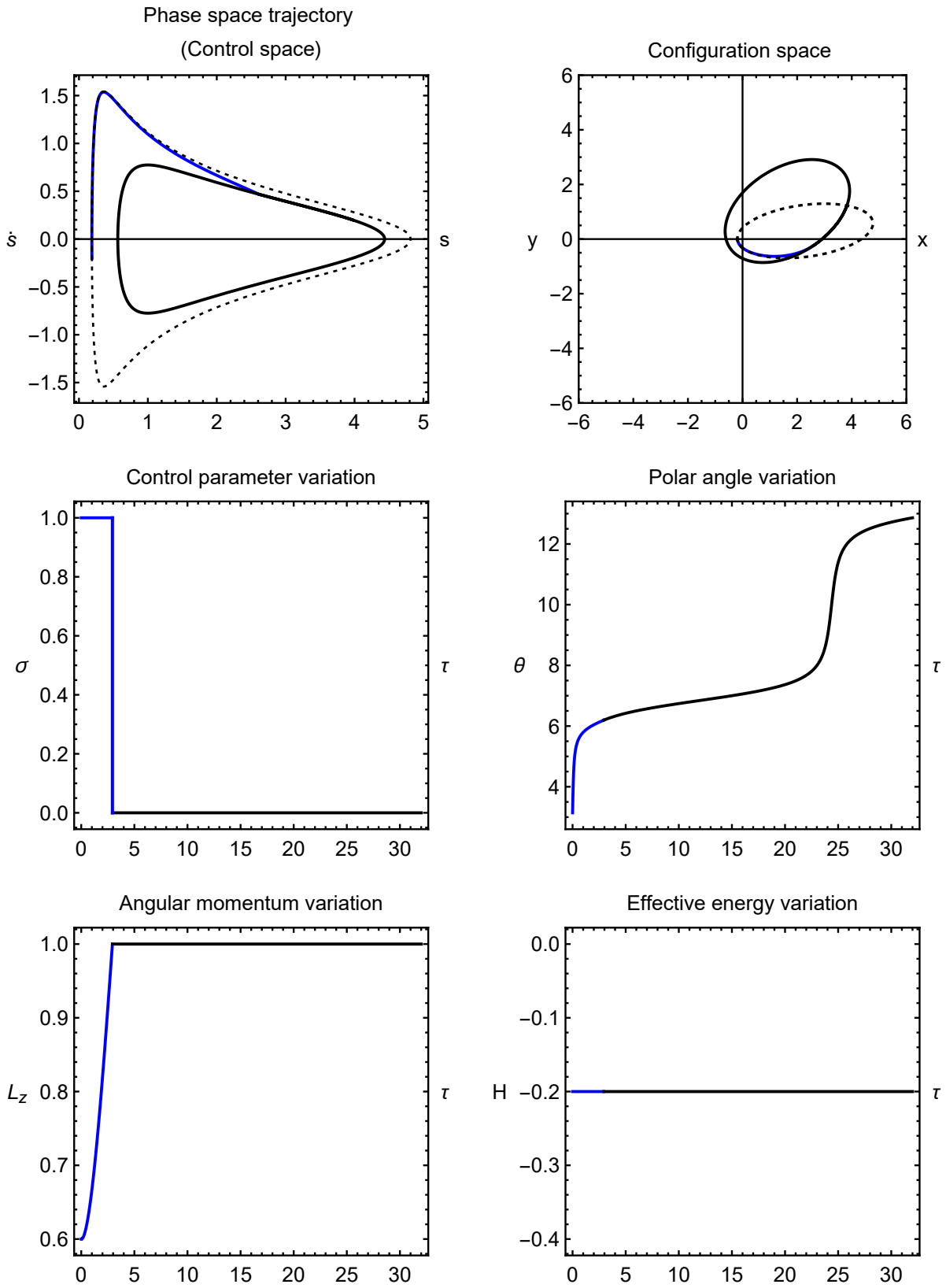

Figure 4.5: Simulation of a transfer with constant effective energy ($H = -0.2$) and between two elliptical orbits: the initial with an effective energy ($L_{z0} = 0.6$) and the final with ($L_{zf} = 1$). The initial orbit is represented by the dashed line, the transfer by the blue line and the final orbit by the black one. The transfer starts at the point $(s_0, \dot{s}_0) = (0.1878, 0.2)$ with $\theta_0 = \pi$. The normalized transfer time is 2.9.

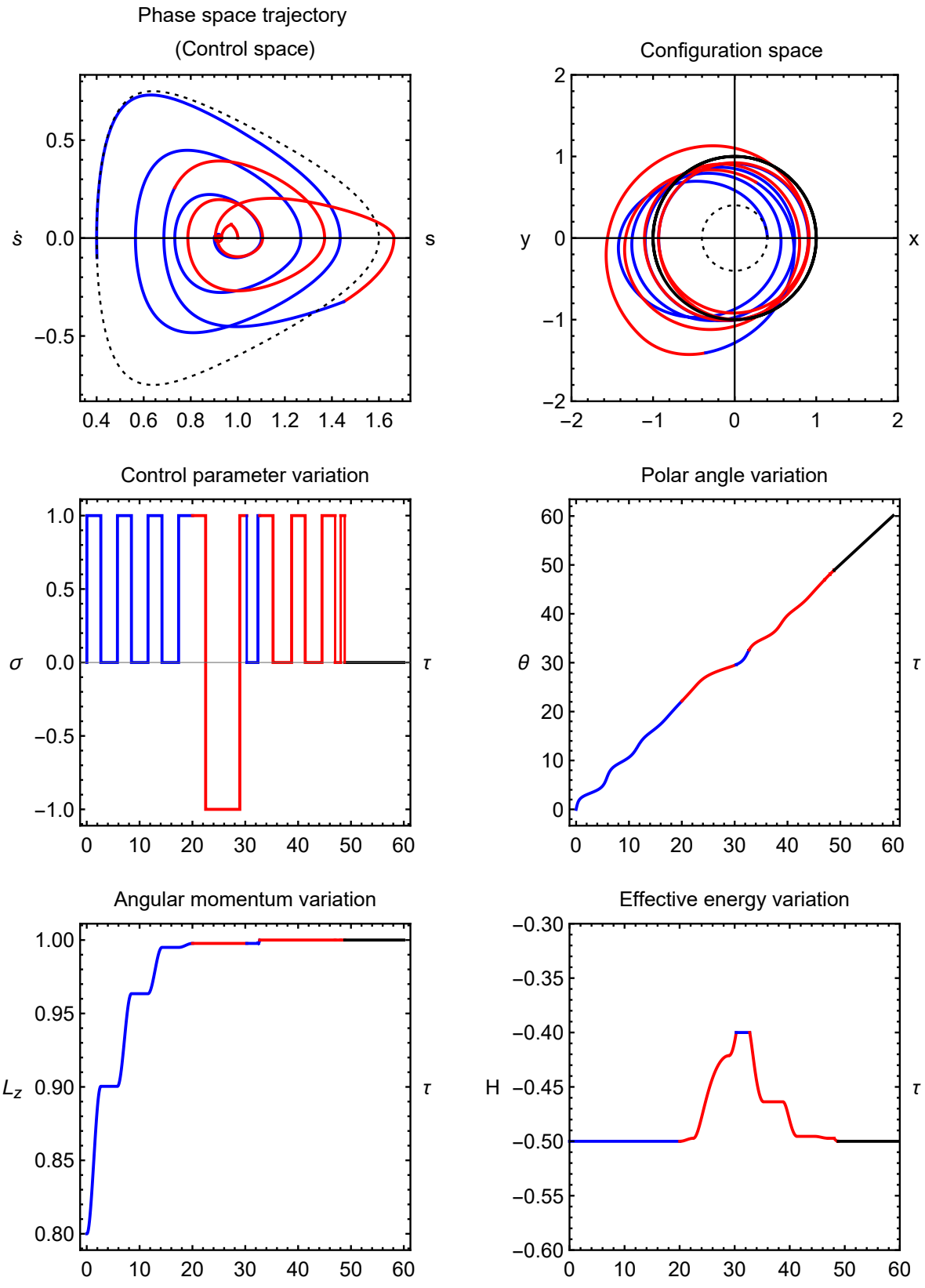

Figure 4.6: Simulation of a transfer between elliptic and circular Keplerian orbits with $H = -0.5$. The initial and final angular momenta are $L_{z0} = 0.8$ and $L_{zf} = 1$, respectively. The transfer starts at the point $(s_0, \dot{s}_0) = (0.4013, -0.1)$ and $\theta_0 = 0$. The initial orbit is represented by the dashed line, constant effective energy transfers by blue lines, constant angular momentum transfers by red lines and the final orbit by the black line. The normalized transfer time is $\Delta\tau = 48.8$.

Chapter 5

Transfers with both variable angular momentum and effective energy

Now we consider transfers with both variable angular momentum and effective energy. We want to make a transfer between an orbit with L_{z0} and H_0 and another with L_{zf} and H_f. Thus, we can have four cases: i) $H_0 < H_f$ and $L_0 < L_f$, ii) $H_0 > H_f$ and $L_0 < L_f$, iii) $H_0 < H_f$ and $L_0 > L_f$ and iv) $H_0 > H_f$ and $L_0 > L_f$.

There are two different ways to obtain these transfers. The first consists of grouping transfers with constant effective energy with transfers with constant angular momentum exactly as described in the previous chapters; the second is obtained through conservation laws. These two methods are explained in detail in Sections 5.1 and 5.2.

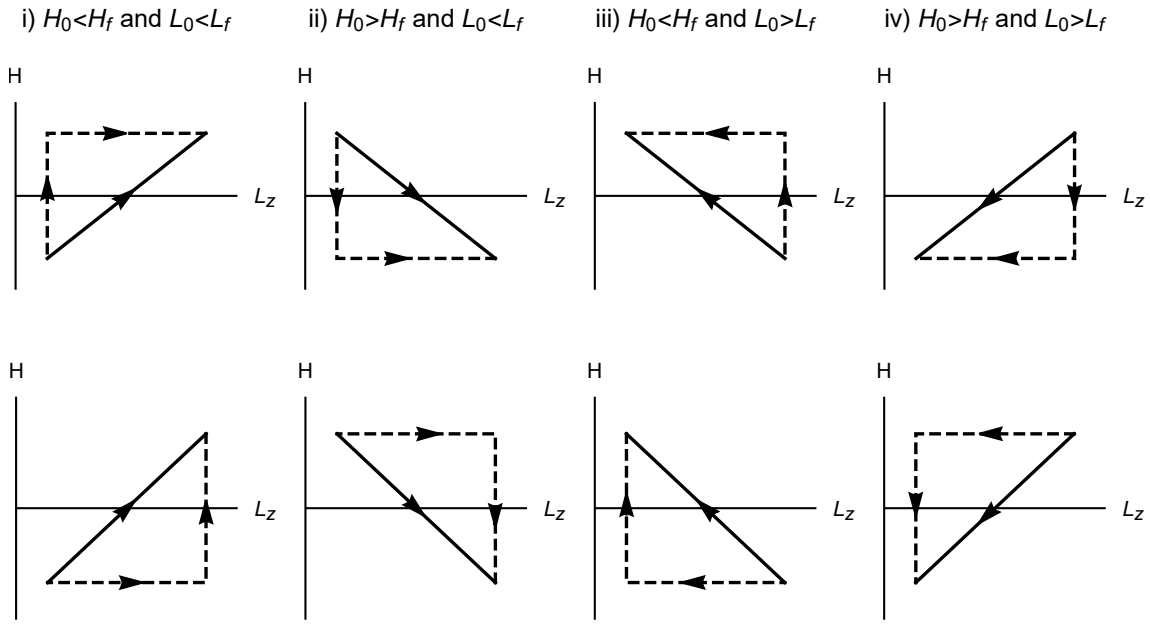

Figure 5.1: Scheme to better understand the order of transfers with effective energy and angular momentum both variable.

5.1 First case of transfers with both variable H and L_z

For the first case, we combine transfers with constant angular momentum and transfers with constant effective energy. Therefore, for each one of the four cases mentioned above, we can have two ways of making this, which is schematically represented in Figure 5.1:

a) making a transfer with constant L_z followed by a transfer with constant H (top);

b) making a transfer with constant H followed by a transfer with constant L_z (bottom).

Simulations

Using the control conditions mentioned above, we obtained some simulation transfers between circular, elliptical, and hyperbolic orbits to each one of the four possible cases - i) to iv) - and with the two possible transfer combinations - a) and b). These results are summarized in Table 5.1.

Note cases i) and iv), where both angular momentum and effective energy increase or decrease, and when the transfer involves a circular orbit, there only is a way to implement the transfer. When $H_0 < H_f$ and $L_{z0} < L_{zf}$, case i), we were unable to transfer the satellite to a circular orbit by first implementing a transfer with constant effective energy followed by another with constant angular momentum because in the first the minimum energy value (circular orbit) is exceeded. The problem in case iv) is similar to this: when $H_0 > H_f$ and $L_{z0} > L_{zf}$, if the satellite is in a circular orbit and we want to transfer it to any other orbit, it will only be possible if we first implement a transfer with constant H followed by another with constant L_z. Otherwise, the minimum energy value will be exceeded and this is not physically possible. This will be discussed in detail in Chapter 6.

In the examples presented, the final orbit orientation is once again different from the initial orbit. The technique described in Chapter 7 to rotate the final orbit can also be used in this case.

Figure 5.2 shows an example of a transfer simulation with both increasing effective energy and angular momentum: a transfer between elliptical and hyperbolic orbits. The initial and final conditions are referenced in the first example in Table 5.1. First, we apply for a constant effective energy transfer and then another with constant angular momentum. However, in the same figure, on the plot of the effective energy variation, we observe two transfers with constant angular momentum (red lines) and another two with constant effective energy (blue lines). This is due to the fact that the satellite enters the problematic region studied in Chapter 4. To solve this, we implement the strategy described in that chapter to the circular orbits (which includes three more types of transfers) but we stop it when the desired angular momentum value L_{zf} is reached. Only after that the transfer with constant L_z begins and takes $\Delta\tau = 38.5$ (normalized time). In fact, in this particular case, the first transfer takes a normalized time $\Delta\tau = 17.1$ and includes an initial transfer with constant H until $\dot{s} = 0$ and $s_1^* < s < s_0^*$ be reached, another with constant L_z up to a chosen value close to H_0 (in this case $H = -0.2$) followed by another one with constant H until the final value L_{zf}. Therefore, the total normalized transfer time is $\Delta\tau = 55.6$.

In Figure 5.3 we present another example of a transfer simulation with $H_0 < H_f$ and $L_{z0} > L_{zf}$ between two hyperbolic Keplerian orbits. Once again, the initial and final conditions of this transfer

are summarized in the first example of case iii) in Table 5.1. Here, we choose to represent the point a) mentioned at the beginning of this section: a transfer with constant angular momentum followed by a transfer with constant effective energy, which takes a normalized time $\Delta\tau = 4.5$ and $\Delta\tau = 0.5$, respectively, to be completed.

case	orbit geometry	initial conditions	final conditions	$\Delta\tau$
i)	elliptic to hyperbolic	$s_0 = 1.1857$ $\dot{s}_0 = -0.25$ $\theta_0 = 0$ $H_0 = -0.3$ $L_{z0} = 1.2$	$H_f = 0.1$ $L_{zf} = 1.5$	$\Delta\tau_a = 8.9$ $\Delta\tau_b = 24.7$
i)	elliptic to circular	$s_0 = 0.8$ $\dot{s}_0 = -0.5$ $\theta_0 = 0$ $H_0 = -0.3438$ $L_{z0} = 1$	$H_f = -0.3$ $L_{zf} = 1.2909$	$\Delta\tau_a = 52.5$ b) inaccessible
ii)	hyperbolic to circular	$s_0 = 0.1878$ $\dot{s}_0 = -0.2$ $\theta_0 = \pi$ $H_0 = 0.2$ $L_{z0} = 0.6231$	$H_f = -0.5$ $L_{zf} = 1$	$\Delta\tau_a = 76.7$ $\Delta\tau_b = 61.1$
ii)	elliptic to elliptic	$s_0 = 0.4445$ $\dot{s}_0 = 0$ $\theta_0 = 0$ $H_0 = -0.2$ $L_{z0} = 0.9$	$H_f = -0.4$ $L_{zf} = 1.1$	$\Delta\tau_a = 44.0$ $\Delta\tau_b = 37.5$
iii)	hyperbolic to hyperbolic	$s_0 = 0.4772$ $\dot{s}_0 = 0$ $\theta_0 = 3\pi/2$ $H_0 = 0.1$ $L_{z0} = 1$	$H_f = 0.6$ $L_{zf} = 0.7$	$\Delta\tau_a = 5.0$ $\Delta\tau_b = 7.07$
iii)	circular to elliptic	$s_0 = 2.25$ $\dot{s}_0 = 0$ $\theta_0 = 0$ $H_0 = -0.2222$ $L_{z0} = 1.5$	$H_f = -0.1$ $L_{zf} = 0.9$	$\Delta\tau_a = 7.1$ $\Delta\tau_b = 8.95$
iv)	hyperbolic to hyperbolic	$s_0 = 0.4148$ $\dot{s}_0 = -0.1$ $\theta_0 = 0$ $H_0 = 0.5$ $L_{z0} = 1$	$H_f = 0.2$ $L_{zf} = 0.8$	$\Delta\tau_a = 3.2$ $\Delta\tau_b = 4.4$
iv)	circular to elliptic	$s_0 = 1$ $\dot{s}_0 = 0$ $\theta_0 = 0$ $H_0 = -0.5$ $L_{z0} = 1$	$H_f = -0.7$ $L_{zf} = 0.8$	a) inaccessible $\Delta\tau_b = 8.5$

Table 5.1: Examples of transfers with both varying angular momentum and effective energy.

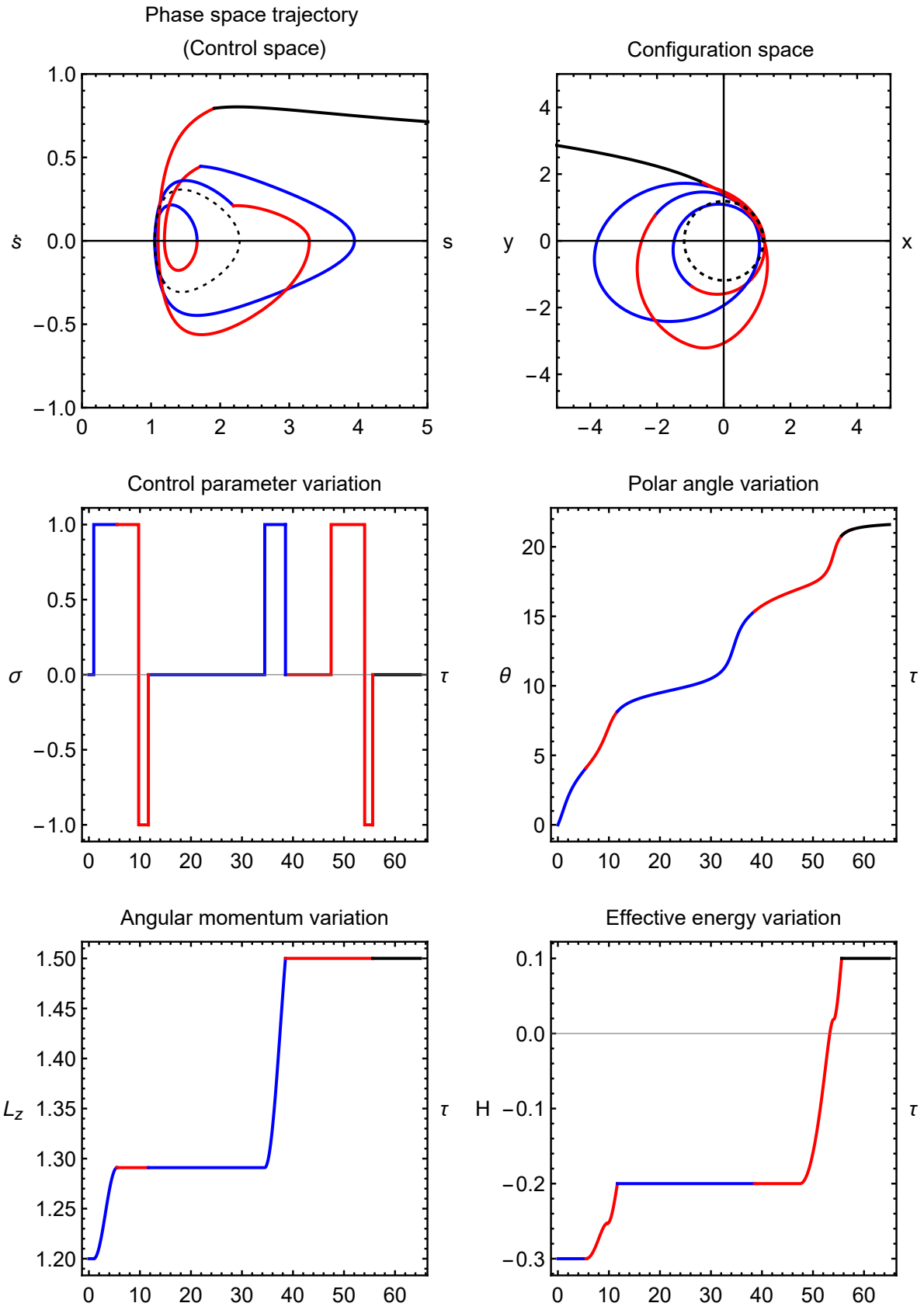

Figure 5.2: Simulation of a transfer with both varying angular momentum and effective energy between elliptical and hyperbolic orbits: the initial one with $L_{z0} = 1.2$ and $H_0 = -0.3$ and the final with $L_{zf} = 1.5$ and $H_f = 0.1$. The initial orbit is represented by the dashed line, the first transfer (with constant H) by the blue line, the second transfer (with constant L_z) by the red line and the final orbit by the black one. The transfer starts at the point $(s_0, \dot{s}_0, \theta_0) = (1.1857, -0.25, 0)$. The normalized transfer time is $\Delta\tau = 55.6$.

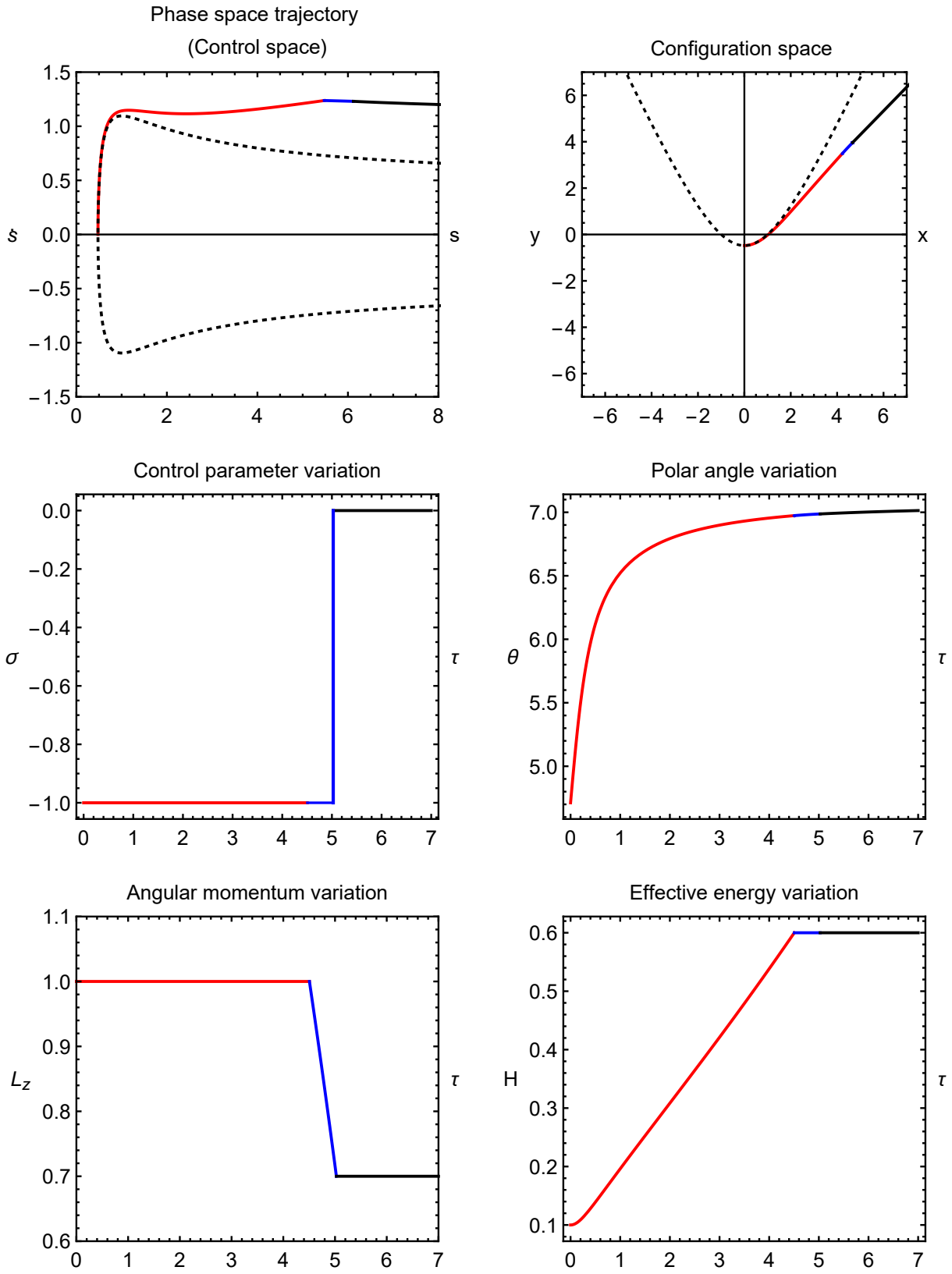

Figure 5.3: Simulation of a transfer with both varying angular momentum and effective energy between two hyperbolic orbits: the initial one with $L_{z0} = 1$ and $H_0 = 0.1$ and the final with $L_{zf} = 0.7$ and $H_f = 0.6$. The initial orbit is represented by the dashed line, the first transfer (with constant H) by the blue line, the second transfer (with constant L_z) by the red line and the final orbit by the black one. The transfer starts at the point $(s_0, \dot{s}_0, \theta_0) = (0.4772, 0, 3\pi/2)$. The normalized transfer time is $\Delta\tau = 5.0$.

5.2 Second case of transfers with both variable H and L_z

Although we have already obtained transfers with both variable angular momentum and effective energy, there is a second hypothesis to compute them, using control conditions given by the conservation laws.

Looking at the plots of $H(L_z)$ - Figure 5.1 - of any of the transfers we are considering, we see this is represented by a straight segment with a slope k. So, we can write

$$\frac{dH}{dL_z} = \frac{H_f - H_0}{L_{zf} - L_{z0}} = k, \tag{5.1}$$

where k is a constant that can be positive or negative according to the case we are analyzing. $k > 0$ if L_z and H increase or decrease; $k < 0$ if one increases and the other decreases. Therefore, this new equation is the other condition that will help us to implement these transfers.

We know that the equations that describe these transfers are given by (2.8) and (2.11):

$$\begin{cases} \ddot{s} = \frac{L_z^2}{s^3} - \frac{1}{s^2} + \epsilon\sigma\cos(\theta - \phi) \\ \dot{L_z} = -\epsilon\sigma s\sin(\theta - \phi) \\ \dot{H} = \epsilon\sigma\left[\dot{s}\cos(\theta - \phi) - s\dot{\theta}\sin(\theta - \phi)\right], \end{cases} \tag{5.2}$$

If we replace the last two equations of (5.2) in (5.1), we obtain

$$\tan(\theta - \phi) = \frac{\dot{s}}{s\dot{\theta} - ks} \Rightarrow \begin{cases} \sin(\theta - \phi) = \frac{\dot{s}}{\left[\dot{s}^2 + (s\dot{\theta} - ks)^2\right]^{\frac{1}{2}}} \\ \cos(\theta - \phi) = \frac{s\dot{\theta} - ks}{\left[\dot{s}^2 + (s\dot{\theta} - ks)^2\right]^{\frac{1}{2}}} \end{cases}, \tag{5.3}$$

and if we still replace these equations in (5.2) we have the final equations to use in transfer simulations:

$$\begin{cases} \ddot{s} = \frac{L_z^2}{s^3} - \frac{1}{s^2} + \epsilon\sigma\frac{s\dot{\theta} - ks}{\left[\dot{s}^2 + (s\dot{\theta} - ks)^2\right]^{\frac{1}{2}}} \\ \dot{L_z} = -\epsilon\sigma s\frac{\dot{s}}{\left[\dot{s}^2 + (s\dot{\theta} - ks)^2\right]^{\frac{1}{2}}} \\ \dot{H} = -\epsilon\sigma s\frac{\dot{s}k}{\left[\dot{s}^2 + (s\dot{\theta} - ks)^2\right]^{\frac{1}{2}}} = k\dot{L_z} \\ \dot{\theta} = \frac{L_z}{s^2} \end{cases} \tag{5.4}$$

Note that these transfers have both varying effective energy and angular momentum and for each one of the four possible cases it is still necessary to impose other conditions: i) when $s\dot{s} > 0$ implies $\sigma = 1$ and $s\dot{s} < 0$, $\sigma = 1$, and ii) when $s\dot{s} > 0$ implies $\sigma = -1$ and $s\dot{s} < 0$, $\sigma = 1$.

We present two examples of this type of transfers, one for the case i) - Figure 5.4 - and another for ii) - Figure 5.5. However, we have not yet been able to obtain transfer simulations for any values of H and L_z because there are still problematic regions (close to the fixed points). This may imply a different choice of control parameters, but we leave our suggestion for possible future work on this subject. Besides, we also call for the study of these transfers when one of the quantities (H or L_z) increases, and the other

decreases. This type of transfers may be important since, as we will see next, they are more efficient than those studied in the previous section.

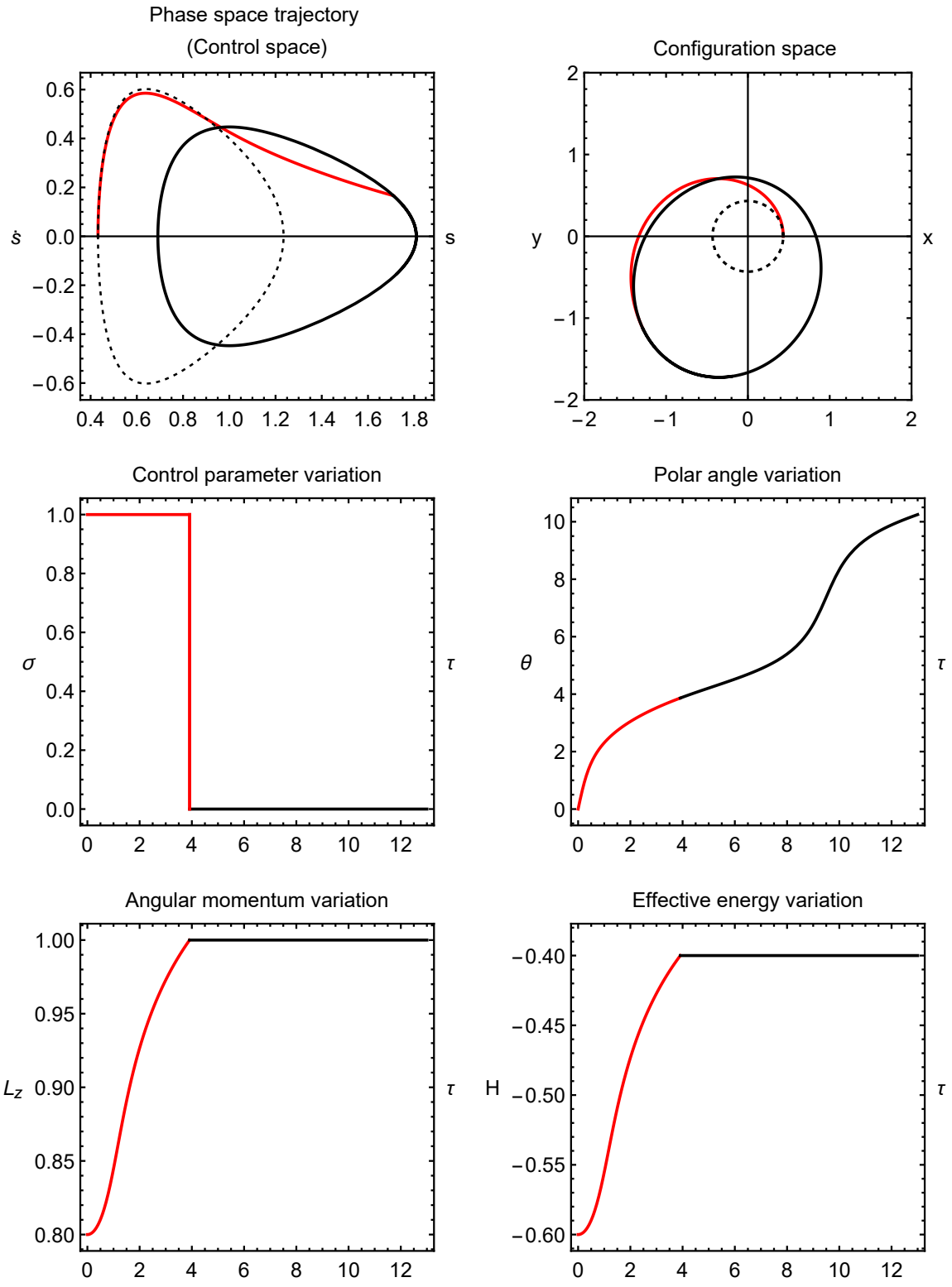

Figure 5.4: Simulation of a transfer with angular momentum and effective energy, both varying, between two elliptical orbits: the initial with $L_{z0} = 0.8$ and $H_0 = -0.6$ and the final with $L_{zf} = 1$ and $H_f = -0.4$. The initial orbit is represented by the dashed line, the transfer (with both variable H and L_z) by the red line and the final orbit by the black one. The transfer starts at the point $(s_0, \dot{s}_0, \theta_0) = (0.4395, 0, 0)$ and its normalized time is $\Delta\tau = 3.9$.

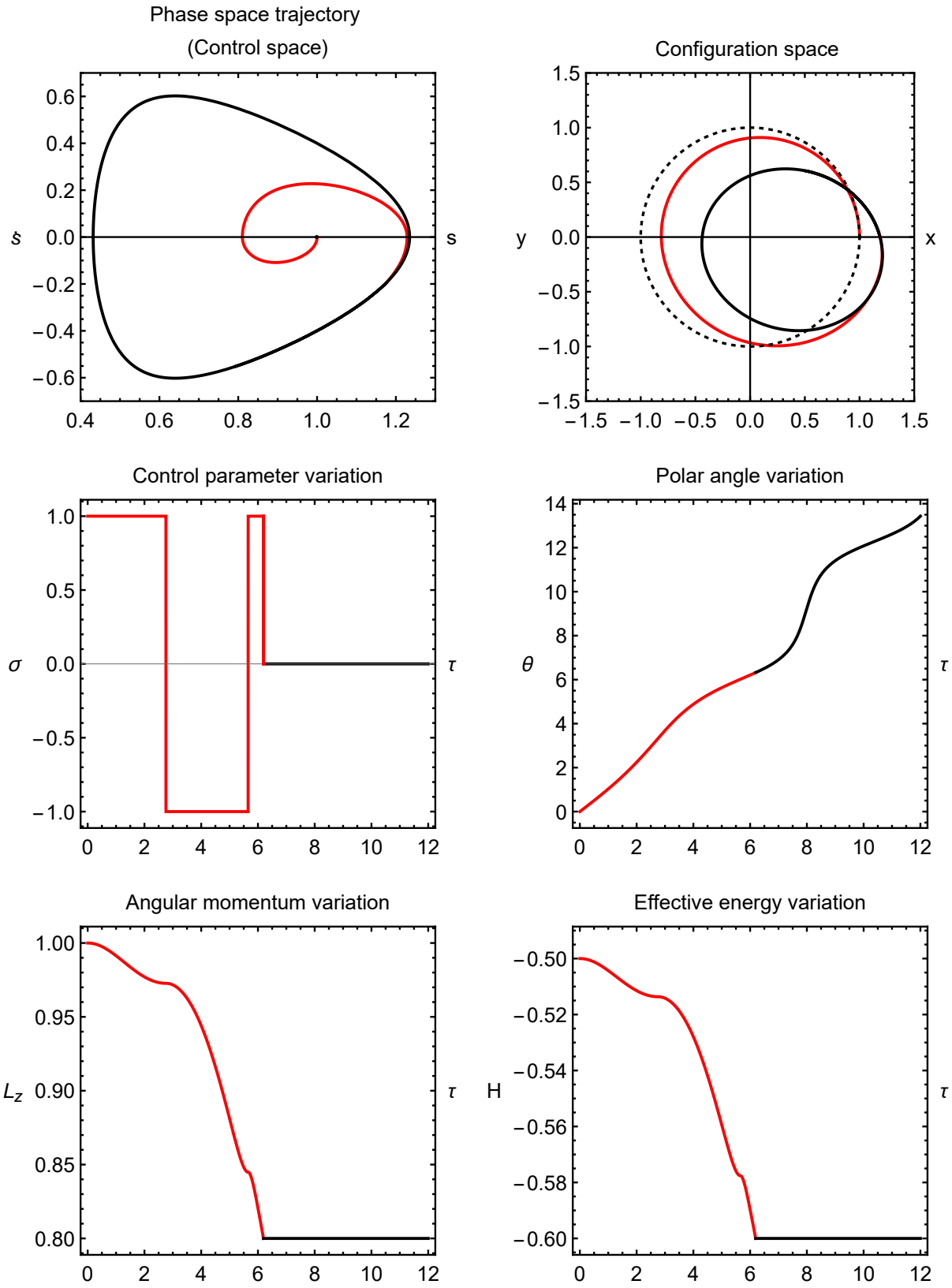

Figure 5.5: Simulation of a transfer with angular momentum and effective energy both variable between a circular and an elliptical orbits: the initial with $L_{z0} = 1$ and $H_0 = -0.5$ and the final with $L_{zf} = 0.8$ and $H_f = -0.6$. The initial orbit is represented by the dashed line, the first transfer (with both variable H and L_z) by the blue line, the second transfer (with constant H) by the red line and the final orbit by the black one. The transfer starts at the point $(s_0, \dot{s}_0, \theta_0) = (1, 0, 0)$ and its normalized time is $\Delta\tau = 6.2$.

5.3 Comparison between the two techniques

This section aims to prove that the method used in Section 5.2 is more efficient than that of Section 5.1 and this is obvious and predictable: while in the former we use two transfers until the desired end-point is reached, in the latter we only use one transfer, obtaining the control conditions directly through conservation laws.

To simplify, for the method implemented in Section 5.2 we call it method c), since at the beginning of Section 5.1 we implement the simulations using transfers with constant angular momentum followed by transfers with constant effective energy and vice-versa and we called them methods a) and b), respectively.

In Table 5.2 we present the main characteristics of two simulations examples of transfers, each one performed with methods a), b) and c). The first is a transfer with both increasing effective energy and angular momentum, and the second with both these parameters decreasing. Comparing transfer times, $\Delta\tau_{a,b} > \Delta\tau_b$, we conclude that, in fact, method c) is the most efficient.

However, note that method c) is not yet fully operational but we predicted that it will continue to be more efficient than methods a) and b).

initial conditions	final conditions	$\Delta\tau$
$L_{z0} = 0.8$ $H_0 = -0.6$ $s_0 = 0.4319$ $\dot{s}_0 = 0$ $\theta_0 = 0$	$L_{zf} = 1$ $H_f = -0.4$	$\Delta\tau_a = 15.9$ $\Delta\tau_b = 31.8$ $\Delta\tau_c = 3.9$
$L_{z0} = 0.85$ $H_0 = -0.6388$ $s_0 = 0$ $\dot{s}_0 = 0$ $\theta_0 = 0$	$L_{zf} = 0.8$ $H_f = -0.6920$	$\Delta\tau_a = 18.7$ $\Delta\tau_b = 11.6$ $\Delta\tau_c = 1.3$

Table 5.2: Results of the simulation of two transfers with both varying effective energy and angular momentum, each one implemented by the methods a) and b).

Chapter 6

Transfers between two circular orbits

In this chapter, we are going to obtain transfers between two circular orbits combining the transfers studied previously.

In Figure 6.1 are represented schematically all types of transfers carried out until now:

1. transfer with constant angular momentum (Chapter 3);
2. transfer with constant effective energy (Chapter 4);
3. transfer with varying angular momentum and varying effective energy (Chapter 5);

and also the method of transfers between two circular orbits that we are studying in this chapter, depicted by the orange line.

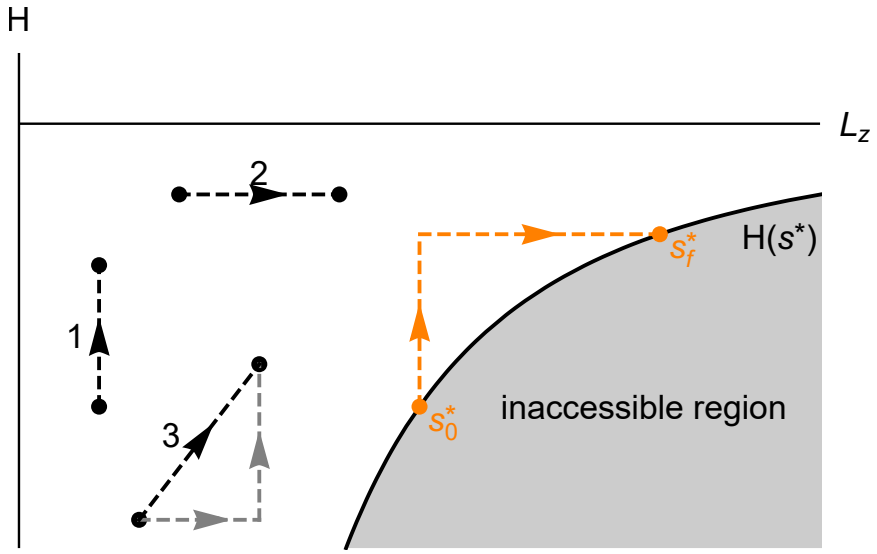

Figure 6.1: Effective energy diagram as a function of the angular momentum of the various transfers simulated in this project. 1) Transfer with constant angular momentum; 2) transfer with constant effective energy; 3) transfer with both varying effective energy and angular momentum. The solid black line corresponds to all possible circular orbits and in the region below that line, transfers cannot be simulated because the energy of a circular orbit is the minimum allowed in Keplerian orbits. In orange, we depicted the path to obtain transfers between two circular orbits.

Still in Figure 6.1 all the possible circular orbits are represented by the solid black line, which coincides with the fixed point $(s, \dot{s}) = (s_0^*, 0)$ and the angular momentum and effective energy expressions are

$L_z(s_0^*, 0) = \sqrt{s_0^*}$ and $H(s_0^*) = -1/(2s_0^*)$, respectively. Since the black line corresponds to circular orbits and since they have the possible minimum energy, the gray region is not accessible and it is impossible to simulate transfers there. This way, it is now possible to understand why for transfers with constant effective energy it is necessary that $H \geq -1/(2L_{z0}^2)$ if $L_{z0} > L_{zf}$ and $H \geq -1/(2L_{zf}^2)$ if $L_{zf} > L_{z0}$.

From here, we conclude that, to obtain transfers between two circular orbits, both effective energy and angular momentum must increase or decrease simultaneously as the radius of the final orbit increases or decreases relative to the initial one, respectively.

Considering the two orange points represented in the figure as the initial and final points of a transfer between two circular orbits, we can see that the most effective way to obtain the endpoint would be to follow the trajectory of the continuous black line that joins the two points. However, this is not possible with using the numerical method of integration Runge-Kutta 4^{th} order because it does not allow us to obtain such an exact result.

Through the scheme represented in Figure 6.1, we conclude that the order of transfers to be implemented is:

i) a constant effective energy transfer followed by a constant angular momentum transfer if $s_0 > s_f$;

ii) a constant angular momentum transfer followed by a constant effective energy transfer if $s_f > s_0$.

Note that in the latter case, when we apply for transfers with constant effective energy, we implement the strategy described in Chapter 4 and, therefore, it is not just a transfer to constant H but three different transfers interchanged between transfers with constant H and transfers with constant L_z.

In Figure 6.2 we present an example of a transfer simulation between two circular orbits through the implementation of method i) where $s_0 > s_f$. The initial orbit is characterized by $L_{z0} = 1$ and $H_0 = -0.5$ and the final one by $L_{zf} = 0.9$ and $H_f = -0.6173$. The transfer starts at the point $(s_0, \dot{s}_0 = 1, 0)$ with $\theta_0 = 0$ and it takes a normalized time $\Delta\tau = 26.6$ to be completed.

As an example of method ii) we present the simulation of Figure 6.3. The transfer begins in an orbit with $L_{z0} = 1$ and $H_0 = -0.5$ and finishes in another with $L_{zf} = 1.2909$ and $H_f = -0.3$ where $s_f > s_0$. The starting point of the transfer is $(s_0, \dot{s}_0 = 1, 0)$ with $\theta_0 = 0$. The normalized transfer time is 71.6, where 17.1 were occupied in the transfer at constant angular momentum and the rest 54.5 in the transfer at constant effective energy (which also implies two transfers with constant angular momentum, as explained at the end of section 4.1).

In both figures, the control parameter variation σ has a different definition depending on the type of transfer, following the control choices of Chapter 3 during the constant angular momentum transfer (red line) and of Chapter 4 during the constant effective energy transfer (blue line).

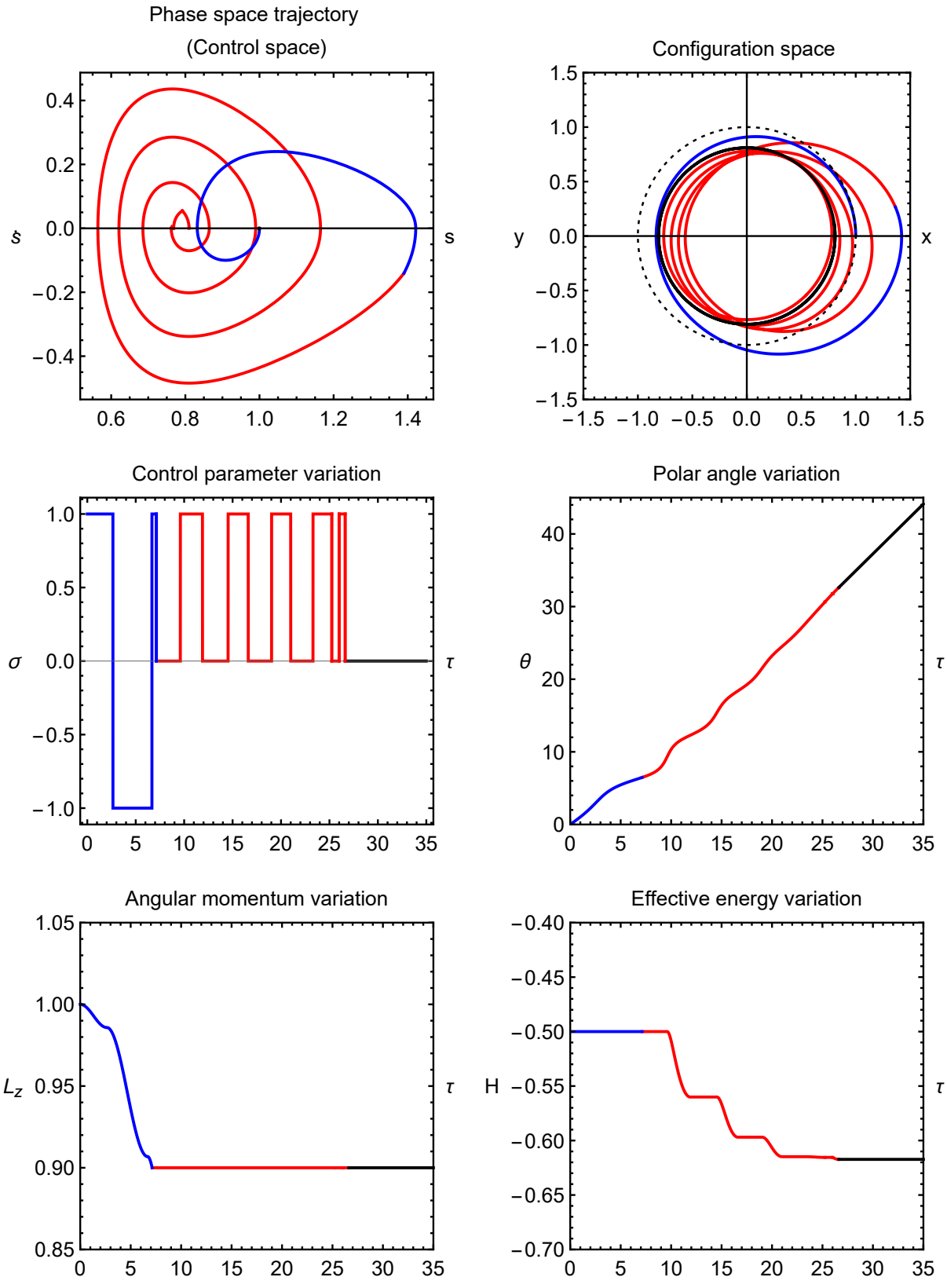

Figure 6.2: Simulation of a transfer with both variable angular momentum and effective energy between two circular orbits $s_0 > s_f$: the initial with $L_{z0} = 1$ and $H_0 = -0.5$ and the final with $L_{zf} = 0.9$ and $H_f = -0.6173$. The initial orbit is represented by the dashed line, the first transfer (with constant H) by the blue line, the second (with constant L_z) by the red line and the final orbit by the black one. The transfer starts at the point $(s_0, \dot{s}_0) = (1, 0)$ with $\theta_0 = 0$. The transfer time is $\Delta\tau = 26.6$ (dimensionless).

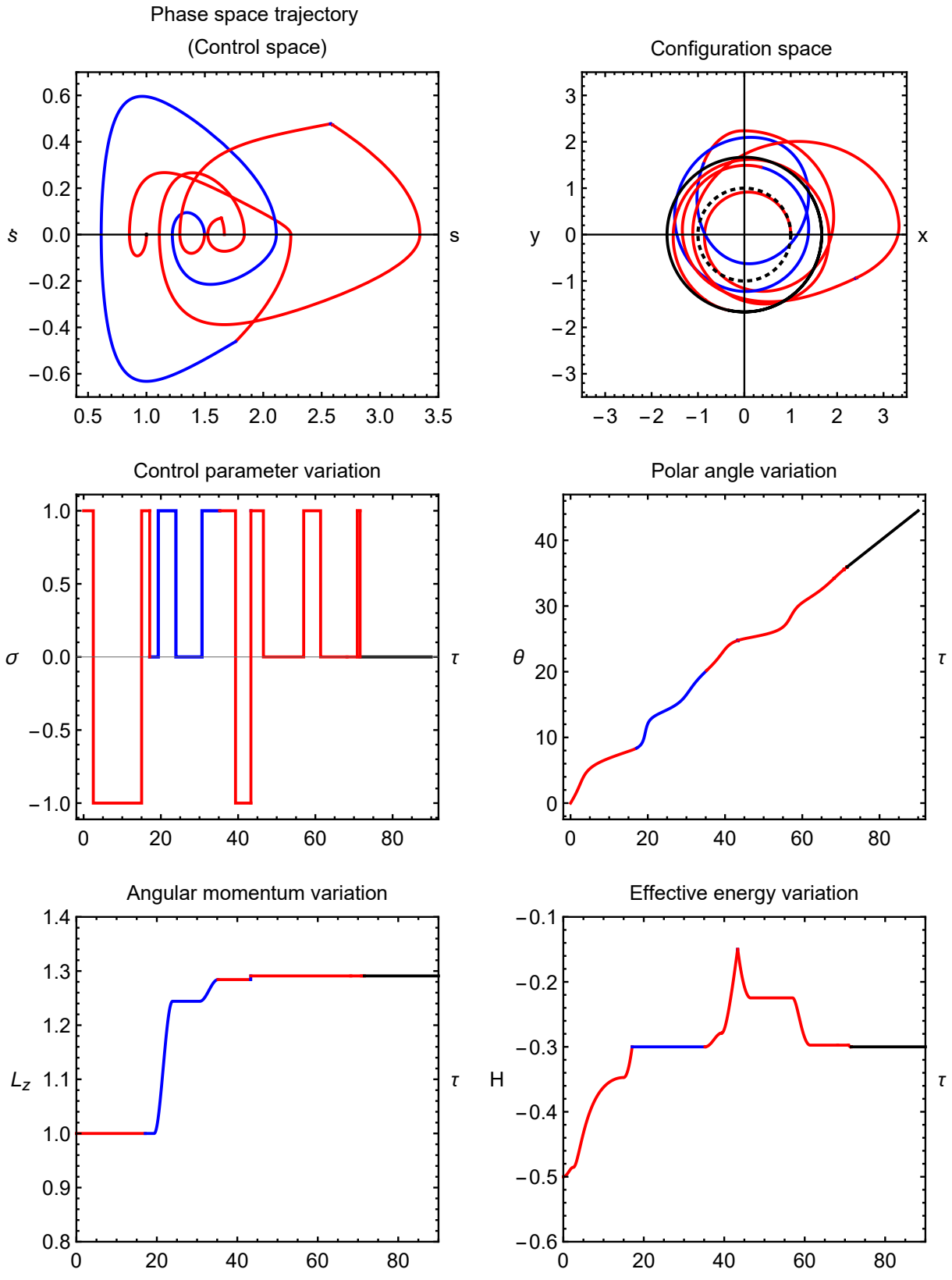

Figure 6.3: Simulation of a transfer with both variable angular momentum and effective energy between two circular orbits with $s_f > s_0$: the initial with $L_{z0} = 1$ and $H_0 = -0.5$ and the final with $L_{zf} = 1.2909$ and $H_f = -0.3$. The transfer starts at the point $(s_0, \dot{s}_0) = (1, 0)$ with $\theta_0 = 0$ and its time is $\Delta\tau = 71.6$ (dimensionless). The initial orbit is represented by the dashed line, the first transfer (with constant H) by the blue line, the second (with constant L_z) by the red line and the final orbit by the black one.

Chapter 7

Final orbit rotation through the Laplace-Runge-Lenz vector

As described by the examples given in the previous chapters, after a transfer, the final orbit rotates relative to the initial one. This is true both for transfers with constant angular momentum as well as for transfers with constant effective energy.

In this chapter, we create a strategy to rotate the final orbit until it is in the initial orbit orientation. For this, we resort to the third constant of motion of the Kepler problem - the Laplace-Runge-Lenz vector (LRL).

7.1 Method description of rotating an orbit

Since it is a constant of motion of the Kepler problem, the LRL vector is invariant for any point in a certain orbit and it is calculated using the equation (2.13). This way, we can calculate the LRL vectors for the initial and final orbits and the scalar product of these two vectors allows us to discover the angle of rotation $\Delta\alpha$ between the orbits:

$$\Delta\alpha = \arccos\left[\frac{A_{x0}A_{xf} + A_{y0}A_{yf}}{\left(A_{x0}^2 + A_{y0}^2\right)^{\frac{1}{2}}\left(A_{xf}^2 + A_{yf}^2\right)^{\frac{1}{2}}}\right], \tag{7.1}$$

where A_{x0} and A_{y0} are the components of the LRL vector relative to the initial orbit, and A_{xf} and A_{yf} are also the components of the LRL vector but relative to the final orbit.

Since we want the final orbit to have the same orientation as the initial one, we have to rotate the final orbit by an angle $-\Delta\alpha$. The control is done as described in Section 2.3.5 of reference [1]: depending on the case we are considering, we use transfers with constant angular momentum or transfers with constant effective energy and we turn the control on with $\sigma = 1$ at a point $(s_r, \dot{s}_r)$ of the final orbit and turn it off when $(s_r, -\dot{s}_r)$ is reached. The phase space is invariant under rotations but we reach a Keplerian orbit defined by the same angular momentum and energy as the initial one with a different

orientation, which means that the orbit precesses in configuration space but rarely at the desired angle $-\Delta\alpha$. Then, for the orbits to have the same orientation, it is necessary to find the initial angle θ_r that satisfies these conditions. This method can be applied for the rotation of elliptic and hyperbolic Keplerian orbits.

To a better understand of the orbital phase space, we have to consider two cases: i) $\dot{s}_r > 0$ and ii) $\dot{s}_r < 0$. For each one of these cases, we present a detailed example of the method used to rotate the final orbit.

7.2 When $\dot{s}_r > 0$

Based on Chapter 3, we consider a transfer simulation with constant angular momentum ($L_z = 1$) which starts at point $(s_0, \dot{s}_0) = (0.8, 0.1)$ with $\theta_0 = 0$ and $H_0 = -0.4638$. When the transfer ends, the effective energy is $H_f = -0.2$, the normalized transfer time is $\Delta\tau = 9.8$ and the rotation angle is $1.2667 = 72.5778°$. This simulation is depicted in Figure 7.1 and each of the LRL vectors is represented in the respective orbit.

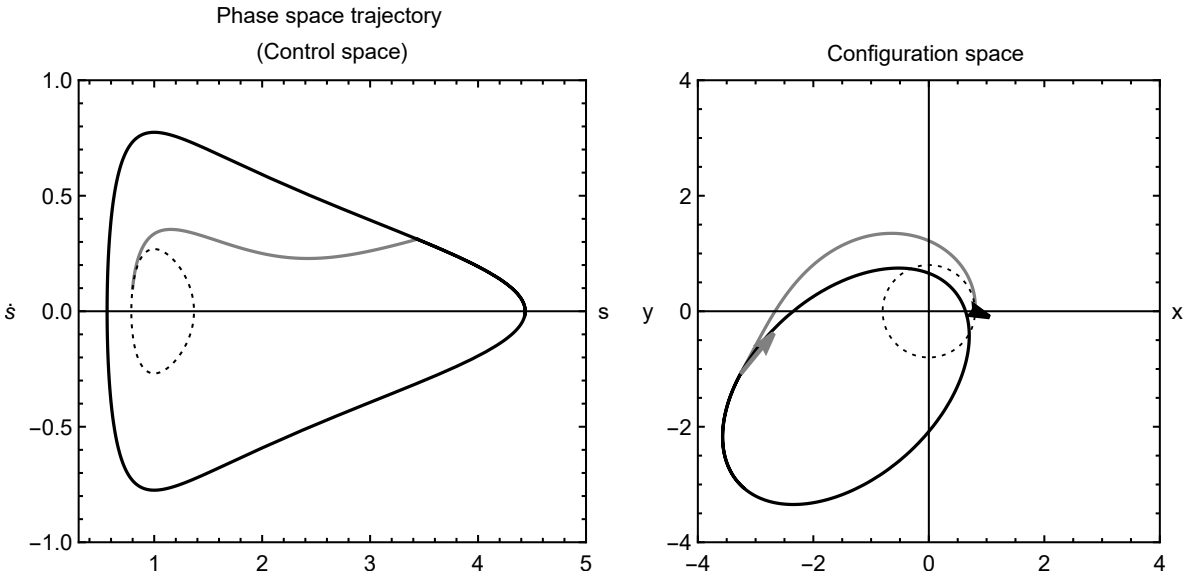

Figure 7.1: Simulation of a transfer with constant angular momentum ($L_z = 1$) between two elliptical orbits: the initial with an effective energy $H_0 = -0.4638$ and the final with $H_f = 0.2$. The initial orbit is represented by the dashed line, the transfer by the gray line and the final orbit by the black one. The transfer starts at the point$(s_0, \dot{s}_0, \theta_0) = (0.8, 0.1, 0)$ and takes 9.8 (dimensionless) to be completed. The final orbit rotates an angle $\Delta\alpha = 1.2667 = 72.5778°$ relative to the initial one. The LRL vectors of the initial and final orbits are represented in black and gray, respectively.

Since we want to rotate the final orbit by an angle $-\Delta\alpha$, we have to align the final LRL vector with the first one. To do that, we turn the control on with $\sigma = 1$ at the point where the final effective energy is reached, $(s_r, \dot{s}_r)$, and turn it off at $(s_r, -\dot{s}_r)$. Note that, in this case, $\dot{s}_r > 0 = 0.3118$ and $s_r = 3.4375$, and we can find the simulation corresponding to this case in Figure 7.2: the initial point is represented by green and the final by orange. During this process, the angular momentum remains constant but the effective energy does not: when the control is turned on, it starts to decrease and when it reaches

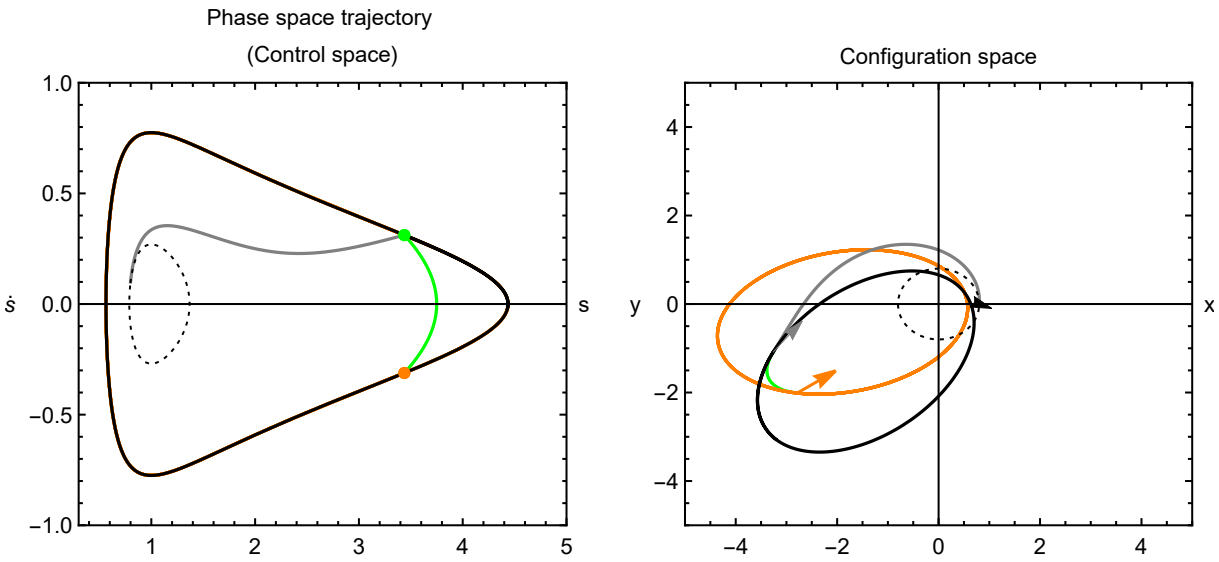

Figure 7.2: Simulation of the implemented method to rotate an orbit. The control is turned on with $\sigma = 1$ at the point $(s_r, \dot{s}_r) = (3.4375, 0.3118)$ with $\theta = 3.4629$ and is turned off when the point $(s, \dot{s}) = (s_r, -\dot{s}_r)$ is reached. The angular momentum and effective energy remain constant and are $L_z = 1$ and $H = -0.2$, respectively. The green line corresponds to the orbit change while the control parameter is on and the orange one to the final orbit already rotated. This corresponds to a rotation angle of $\Delta\alpha = 0.3001 = 17.1941°$. On the left plot, the black and orange orbits coincide.

$\dot{s} = 0$ it starts to increase until the H_f value. On the left plot, in the orbital phase space trajectory, the satellite describes the same closed orbit (black line) before the control is on and after the control is again turned off. Thus, it is proven that the phase space is invariant according to rotations. On the right, we verify a rotation of the final orbit (the orange one) in configuration space, which means that its orientation changes continuously when we implement this control method. However, the rotation angle, $\Delta\alpha = 0.3001 = 17.1941°$, is not sufficient to align the LRL vectors (orange and black).

To solve this problem, we have to manipulate the initial polar angle θ_r that leads to a rotation of the final orbit with the desired angle $-\Delta\alpha$. When we find the value of θ_r that satisfies this condition, we start the orbit rotation itself. Then, in the end, both orbits have the same orientation.

For the example that we are considering, $\theta_r = 2.8575$. Through Figure 7.3, we can verify that both LRL vectors of the rotated and of the initial orbits have the same orientation. Thus, the process is complete and we obtain a transfer with constant angular momentum and where the initial and final orbits have the same orientation, using the constants of motion of the Kepler problem.

Note that, with this method, it is not possible to measure the time it takes to obtain an orbit with the desired orientation. We are only able to discover one condition (in this case the initial polar angle) for this to happen. We can only know, for any θ_r, how long it takes from the moment we start to rotate the orbit until it has the desired orientation. This value is constant and independent of the θ_r value. In this case, it corresponds to 4.0.

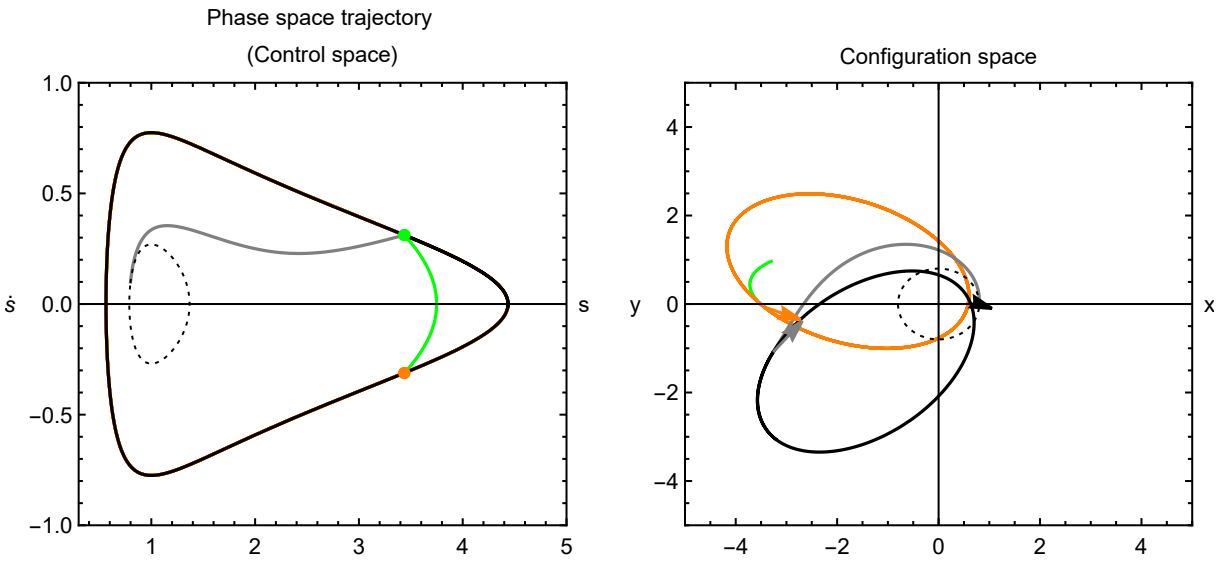

Figure 7.3: Rotation of an orbit resulting from a transfer with constant angular momentum ($L_z = 1$). The rotation is also done with constant angular momentum. The initial conditions are $(s_r, \dot{s}_r, \theta_r) = (3.4375, 0.3118, 2.8575)$ and it takes a normalized time $\Delta\tau = 4.0$ to reach the point $(s_r, -\dot{s}_r)$. The initial and final orbits are represented by the dashed and black lines, respectively, and the rotated orbit by the orange line. In green (left plot), the phase space is shown when the control is on, and we confirm that when it is turned off, we remain in the same orbit but with a different orientation (right plot).

7.3 When $\dot{s}_r < 0$

In this example, we consider a transfer with constant effective energy ($H = -0.5$) starting at the point $(s_0, \dot{s}_0) = (0.5, -0.2)$ with $\theta_0 = 0$ and $L_{z0} = 0.8602$ and ending when $L_{zf} = 0.5$ is reached. We use the control choices described in Chapter 4 and this transfer simulation is presented in Figure 7.4. The normalized transfer time is 5.96588 and the final orbit rotates an angle $\Delta\alpha = 0.2558 = 14.6589°$ relative to the initial one.

After the transfer, we verify that we need to rotate the final orbit by an angle $-\Delta\alpha = -0.2558 = -14.6589°$. Letting the effective energy invariant, we turn on the control with $\sigma = 1$ at the point where the final angular momentum is reached, at $(s_r, \dot{s}_r)$, and turn it off at point $(s_r, -\dot{s}_r)$. The angular momentum is the same in both points but when the control is turned on ceases to be constant: it decreases until $\dot{s} = 0$ and then increases again to L_{zf}. In this case, $s_r = 1.1194$ and $\dot{s}_r < 0 = -0.7663$ with $\theta_r = 3.9021$. This is presented in Figure 7.5. On the left plot, the green and orange points correspond to the positions where the control is turned on and off, respectively. The orange and black lines overlap meaning that the satellite remains in the same orbit (with the same angular momentum and effective energy). Again, we prove that the phase space is invariant according to rotations. On the right plot, in configuration space, the final orbit (the orange line) rotates relatively to the black one. Again, this rotation angle $\Delta\alpha = 0.1436 = 8.2264°$ is not sufficient to align the LRL vectors (orange and black).

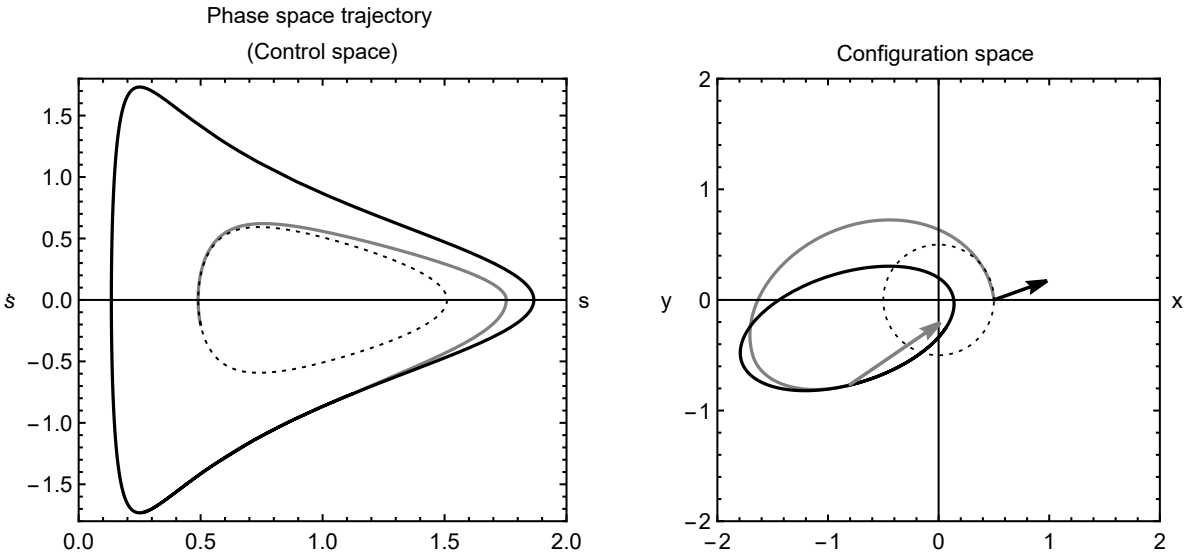

Figure 7.4: Simulation of a transfer with constant effective energy ($H = -0.5$) between two elliptical orbits: the initial with an effective energy $L_{z0} = 0.8602$ and the final with $L_{zf} = 0.5$. The initial orbit is represented by the dashed line, the transfer by the gray line and the final orbit by the black one. The transfer starts at the point $(s_0, \dot{s}_0, \theta_0) = (0.5, -0.2, 0)$ and takes a normalized time $\Delta\tau = 5.9$ (dimensionless) to be completed. The final orbit rotates an angle $\Delta\alpha = 0.25585 = 14.6589°$ relative to the initial one. The LRL vectors of the initial and final orbits are represented in black and gray, respectively.

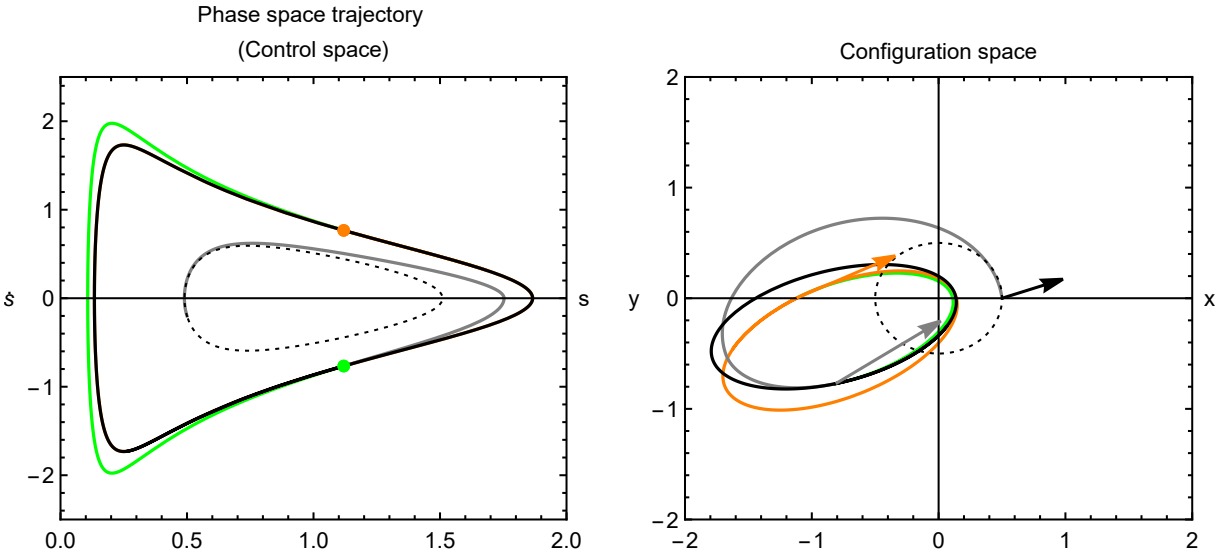

Figure 7.5: Simulation of the implemented method to rotate an orbit. The control is turned on the control with $\sigma = 1$ at the point $(s_r, \dot{s}_r) = (1.1194, -0.7663)$ with $\theta_r = 3.9021$ and is turned off when the point $(s, \dot{s}) = (s_r, -\dot{s}_r)$ is reached. The effective energy remains constant ($H = -0.5$). The green line corresponds to the orbit trajectory change while control parameter is on and the orange one to the final orbit already rotated. This corresponds to a rotation angle of $\Delta\alpha = 0.1436 = 8.2264°$. On the left plot, the green and orange points at the point where the control is turned on and off, respectively. The black and orange orbits coincide.

Similar to what was done in the previous example, we have to manipulate the initial polar angle θ_r which leads to a rotation of the final orbit with the desired angle $-\Delta\alpha$. Thus, we find an angle $\theta_r = 3.8265$ and, by Figure 7.6, the orbits have the same orientation.

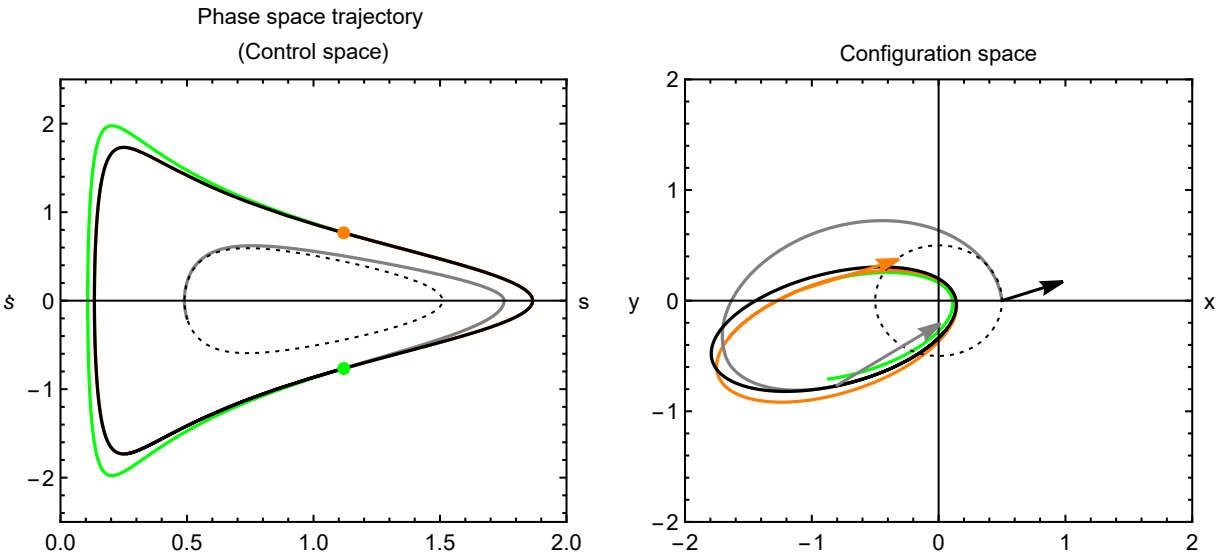

Figure 7.6: Rotation of an orbit resulting from a transfer with constant effective energy ($H = -0.5$). The rotation is also done with constant effective energy. The initial conditions are $(s_r, \dot{s}_r, \theta_r) = (1.1194, 0.7663, 3.8265)$ and it takes a normalized time $\Delta\tau = 1.7$ to reach the point $(s_r, -\dot{s}_r)$. The initial and final orbits are represented by the dashed and black lines, respectively, and the rotated orbit by the orange line. In green (left plot), the phase space is shown when the control is on, and it is confirmed that when it is turned off, we remain in the same orbit but with a different orientation (right plot).

Chapter 8

Conclusions

The main goal of this master thesis was to develop a control strategy to be applied in satellites' low-thrust transfers between two-dimensional Keplerian orbits through conservation laws. The starting point of this project was Mariana Fernandes 2017 master thesis [1], where transfers with constant angular momentum, transfers with constant effective energy, and a particular case of transfers with both variable angular momentum and effective energy were studied. Based on this work, we simplified the *Mathematica* code for the transfers mentioned above and we deepened the study of these for any value of the effective energy and angular momentum. For each transfer, we used different control choices depending on its phases space. We used a *bang-bang* control, where the parameter control, σ, could only be ± 1 or 0 (which the latter corresponds to the control being turned off).

We started our work by presenting the mathematical formalism of the two-dimensional variable mass Kepler problem in Chapter 2. We assumed that the thrusters exhaust gases intensity were constant and we obtained the equations of motion for this problem, which has three constants of motion: the angular momentum vector, the effective energy, and the Laplace-Runge-Lenz vector, where the latter is used to control the final orbit orientation. However, during transfers, they are no longer constants. This means that, initially, the satellite is in an initial orbit with a certain angular momentum, effective energy, and LRL vector. When the control is turned on, one or two of these constants (depending on the type of transfer we are considering) are no longer constant and the satellite moves to another orbit. When the desired value is reached, the control turns off and we have the three constants of motion again but now with different values according to the final orbit. Also in Chapter 2, we derived the energy expenditure equation for a transfer. However, we did not think it would make sense to calculate the energy cost involved in each transfer simulation since, by equation (2.16), it depends on the initial satellite mass and the gamma parameter, which is given by the satellite manufacturer and we were considering a general satellite and not a specific one.

The following chapters were dedicated to the various types of transfers. We started by studying transfers with constant angular momentum, which were explained in Chapter 3. In Table 3.2 we summarize the control choices made for the two possible cases of these transfers: $H_0 < H_f$ and $H_f < H_0$. When $H_f < H_0$ and after analyzing the phases space trajectories, we were able to obtain more general

transfers for any angular momentum value by choosing different control parameters from those used in [1]. We combined only $\sigma = 1$ with the control off ($\sigma = 0$). The great advantage of not using the solution of $\sigma = -1$ is that the orbits with $\sigma = 1$ are always stable and we can obtain transfers for any angular momentum value.

In Chapter 4 we studied transfers with constant effective energy and, in order to guarantee the stability of the orbits, we again only chose the control parameters $\sigma = 1$ and $\sigma = 0$ when $L_{zf} > L_{z0}$. The control choices are summarized in equations (4.4) and (4.7).

In both types of transfers, due to the orbital phase spaces, it was not possible to reach directly the circular orbit. To solve this, we implemented a new strategy that is discussed in the final of Sections 3.1 and 4.1.

We proceeded with our study in Chapter 5 by simulating transfers with both variable effective energy and angular momentum. Firstly, in Section 5.1, we analyzed a particular case of this type of transfers: a simpler case that consists of combining transfers with constant angular momentum with transfers with constant effective energy, as discussed earlier. Then, in Section 5.2, we implemented a more efficient way to obtain these transfers using only conservation laws of effective energy and angular momentum. However, this method is not yet totally completed because some problems related to the regions near the fixed points were not being solved. We encourage anyone who wants to study this topic to explore this method as it is more efficient than the first one since both angular momentum and effective energy vary simultaneously. This was also discussed in Section 5.3.

To prove the effectiveness of the method used, in all chapters mentioned so far, we presented some examples of transfers between elliptical, circular, or hyperbolic orbits. Besides, another very important aspect is the fact that we can start transfers at any point in the orbit.

After this, we simulated in Chapter 6 a particular type of transfers: between two circular orbits. We obtained it using a method schematically depicted in Figure 6.1 by the orange lines. This method resulted from joining the previous transfers (with constant angular momentum and with constant effective energy). Note that the most efficient way to obtain these transfers would be to follow the black line that joins the initial and final points in Figure 6.1. However, we were using a method of numerical integration (Runge-Kutta 4^{th} order) that did not allow us to obtain this trajectory exactly. Another possibility to consider in future work in this field is to simulate these transfers by implementing the second (and more efficient) method studied in Chapter 5.

Finally, we used the third constant of motion of the Kepler problem: the LRL vector. When we simulated transfers with constant effective energy and with constant angular momentum we verified that the final orbit had rotated relative to the initial one. So, using the LRL vector, we implemented an algorithm to rotate the final orbit. This is covered in Chapter 7.

In addition to the suggestions mentioned above, we propose two more topics that we consider crucial for the development of the field of orbital transfers using low-thrust satellites:

- the simulation of a real transfer, using known thrust parameters. However, this may take a long time to run on a "normal" computer.
- the implementation of a similar strategy to three-dimensional transfers. We have already started

to take a look at this case and perhaps the best approach will be to consider that transfers should occur along an orbit contained in the sphere that contains the initial orbit. Therefore, the initial orbit must always be circular. If not, we use the 2-dimensional transfers described in this project to transform the initial orbit into a circular one. Likely, the most complicated task will be to find the transfer stop condition when the satellite reaches the desired angular momentum value.

References

[1] M. da Silva Fernandes, “Orbit Transfers Between Keplerian Orbits,” Master’s thesis, Instituto Superior Técnico, October 2017.

[2] W. J. Larson and J. R. Wertz, *Space Mission Analysis and Design*. Space Technology Library, 1992 (3rd edition). ISBN 1881883108.

[3] R. Dilão, M. Fernandes, and M. Sá, “Low-Thrust Orbit Transfers Between Two-Body Keplerian Orbits,” *Preprint*, December 2020.

[4] L. G. Taff, *Celestial Mechanics: A Computational Guide for the Practitioner*. Wiley, 1985. ISBN 9780471893165.

[5] M. Kaplan, *Modern Spacecraft Dynamics and Control*. John Wiley and Sons, 1976. ISBN 978-0486819181.

[6] W. Hohmann, *The Attainability of Heavenly Bodies*. National Aeronautics and Space Administration (NASA), 1960 (technical translation).

[7] W. E. Wiesel, *Spaceflight Dynamics*. McGraw-Hill, 1997 (2nd edition). ISBN 0-07-070110-5.

[8] W. D. Dickerson and D. B. Smith, “Trajectory Optimization for Solar-Electric Powered Vehicles,” *AIAA Paper 67-583*, August 1967.

[9] C. G. Sauer, “Optimization of a Solar-Electric-Propulsion Planetary Orbiter Spacecraft,” *American Astronautical Society Paper 68-104*, September 1968.

[10] R. E. Oglevie, P. D. Andrews, and T. P. Jasper, “Attitude Control Requirements for an Earth-Orbital Solar Electric Propulsion Stage,” *AIAA PAPER 75-353*, March 1975.

[11] C. R. Mercer, M. L. McGuire, S. R. Oleson, and M. J. Barrett, “Solar Electric Propulsion Concepts for Human Space Exploration,” *AIAA–2015–4521*, March 2016. NASA/TM—2016-218921.

[12] R. S. Matlock, J. R. Feig, and M. R. Dickey, “Paper Session II-B - The Electric Insertion Transfer Experiment (ELITE): An Air Force Critical Experiment to Revolutionize Space Transportation,” *The Space Congress Proceedings*, 1990. 13. https://commons.erau.edu/space-congress-proceedings/proceedings-1990-27th/april-25-1990/13.

[13] E. R. Avila, “ELITE Program Overview,” *AIAA Paper 92-1559*, March 1992.

[14] R. Dudney, “Rescue in Space,” *Air Force Magazine*, p. 38–41, January 2012.

[15] R. Killinger, R. Kukies, M. Surauer, A. Tomasetto, and L. van Holtz, “ARTEMIS Orbit Raising Inflight Experience with Ion Propulsion,” *Acta Astronautica*, vol. 53, no. 4, p. 607–621, 2003.

[16] S. Zhao and J. Zhang, “Minimum-Fuel Station-Change for Geostationary Satellites Using Low-Thrust Considering Perturbations,” *Acta Astronautica*, p. 296–307, October–November 2016.

[17] D. E. Kirk, *Optimal Control Theory-An Introduction*. Prentice-Hall Inc., 1970. ISBN 0-486-43484-2.

[18] H. J. Sussmann and J. C. Willems, “300 Years of Optimal Control: From The Brachystochrone to the Maximum Principle,” *IEEE Control Systems*, pp. 32–44, 1997.

[19] D. W. Bushaw, *Optimal discontinuous forcing terms. Contributions to the Theory of Nonlinear Oscillations*. PhD thesis, Department of Mathematics, Princeton University, 1952.

[20] R. Dilão, *Uma Introdução Informal à Teoria dos Sistemas Dinâmicos e do Caos*. 2016.

[21] D. F. Lawden, *Advances in Space Science - Interplanetary Rocket Trajectories*. Academic Press, 1959. vol. 1.

[22] H. Munick, R. McGill, and G. E. Taylor, “Analytic Solutions to Several Optimum Orbit Transfer Problems,” *Journal of the Astronautical Sciences*, vol. 7, no. 4, pp. 73–77, 1960.

[23] T. N. Edelbaum, “Propulsion Requirements for Controllable Satellites,” *ARS Journal*, vol. 32, no. 8, p. 1079–1089, 1961.

[24] G. A. Flandro, “Asymptotic Solution for Solar Electric Low-Thrust Orbit Raising with Eclipse Penalty,” *AIAA Mechanics and Control of Flight Conference*, 1974. AIAA Paper 1974-0802.

[25] R. G. Brusch and T. L. Vincent, “Low-Thrust, Minimum Fuel, Orbit Transfers,” *Acta Astronautica*, vol. 16, no. 2, p. 65–73, 1971.

[26] S. Alfano, “Low-Thrust Orbit Transfer,” Master’s thesis, Air Force Institute of Technology (Dept. of Aeronautics and Astronautics), December 1982.

[27] S. Alfano and W. Wiesel, “Optimal Many-Revolution Orbit Transfer,” *Journal of Guidance, Control, and Dynamics*, vol. 8, no. 1, p. 155–157, 1985.

[28] D. C. Redding and J. V. Breakwell, “Optimal Low-Thrust Transfers to Geosynchronous Orbit,” *Journal of Guidance, Control, and Dynamics*, vol. 7, no. 2, pp. 148–155, 1983.

[29] D. Lawden, *Optimal Trajectories for Space Navigation*. Butterworths, 1963.

[30] B. A. Conway, *Spacecraft Trajectory Optimization*. Cambridge University Press, 2010. ISBN 978-0-511-90945-0.

[31] C. R. Hargraves and S. W. Paris, “Direct Trajectory Optimization Using Nonlinear Programming and Collocation,” *Journal of Guidance, Control, and Dynamics*, vol. 10, no. 4, p. 338–342, 1987.

[32] D. B. Spencer, *An Analytical Solution Method for Near-Optimal Continuous-Thrust Orbit Transfers*. PhD thesis, University of Colorado (Dept. of Aerospace Engineering Sciences), 1994.

[33] A. L. Herman, *Improved Collocation Methods with Application to Direct Trajectory Optimization*. PhD thesis, University of Illinois at Urbana–Champaign (Dept. of Aeronautical and Astronautical Engineering), September 1995.

[34] A. L. Herman and D. B. Spencer, "Optimal, Low-Thrust Earth-Orbit Transfers Using Higher-Order Collocation Methods," *Journal of Guidance, Control, and Dynamics*, vol. 25, no. 1, January–February 2002.

[35] D. J. Stewart and R. G. Melton, "Approximate Analytic Representation for Low-Thrust Trajectories," *American Astronautical Society Paper 91-512*, August 1991.

[36] T. A. Bauer, "Near-Optimum Low-Thrust Transfer in Semimajor Axis and Eccentricity," *American Astronautical Society Paper 92-134*, February 1992.

[37] S. Alfano and J. D. Thorne, "Circle-to-Circle Constant-Thrust Orbit Raising," *Journal of the Astronautical Sciences*, vol. 42, no. 1, pp. 35–45, 1994.

[38] J. A. Kechichian, "Optimal Low-Earth-Orbit? Geostationary-Earth- Orbit Intermediate Acceleration Orbit Transfer," *Journal of Guidance, Control, and Dynamics*, vol. 20, no. 4, p. 803–8117, 1997.

[39] J. A. Kechichian, "Reformulation of Edelbaum's Low-Thrust Transfer Problem Using Optimal Control Theory," *Journal of Guidance, Control, and Dynamics*, vol. 20, no. 5, September–October 1997.

[40] J. A. Kechichian, "Low-Thrust Eccentricity-Constrained Orbit Raising," *Journal of Spacecraft and Rockets*, vol. 35, no. 3, p. 327–335, 1998.

[41] J. A. Kechichian, "Orbit Raising with Low-Thrust Tangencial Acceleration in Presence of Earth Shadow," *Journal of Spacecraft and Rockets*, vol. 35, no. 4, p. 516–525, 1998.

[42] J. A. Kechichian, "Low-Thrust Inclination Control in Presence of Earth Shadow," *Journal of Spacecraft and Rockets*, vol. 35, no. 4, p. 526–532, 1998.

[43] M. W. Marasch and C. D. Hall, "Application of Energy Storage to Solar Electric Propulsion Orbital Transfer," *Journal of Spacecraft and Rockets*, vol. 37, no. 5, p. 645–652, 2000.

[44] C. H. Ferrier and R. Epenoy, "Optimal Control for Engines with Electro-Ionic Propulsion under Constraint of Eclipse," *Acta Astronautica*, vol. 48, no. 4, p. 181–192, 2001.

[45] J.-B. Caillau and J. Noailles, "Coplanar Control of a Satellite aroud the Earth," *ESAIM: Control, Optimisation and Calculus of Variations*, vol. 6, p. 239–258, February 2001.

[46] T. Haberkorn, P. Martinon, and J. Gergaud, "Low-Thrust Minimum-Fuel Orbital Transfer: A Homotopic Approach," *Journal of Guidance, Control, and Dynamics*, vol. 27, no. 6, November–December 2004.

[47] J. Gergaud and T. Haberkorn, "Homotopy Method for Minimum Consumption Orbit Tranfer Problem," *ESAIM: Control, Optimisation and Calculus of Variations*, vol. 12, p. 294–310, February 2005.

[48] G. Colasurdo and L. Casalino, "Optimal Low-Thrust Maneuvers in Presence of Earth Shadow," *AIAA/AAS Astrodynamics Specialist Conference and Exhibit*, vol. 35, 2004. AIAA Paper 2004-5087.

[49] C. Kluever, "Using Edelbaum's Method to Compute Low-Thrust Transfers with Earth-Shadow Eclipses," *Journal of Guidance, Control, and Dynamics*, vol. 34, no. 1, p. 300–303, 2011.

[50] S. Lee, P. von Allmen, W. Fink, A. E. Petropoulos, and R. J. Terrile, "Design and Optimization of Low-Thrust Orbit Transfers," *IEEE Aerospace Conference*, 2005.

[51] D. Izzo, D. Hennes, L. F. Simões, and M. Martens, "Designing Complex Interplanetary Trajectories for the Global Trajectory Optimization Competitions," 2016. arXiv:1511.00821v3 [physics.space-ph].

[52] H. C. Henninger, "Study of the solutions of low-thrust orbital transfers in the two and three body problem," Master's thesis, Université Nice Sophia Antipolis, October 2015.

[53] S. Marcuccio, P. Pergola, S. Gregucci, and M. Andrenucci, "Low-Thrust Propulsion Systems For Small Satellites," *66th International Astronautical Congress*, vol. IAC-15-C4.6.7, October 2015.

[54] J. Zhu, E. Trélat, and M. Cerf, "Gometric Optimal Control and Applications to Aerospace," *Pacific Journal of Mathematics for Industry*, 2017.

[55] S. Lee, P. von Allmen, W. Fink, A. E. Petropoulos, and R. J. Terrile, "Fast and Robust Computation of Low-Thrust Orbit-Raising Trajectories," *Journal of Guidance, Control, and Dynamics*, vol. 41, no. 9, 2018.

[56] M. Swenson and J. Fonseca, "A direct collocation method for orbital transfers," *a private communication to Professor Rui Dilão*, 2019.

[57] J.-P. Marec, *Optimal Space Trajectories*. Elsevier, January 1979.

[58] W. E. Wiesel, *Modern Orbit Determination*. Aphelion Press, 2003.

[59] W. E. Wiesel, *Modern Astrodynamics*. Aphelion Press, 2003.

[60] E. Hairer, C. Lubich, and G. Wanner, *Geometric Numerical Integration*. Springer, 2002.

[61] H. Goldstein, C. Poole, and J. Safko, *Classical Mechanics*. Addison Wesley, 2002 (3rd edition).

[62] R. Fitzpatrick, *An Introduction to Celestial Mechanics*. Cambridge Press University, 2012. ISBN 978-1-107-02381-9.

[63] H. D. Curtis, *Orbital Mechanics for Engineering Students*. Elsevier Aerospace Engineering Series, 2020 (4th edition). ISBN 978-0-08-102133-0.

[64] J. M. Longuski, J. J. Guzmán, and J. E. Prussing, *Optimal Control with Aerospace Applications*. Microcosm Press and Springer, 2014. ISBN 978-1-4614-8944-3.

[65] F. Hale, *Introduction to Space Flight*. Prentice-Hall, 1994. ISBN 978-0134819129.

[66] P. W. Keaton, “Low-Thrust Rocket Trajectories,” *Los Alamos National Laboratory*, 1987. Revised by Physics Ware Consulting November 2002. LA-10625-MS.

[67] P. J. S. Gil, *Elementos de Mecânica Orbital*. Lecture notes of "Satellites Dynamics" course at Instituto Superior Técnico., 2015.

Appendix A

Circular orbits approaching

Throughout the development of this project, we encountered some difficulties in obtaining transfers to circular orbits. After analyzing the phases space for each case, we are faced with the existence of a problematic region that did not respect our control choices and that coincided with the region near the circular orbits. In this appendix, we show the calculations that were made so that we can implement the new control choices in that region and, thus, obtain final circular orbits.

A.1 Transfers with constant angular momentum and decreasing effective energy

In Chapter 3 we analyzed transfers with constant angular momentum with i) $H_f > H_0$ and ii) $H_f < H_0$ and presented the control choices to each case (Table 3.2). However, in the second case we found that there was a problematic region when $s_1^* < s < s_0^*$ and that did not allow us to obtain circular orbits.

To solve this problem, we carefully analyzed the orbits phase space with $\sigma = 0$ and $\sigma = 1$. In Figure A.1 we find an example of a simulation for a circular orbit. When $s_1^* < s < s_0^*$ and $\dot{s} = 0$ we keep the s value and call it s_a. When $\dot{s} > 0$, the control should go to 1 but now we will keep it off and the satellite remains in the same Keplerian orbit. When intercepting the orbit with $\sigma = 1$ (red line) with the effective energy corresponding to that of the circular orbit, we turn the control back on and turn it off when $\dot{s}$ is zero again. At that time, the satellite will be in the circular orbit.

To implement this strategy we need to calculate the value of the coordinate s_i. To do this, we have to solve some orbit equations.

The first step is to find the orbit equation with $\sigma = 1$ that connects s_b to s_0^* (green line of Figure A.1). At the fixed point $(s_0^*, 0) = (L_z^2, 0)$, using equation (2.10), we know that the effective energy is given by

$$H_{s_0^*}^{\epsilon} = -\frac{1}{2L_z^2} - \epsilon L_z^2. \tag{A.1}$$

This effective energy value is constant at any point in the orbit and, therefore, we can equate this to a

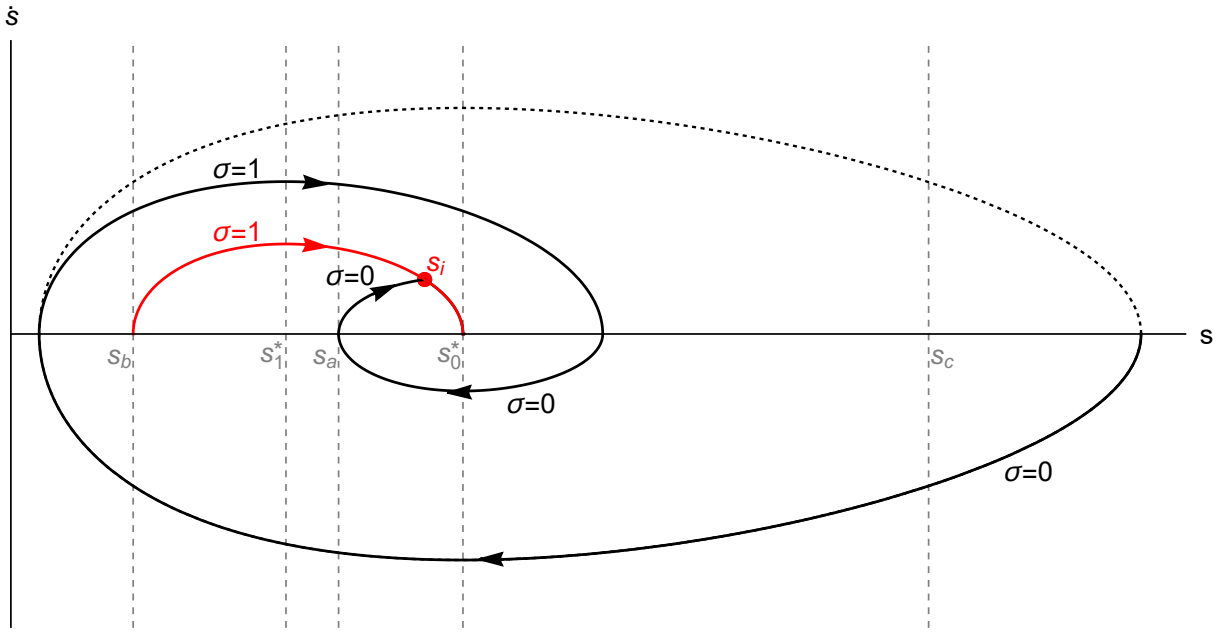

Figure A.1: Phase spaces with $\sigma = 0$ and $\sigma = 1$ in the approach to circular orbits.

general expression:

$$-\frac{1}{2L_z^2} - \epsilon L_z^2 = \frac{1}{2}\left(\dot{s}^2 + \frac{L_z^2}{s^2}\right) - \frac{1}{s} - \epsilon s. \tag{A.2}$$

Solving it in order to $\dot{s}$ we obtain:

$$\dot{s} = \pm\left(-\frac{1}{L_z^2} - 2\epsilon L_z^2 - \frac{L_z^2}{s^2} + \frac{2}{s} + 2\epsilon s\right)^{\frac{1}{2}}, \tag{A.3}$$

where we only consider the positive value since we are analyzing the part with $\dot{s} > 0$ of the orbit. This equation has three zeros but one of them is negative and, therefore, is neglected. So, when $\dot{s} = 0$, its solutions are: $s_0^* = L_z^2$ and $s_b = \frac{1-(1-8\epsilon L_z^4)^{\frac{1}{2}}}{8\epsilon L_z^2}$.

Next, we have to find the orbit equation with $\sigma = 0$ that connects s_b to s_c. When $s = s_b$, the effective energy corresponding to the orbit with $\sigma = 0$ is

$$H_{s_b}^0 = -\frac{1 + (1 - 8\epsilon L_z^4)^{\frac{1}{2}} + 4\epsilon L_z^4}{4L_z^2}. \tag{A.4}$$

Equating this to the general expression of effective energy given by equation (2.10) and solving it in order to $\dot{s}$, we obtain two solutions. As we are only considering the negative part of the orbit, we choose the minus sign. From here, when $\dot{s} = 0$ we obtain two solutions: s_b and s_c, as expected. The expression for s_c is very long and we are not going to write it. Furthermore, it will not be necessary for what we are studying.

Finally, we just need to get the expression for an orbit with $\sigma = 0$ crossing $\dot{s} = 0$ when $s = s_a$ with $s_1^* < s_a < s_0^*$ (problematic region) and $s_0^* < s_a < s_c$. The procedure is similar to what was done previously for the other two orbits. If we equate the expressions of the effective energy at the point $(s_a, 0)$

with the effective energy of the orbit with $\sigma = 0$, we obtain

$$\frac{1}{2}\frac{L_z^2}{s_a^2} - \frac{1}{s_a} = \frac{1}{2}\left(\dot{s}^2 + \frac{L_z^2}{s^2}\right) - \frac{1}{s}. \tag{A.5}$$

The intersection between the orbit with $\sigma = 0$ that leaves s_a and the orbit with $\sigma = 1$ that reaches the fixed point s_0^* (red orbit) is given by joining equations (A.3) and (A.5). So, the s intersection coordinate is

$$s_i = \frac{L_z^2}{2\epsilon s_a^2} - \frac{1}{\epsilon s_a} + \frac{1}{2\epsilon L_z^2} + L_z^2. \tag{A.6}$$

Using this expression, we are ready to simulate transfers to a final circular orbit.